Final Report

Site amplification factors for deep deposits and their application in seismic hazard analysis for Central U.S

Prepared for

USGS

Under USGS/NEHRP Grant: G09AP00123

Grant Tem: - August/15/2009-August/15/2011

Prepared by

Principle Investigator: Youssef Hashash, Professor, hashash@illinois.edu

Graduate Research Assistant: Sungwoo Moon, moon9@illinois.edu

University of Illinois at Urbana-Champaign

205 N. Mathews Ave, Urbana, IL 61801

Ph: 217-333-6986, Fax: 217-265-8041

November 30, 2011

TABLE OF CONTENTS

1. Introduction 1

2. Review of prior work on depth dependent site factors. 3

3. Proposed PSHA-NL(FF)(2011) procedure 8

2.1 Source characterization 8

2.2 Generation of ground motion time series 9

2.2.1 Smoothed seismic sources/Gridded seismicity 10

2.2.2 Finite Fault sources/Characteristic earthquakes 11

2.2.3 Evaluation of resulting UHRS at B/C boundary 13

2.3 Site response analysis 13

2.3.1. Randomization of shear wave velocities 14

2.3.2. Selection of the modulus reduction and damping curves 15

4. Evaluation of developed UHRS and site coefficients 39

3.1 UHRS and site coefficients for 30m depth profiles 39

3.2 Depth-dependent site coefficients 40

5. Summary and Conclusions 55

6. References 56

APPENDIX A - Site Class C 59

APPENDIX B - Site Class D 70

APPENDIX C - Site Class E 81

LIST OF TABLES

Table 2.1 Comparison of conventional USGS PSHA/NEHRP procedure and PSHA-NL to derive surface ground motions 6
Table 3.1 Point source and finite fault models, calibrated to selected attenuation relationships, us ed in PSHA-NL(FF) to generate ground motions for smoothed sources and finite-fault sources. 17
Table 3.2 Selected locations at which simulations are made to develop UHRS and corresponding 2008 USGS spectral accelerations and NEHRP site coefficients. 18
Table 3.3 PS models and revised parameters based on 2008 USGS attenuation relationships 19
Table 3.4 FF models and revised parameters based on 2008 USGS attenuation relationships 20
Table 3.5 Average 30m shear wave velocities (V_{s30}) corresponding to site classes 21
Table 3.6 Weights assigned to dyamic soil properties for each profile..... 21
Table 3.7 Matrix for PSHA-NL(FF)(2011)..... 21
Table 4.1 Recommended site coefficients at site class C, Fa corresponding to soil column thickne ss and 0.2 sec period spectral acceleration based on 2008 USGS hazard map..... 42
Table 4.2 Recommended site coefficients at site class C, Fv corresponding to soil column thickne ss and 1.0 sec period spectral accelelration bsed on 2008 USGS hazard map 42
Table 4.3 Recommended site coefficients at site class D, F_a corresponding to soil column thickne ss and 0.2 sec period spectral acceleration based on 2008 USGS hazard map..... 43
Table 4.4 Recommended site coefficients at site class D, F_v corresponding to soil column thickne ss and 1.0 sec period spectral acceleration based on 2008 USGS hazard map..... 43
Table 4.5 Recommended site coefficients at site class E, F_a corresponding to soil column thickne ss and 0.2 sec period spectral acceleration based on 2008 USGS hazard map..... 44
Table 4.6 Recommended site coefficients at site class E, F_v corresponding to soil column thickne ss and 1.0 sec period spectral acceleration based on 2008 USGS hazard map..... 44

LIST OF FIGURES

Figure 2.1 PSHA-NL for estimation of site coefficients (after Park and Hashash (2005b)..... 7
Figure 3.2 Transfer function to convert a motion from site class A to site class B (B/C boundary) 22
Figure 3.3 Fictitious faults in NMSZ and selected locations for PSHA-NL analysis 22
Figure 3.4 Comparison of calibrated PS simulation (SMSIM) and Frankel (1996) attenuation relationship at selected epicentral distances for NEHRP B/C and hard rock boundary. 23
Figure 3.5 Comparison of calibrated PS simulation (SMSIM) and Campbell (2003) attenuation relationship at selected epicentral distances for NEHRP B/C and hard rock boundary..... 24
Figure 3.6 Comparison of calibrated PS simulation (SMSIM) and Tavakoli & Pezeshk (2003) attenuation relationship at selected epicentral distances for NEHRP B/C and hard rock boundary. 25
Figure 3.7 Comparison of calibrated FF simulation (EXSIM) and Toro (1997) attenuation relationship at selected epicentral distances for NEHRP B/C and hard rock boundary..... 26
Figure 3.8 Comparison of calibrated FF simulation (EXSIM) and Atkinson & Boore (2006) with stress drop 140 attenuation relationship at selected epicentral distances for NEHRP B/C and hard rock boundary. 27
Figure 3.9 Comparison of calibrated FF simulation (EXSIM) and Atkinson & Boore (2006) with stress drop 200 attenuation relationship at selected epicentral distances for NEHRP B/C and hard rock boundary. 28
Figure 3.10 Comparison of calibrated FF simulation (EXSIM) and Silva (2002) attenuation relationship at selected epicentral distances for NEHRP B/C and hard rock boundary..... 29
Figure 3.11 Comparison of calibrated FF simulation (EXSIM) and Somerville (2001) attenuation relationship at selected epicentral distances for NEHRP B/C and hard rock boundary. 30
Figure 3.12 Comparison of simulated UHRS (PSHA-NL(FF)(2011)) and spectral acceleration taken from 2008 USGS hazard maps at PGA, 0.2, and 1 sec..... 31
Figure 3.13 Comparison of simulated UHRS (PSHA-NL(FF)(2011) and PSHA-NL(FF)(2008)) and PGA, 0.2 and 1 sec spectral acceleration taken from 2002 and 2008 USGS hazard maps at NEHRP B/C boundary 32

Figure 3.14 Shear wave velocity profiles for upland and lowland at site class C (a) mean values (b) 30 randomized profiles at upland (c) 30 randomized profiles at lowland 33
Figure 3.15 Shear wave velocity profiles for upland and lowland at site class D (a) mean values (b) 30 randomized profiles at upland (c) 30 randomized profiles at lowland 34
Figure 3.16 Shear wave velocity profiles for upland and lowland at site class E (a) mean values (b) 30 randomized profiles at upland (c) 30 randomized profiles at lowland 35
Figure 3.17 Dynamic soil properties of ME (a) Modulus reduction curves and (b) damping curve s 36
Figure 3.18 Dynamic soil properties of EPRI (a) Modulus reduction curves and (b) damping curv es 37
Figure 3.19 Dynamic soil properties of Darendeli&Menq (a) Modulus reduction curves and (b) d amping curves 38
Figure 4.1 Comparison of PSHA(FF) (2011) UHRS at 30m depth soil-column and NEHRP design spectra at site class D 45
Figure 4.2 Comparison of PSHA(FF) (2011) UHRS at 30m depth soil-column and NEHRP design spectra at site class C 46
Figure 4.3 Comparison of PSHA(FF) (2011) UHRS at 30m depth soil-column and NEHRP design spectra at site class E 47
Figure 4.4 Comparison of site coefficients obtained from PSHA-NL(FF)(2011) and other studies for 30m thick soil column. 48
Figure 4.5 Comparison of depth-dependent site coefficients obtained from PSHA-NL(FF) and NEHRP site coefficients at site class C (a) Upland (b) Lowland 49
Figure 4.6 Comparison of depth-dependent site coefficients obtained from PSHA-NL(FF) and NEHRP site coefficients at site class D (a) Upland (b) Lowland 50
Figure 4.7 Comparison of depth-dependent site coefficients obtained from PSHA-NL(FF) and NEHRP site coefficients at site class E (a) Upland (b) Lowland 51
Figure 4.8 Comparison of depth-dependent site coefficients obtained from PSHA-NL(FF) and empirical studies at 30m,100m,200m,300m,500m,1000m depth soil column (a) and (b) Uplands, (c) and (d) Lowlands at site class C. 52
Figure 4.9 Comparison of depth-dependent site coefficients obtained from PSHA-

NL(FF) and empirical studies at 30m,100m,200m,300m,500m,1000m depth soil column (a) and (b) Uplands, (c) and (d) Lowlands at site class D. 53
Figure 4.10 Comparison of depth-dependent site coefficients obtained from PSHA-NL(FF)(2011) and empirical studies at 30m,100m,200m,300m,500m,1000m depth soil colu mn (a) and (b) Uplands, (c) and (d) Lowlands at site class E. 54
Figure A 1 Computed PSHA(FF)(2011) UHRS for 30m, 100m, 200m, 300m, 500m, 1000m soil-columns and NEHRP design spectra. Uplands, site 1 60
Figure A 2 Computed PSHA(FF)(2011) UHRS for 30m, 100m, 200m, 300m, 500m, 1000m soil-columns and NEHRP design spectra. Uplands, site 2 60
Figure A 3 Computed PSHA(FF)(2011) UHRS for 30m, 100m, 200m, 300m, 500m, 1000m soil-columns and NEHRP design spectra. Uplands, site 3 61
Figure A 4 Computed PSHA(FF)(2011) UHRS for 30m, 100m, 200m, 300m, 500m, 1000m soil-columns and NEHRP design spectra. Uplands, site 4 61
Figure A 5 Computed PSHA(FF)(2011) UHRS for 30m, 100m, 200m, 300m, 500m, 1000m soil-columns and NEHRP design spectra. Uplands, site 5 62
Figure A 6 Computed PSHA(FF)(2011) UHRS for 30m, 100m, 200m, 300m, 500m, 1000m soil-columns and NEHRP design spectra. Uplands, site 6 62
Figure A 8 Computed PSHA(FF)(2011) UHRS for 30m, 100m, 200m, 300m, 500m, 1000m soil-columns and NEHRP design spectra. Uplands, site 8 63
Figure A 9 Computed PSHA(FF)(2011) UHRS for 30m, 100m, 200m, 300m, 500m, 1000m soil-columns and NEHRP design spectra. Uplands, site 9 64
Figure A 10 Computed PSHA(FF)(2011) UHRS for 30m, 100m, 200m, 300m, 500m, 1000m soil -columns and NEHRP design spectra. Lowlands, site 1 65
Figure A 11 Computed PSHA(FF)(2011) UHRS for 30m, 100m, 200m, 300m, 500m, 1000m soil -columns and NEHRP design spectra. Lowlands, site 2. 65
Figure A 12 Computed PSHA(FF)(2011) UHRS for 30m, 100m, 200m, 300m, 500m, 1000m soil -columns and NEHRP design spectra. Lowlands, site 3. 66
Figure A 13 Computed PSHA(FF)(2011) UHRS for 30m, 100m, 200m, 300m, 500m, 1000m soil -columns and NEHRP design spectra. Lowlands, site 4. 66
Figure A 14 Computed PSHA(FF)(2011) UHRS for 30m, 100m, 200m, 300m, 500m, 1000m soil

-columns and NEHRP design spectra. Lowlands, site 5. 67
Figure A 15 Computed PSHA(FF)(2011) UHRS for 30m, 100m, 200m, 300m, 500m, 1000m soil -columns and NEHRP design spectra. Lowlands, site 6. 67
Figure A 16 Computed PSHA(FF)(2011) UHRS for 30m, 100m, 200m, 300m, 500m, 1000m soil -columns and NEHRP design spectra. Lowlands, site 7. 68
Figure A 17 Computed PSHA(FF)(2011) UHRS for 30m, 100m, 200m, 300m, 500m, 1000m soil -columns and NEHRP design spectra. Lowlands, site 8. 68
Figure A 18 Computed PSHA(FF)(2011) UHRS for 30m, 100m, 200m, 300m, 500m, 1000m soil -columns and NEHRP design spectra. Lowlands, site 9. 69
Figure B 1 Computed PSHA(FF)(2011) UHRS for 30m, 100m, 200m, 300m, 500m, 1000m soil-columns and NEHRP design spectra. Uplands, site 1. 71
Figure B 2 Computed PSHA(FF)(2011) UHRS for 30m, 100m, 200m, 300m, 500m, 1000m soil-columns and NEHRP design spectra. Uplands, site 2. 71
Figure B 3 Computed PSHA(FF)(2011) UHRS for 30m, 100m, 200m, 300m, 500m, 1000m soil-columns and NEHRP design spectra. Uplands, site 3. 72
Figure B 4 Computed PSHA(FF)(2011) UHRS for 30m, 100m, 200m, 300m, 500m, 1000m soil-columns and NEHRP design spectra. Uplands, site 4. 72
Figure B 5 Computed PSHA(FF)(2011) UHRS for 30m, 100m, 200m, 300m, 500m, 1000m soil-columns and NEHRP design spectra. Uplands, site 5. 73
Figure B 6 Computed PSHA(FF)(2011) UHRS for 30m, 100m, 200m, 300m, 500m, 1000m soil-columns and NEHRP design spectra. Uplands, site 6. 73
Figure B 7 Computed PSHA(FF)(2011) UHRS for 30m, 100m, 200m, 300m, 500m, 1000m soil-columns and NEHRP design spectra. Uplands, site 7. 74
Figure B 8 Computed PSHA(FF)(2011) UHRS for 30m, 100m, 200m, 300m, 500m, 1000m soil-columns and NEHRP design spectra. Uplands, site 8. 74
Figure B 9 Computed PSHA(FF)(2011) UHRS for 30m, 100m, 200m, 300m, 500m, 1000m soil-columns and NEHRP design spectra. Uplands, site 9. 75
Figure B 10 Computed PSHA(FF)(2011) UHRS for 30m, 100m, 200m, 300m, 500m, 1000m soil -columns and NEHRP design spectra. Lowlands, site 1. 76
Figure B 11 Computed PSHA(FF)(2011) UHRS for 30m, 100m, 200m, 300m, 500m, 1000m soil

-columns and NEHRP design spectra. Lowlands, site 2. 76
Figure B 12 Computed PSHA(FF)(2011) UHRS for 30m, 100m, 200m, 300m, 500m, 1000m soil -columns and NEHRP design spectra. Lowlands, site 3. 77
Figure B 13 Computed PSHA(FF)(2011) UHRS for 30m, 100m, 200m, 300m, 500m, 1000m soil -columns and NEHRP design spectra. Lowlands, site 4. 77
Figure B 14 Computed PSHA(FF)(2011) UHRS for 30m, 100m, 200m, 300m, 500m, 1000m soil -columns and NEHRP design spectra. Lowlands, site 5. 78
Figure B 15 Computed PSHA(FF)(2011) UHRS for 30m, 100m, 200m, 300m, 500m, 1000m soil -columns and NEHRP design spectra. Lowlands, site 6. 78
Figure B 16 Computed PSHA(FF)(2011) UHRS for 30m, 100m, 200m, 300m, 500m, 1000m soil -columns and NEHRP design spectra. Lowlands, site 7. 79
Figure B 17 Computed PSHA(FF)(2011) UHRS for 30m, 100m, 200m, 300m, 500m, 1000m soil -columns and NEHRP design spectra. Lowlands, site 8. 79
Figure B 18 Computed PSHA(FF)(2011) UHRS for 30m, 100m, 200m, 300m, 500m, 1000m soil -columns and NEHRP design spectra. Lowlands, site 9 80
Figure C 1 Computed PSHA(FF)(2011) UHRS for 30m, 100m, 200m, 300m, 500m, 1000m soil-columns and NEHRP design spectra. Uplands, site 1 82
Figure C 2 Computed PSHA(FF)(2011) UHRS for 30m, 100m, 200m, 300m, 500m, 1000m soil-columns and NEHRP design spectra. Uplands, site 2 82
Figure C 3 Computed PSHA(FF)(2011) UHRS for 30m, 100m, 200m, 300m, 500m, 1000m soil-columns and NEHRP design spectra. Uplands, site 3 83
Figure C 4 Computed PSHA(FF)(2011) UHRS for 30m, 100m, 200m, 300m, 500m, 1000m soil-columns and NEHRP design spectra. Uplands, site 4 83
Figure C 5 Computed PSHA(FF)(2011) UHRS for 30m, 100m, 200m, 300m, 500m, 1000m soil-columns and NEHRP design spectra. Uplands, site 5 84
Figure C 6 Computed PSHA(FF)(2011) UHRS for 30m, 100m, 200m, 300m, 500m, 1000m soil-columns and NEHRP design spectra. Uplands, site 6 84
Figure C 7 Computed PSHA(FF)(2011) UHRS for 30m, 100m, 200m, 300m, 500m, 1000m soil-columns and NEHRP design spectra. Uplands, site 7 85
Figure C 8 Computed PSHA(FF)(2011) UHRS for 30m, 100m, 200m, 300m, 500m, 1000m soil-

columns and NEHRP design spectra. Uplands, site 8..... 85
Figure C 9 Computed PSHA(FF)(2011) UHRS for 30m, 100m, 200m, 300m, 500m, 1000m soil-columns and NEHRP design spectra. Uplands, site 9..... 86
Figure C 10 Computed PSHA(FF)(2011) UHRS for 30m, 100m, 200m, 300m, 500m, 1000m soil -columns and NEHRP design spectra. Lowlands, site 1..... 87
Figure C 11 Computed PSHA(FF)(2011) UHRS for 30m, 100m, 200m, 300m, 500m, 1000m soil -columns and NEHRP design spectra. Lowlands, site 2..... 87
Figure C 12 Computed PSHA(FF)(2011) UHRS for 30m, 100m, 200m, 300m, 500m, 1000m soil -columns and NEHRP design spectra. Lowlands, site 3..... 88
Figure C 13 Computed PSHA(FF)(2011) UHRS for 30m, 100m, 200m, 300m, 500m, 1000m soil -columns and NEHRP design spectra. Lowlands, site 4..... 88
Figure C 14 Computed PSHA(FF)(2011) UHRS for 30m, 100m, 200m, 300m, 500m, 1000m soil -columns and NEHRP design spectra. Lowlands, site 5..... 89
Figure C 15 Computed PSHA(FF)(2011) UHRS for 30m, 100m, 200m, 300m, 500m, 1000m soil -columns and NEHRP design spectra. Lowlands, site 6..... 89
Figure C 16 Computed PSHA(FF)(2011) UHRS for 30m, 100m, 200m, 300m, 500m, 1000m soil -columns and NEHRP design spectra. Lowlands, site 7..... 90
Figure C 17 Computed PSHA(FF)(2011) UHRS for 30m, 100m, 200m, 300m, 500m, 1000m soil -columns and NEHRP design spectra. Lowlands, site 8..... 90
Figure C 18 Computed PSHA(FF)(2011) UHRS for 30m, 100m, 200m, 300m, 500m, 1000m soil -columns and NEHRP design spectra. Lowlands, site 9..... 91

ABSTRACT

This report presents the results of probabilistic seismic hazard analysis with nonlinear site effects, PSHA-NL (FF)(2011), for Central and Eastern United States. This approach consists of the following steps: (a) Develop a synthetic earthquake catalog over a period of simulation years to reflect the seismic sources and their recurrence rates based on 2008 USGS hazard map, (b) Use attenuation relationships to calibrate point source (SMSIM) and finite fault models (EXSIM) for generation of synthetic ground-motion time histories corresponding to the synthetic earthquake catalogue at hard rock, (c) Propagate ground motion through soil columns of varying thickness using equivalent linear and nonlinear site response analysis (DEEPSOIL) to develop a uniform hazard response spectrum, (d) compute soil column depth dependent NEHRP style site amplification factors.

This approach was applied to soil column thickness of 30m, 100m, 200m, 300m, 500m, 1000m, and for site classes C, D and E. Computed UHRS for 30m soil-column profiles of NEHRP site-class D are consistent with NEHRP design spectra. But those of Site class C and D differ somewhat. For all site classes, the site factors exhibited a clear depth dependence, and thus dependent site coefficients are proposed. Comparisons with factors proposed in the literature are also made. It is recommended that future revisions of site factors account for the depth of the soil column to hard rock.

1. Introduction

Widespread damage to infrastructures and massive loss of life have resulted from strong earthquakes throughout the world in the last two decades (Iran, 1990; US, 1994; Japan, 1995; Turkey, 1999; Taiwan, 1999; India, 2001; Pakistan, 2005; Sumatra, 2007; Samoa, 2009, 2009; Chile, 2010; Japan, 2011). Two approaches, deterministic and probabilistic seismic hazard analysis (DSHA and PSHA), for the realistic seismic hazard assessment and risk analyses have been employed to estimate the strong ground motions parameters for engineering design and decision-making purposes.

In 1968, Cornell (1968) developed PSHA to explicitly incorporate the uncertainties (e.g. epistemic, aleatory variability) in earthquake size, location and rate of recurrence of earthquakes, and the variation of resulting ground motion time histories in the evaluation of seismic hazard. PSHA provides the mean annual rate of exceedance of ground-motion parameters at selected locations, based on both the distances between source and site, and the amplitudes of ground motion parameters at selected annual probabilities of exceedance. The United States Geological Survey (USGS) National Hazard Maps, updated by Petersen et al. (2008), and the site coefficients proposed in the 2009 edition of the National Earthquake Hazard Reduction Program (NEHRP) Recommended Provisions for Seismic Regulations of New Building and Other Structures can be applied to develop surface ground-motion parameters for different site conditions.

However, these site coefficients may not be applicable for all site conditions especially for conditions in the Central U.S. Seismic wave amplification due to unconsolidated fluvial or lacustrine deposits has been a major factor in damage and economical losses during strong ground motions (e.g. San Francisco, 1957; Loma Prieta, 1989; Northridge, 1994; and Kobe,

1995). The amplification and attenuation of ground motions associated with the deep soil deposits on the Mississippi Embayment (ME) are not well understood. The site coefficients use in NEHRP cannot account for the effect of deep soil deposits, such as in the Upper Mississippi Embayment(UME) where the deposits can be up to 1000m in thickness, because site coefficients are developed by using the weighted average shear-wave velocity of the top 30m of the profile (V_{s30}).

In this report we utilize an integrated site response-PSHA procedure to evaluate the influence of deep soil deposits on NEHRP style site coefficients in a probabilistically consistent fashion.

2. Review of prior work on depth dependent site factors.

Park and Hashash (2005b) proposed a new integrated PSHA procedure that can consider site effects of selected locations, PSHA-NL(Non Linear), based on the doctoral dissertation of Park (2003). The procedure is illustrated in Figure 2.1 and Table 2.1. The procedure is composed of three main steps: (1) source characterization, (2) generation of ground-motion time histories, and (3) site response analysis. Steps 1 and 2 generate ground-motion time histories and uniform hazard response spectra (UHRS) at hard rock and B/C boundary, and step 3 characterizes the effect of the deep soil deposits of the UME through propagation of generated ground motions. The propagated ground motion through soil-column and the developed UHRS are used to determine depth-dependent NEHRP-style site coefficients for site class D sites only. The PSHA-NL procedure suggested by Park and Hashash (2005b) has two limitations: (1) the use of point source models and parameters to simulate characteristic earthquakes requiring artificial cap usage to avoid unrealistically large ground motions in step 2, (2) the use of only two deterministic soil profiles to account for uncertainty in soil-column profiles that only represent site class D.

Cramer (2006) suggested a procedure to estimate site-specific seismic hazard considering the effect of deep soil deposits of UME. The developed UHRS from the USGS hazard map methodology is obtained on a grid pattern. Ten ground-motion time histories are selected from M ~7 strong motion time series (corresponding to a characteristic earthquake for the New Madrid Seismic Zone (NMSZ)) and scaled to match the USGS UHRS (with 2% possibility of exceedance in 50 yr) at each grid point. The site response analysis is performed using 1-D equivalent linear site response analysis. The scaled ground motions are propagated through 100 randomized soil profiles to account for the uncertainty and variability of soil profiles. However,

this approach has important limitations. Scaling a motion to fit a UHRS is generally not recommended because it is not probabilistically rigorous (Baker and Cornell 2006). The UHRS represents an aggregation of multiple earthquake sources while the ground motion used for site response analysis represents the motion from only a single earthquake. Conversely, NMSZ characteristic earthquakes generally control the seismic hazard at rock sites for return periods of greater than or equal to 1000 years (Wen and Wu 2001). The sole use of the equivalent linear method for site response analysis under strong shaking is generally unsuitable because it does not consider the strongly nonlinear response of the soil (Field 1998). The procedure does not generate a UHRS at the ground surface that meets the strict definition of this type of spectra.

Hashash et al. (2008) enhanced PSHA-NL procedure suggested by Park and Hashash (2005b) via the incorporation of a finite fault model which is able to generate ground-motion time histories for strong earthquakes (M_w>7) compatible with the USGS hazard maps without artificial caps (i.e., peak ground acceleration (PGA) is 1.5g used in Petersen et al. (2008)), and propagate the generated ground motions through randomized soil-column properties. These improvements enhance a more consistent and probabilistic procedure that accounts for the site effects of UME deep soil deposits and overcomes the limitations in the study presented by Cramer (2006) and Park and Hashash (2005b) described earlier.

In this report, new shear wave velocity data collected for the UME soils are added to that of Hashash et al. (2008), to evaluate site classes C, D, and E. The modulus reduction and damping curves proposed by Darendeli (2001) and Menq (2003) are combined with those (ME, EPRI) developed by Hashash et al. (2008) for site response analysis. The updated information regarding hypothetical faults and attenuation relationships for finite-fault (FF) and point-source (PS) is used based on the 2008 USGS hazard map rather than the 2002 USGS hazard map. The PSHA-

NL procedure enhanced by Hashash et al. (2008) is integrated with the program EXSIM (Extended Finite-Fault Simulation; Motazedian and Atkinson (2005)), which is an updated version of FINSIM (Beresnev and Atkinson (1998)), capable of simulating stochastic ground-motion time histories from finite faults, and SMSIM (version 3.1, Boore (2005)), an updated version of SMSIM (version 2.2, Boore (2002)), capable of simulating stochastic ground-motion time histories from point sources. New sets of depth-dependent NEHRP-style site coefficients of the UME corresponding to NEHRP site-classes C, D, and E are developed, and the obtained sets of NEHRP-style site coefficients are compared with site amplification factors from other studies studies in terms of PGA. The methodology proposed by Hashash et al. (2008) is denoted as PSHA-NL (FF)(2008) whereas the enhanced procedure is denoted as PSHA-NL (FF)(2011).

Table 2.1 Comparison of conventional USGS PSHA/NEHRP procedure and PSHA-NL to derive surface ground motions

Step	USGS/PSHA	Hashash/Wen(PSHA-NL(FF))
1. Seismic source characterization	a. Identify seismic sources and geometry. b. Define recurrence parameters for each seismic source.	a. Identify seismic sources and geometry. b. Define recurrence parameters for each seismic source. c. Develop a synthetic earthquake catalog over a period of simulation years to reflect the sources and their recurrence rates.
2. Ground-motion parameters	a. Use attenuation relationships to derive ground-motion parameters. b. Develop spectral parameters corresponding to a given uniform hazard at NEHRP site-class A or B/C.	a. Use attenuation relationships to calibrate PS and FF models for generation of synthetic ground-motion time histories. b. Develop UHRS from the aggregation of all acceleration time histories for NEHRP site-class A and B/C.
3. Site effects	a. Use NEHRP site coefficients to develop NEHRP spectrum at ground surface.	a. Propagate all synthetic motions through randomized soil profile properties to preserve the probabilistic nature of the surface ground-motion parameters. b. Develop UHRS at the ground surface.

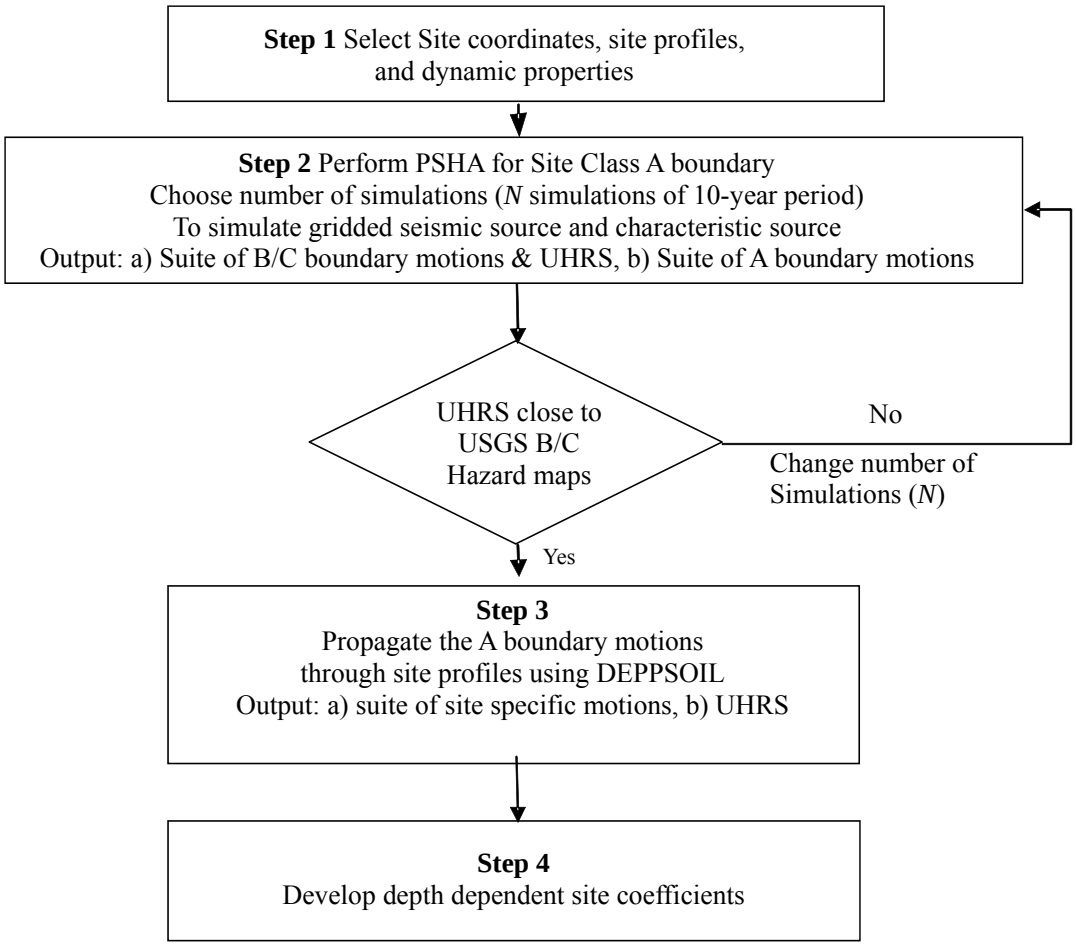

Figure 2.1 PSHA-NL for estimation of site coefficients (after Park and Hashash (2005b)

3. Proposed PSHA-NL(FF)(2011) procedure

Park and Hashash (2005b) proposed PSHA-NL procedure employed a point source model, and Hashash et al. (2008) enhanced this methodology through the incorporation of a finite fault model able to generate ground time histories for strong motions (M_w>7) compatible with the USGS hazard maps without the need for an artificial cap. Similarly the proposed PSHA-NL(FF)(2011), uses a finite fault model artificial cap. As shown in Table 2.1, the USGS/PSHA and the proposed PSHA-NL(PS2005, FF2008 and FF2011) procedures are composed of three main steps; (1) seismic source characterization, (2) ground motion parameters (attenuation relationships), and (3) site effects.

2.1 Source characterization

In this report, the seismic source characterization is composed of three elements: (1) characterization of location and geometry of seismic sources, (2) definition of recurrence parameters for each seismic source, and (3) development of a synthetic earthquake catalog, as shown in Table 2.1.

The USGS hazard maps (Petersen et al. 2008) define two types of seismic sources for the Central United States: (1) finite fault sources and (2) smoothed seismic sources. Finite fault sources are used to represent earthquakes corresponding to the recurrence interval and magnitude which are based on geologic evidences (characteristic earthquakes). Smoothed seismic sources, are considered to represent the historical seismicity and large background source zones (gridded seismicity), and are determined by three components: (1) the recurrence rate, (2) the annual rate of exceedance, and (3) the earthquake magnitude. The finite fault and smoothed seismic sources are considered separately and are added to the final seismic hazard.

Based on USGS hazard maps, seismicity for both finite fault source and smoothed seismic

source is considered, whereas actual sources that occur within a finite number of 10 simulation years (N) are assumed. Wen and Wu (2001) suggest that 9000 simulation years are required to generate recurrence rates compatible with USGS hazard maps, and the same simulation years are used in this report.

2.2 Generation of ground motion time series

Point source (SMSIM, version 3.1, Boore 2005) and finite fault (EXSIM, Motazedian and Atkinson, 2005) models are used to generate ground motions based on the synthetic catalogue developed in the previous step.

The PS and FF model parameters are developed to reflect the attenuation relationships in the 2008 USGS maps as shown in Table 3.2.

The ground motion time series for NEHRP site-class A, hard rock, are generated through both finite fault and point source (smoothed) seismic sources at nine site locations listed in Table 3.2. The nine site locations representing the range of spectral acceleration expected within the upper Mississippi embayment (UME) are selected due to the long time required to perform a hazard analysis on a 0.1°×0.1° grid pattern within the embayment. In step 3, the hypothetical sediment thicknesses from 30m to 1000m are used for site response analysis to represent the range of the sediment thickness encountered in the UME, described in the following section. Site locations 1-6 were considered in the report by Park and Hashash (2005b), and site locations 7-9 were added in the report by Hashash et al. (2008), to examine NEHRP site coefficients for very strong motions and weak motion within UME.

In Hashash et al. (2008), a spectral decay parameter (κ) with a value of 0.006 was used to produce a gradual attenuation of high frequency and to generate rock motions by PSHA-NL(FF). In this report, a kappa of 0.01, as recommended for NEHRP site-class A for the Central and Eastern United States (CEUS) (Frankel et al. 1996), is applied to generate proper

rock motions at selected site locations.

As shown in Figure 3.1, the transfer function from Frankel et al. (1996) is applied to convert generated hard rock ground motions to B/C boundary ground motions, and the generated hard rock ground motions are applied directly to perform site response analysis as described in step 3.

2.2.1 Smoothed seismic sources/Gridded seismicity

In order to generate the ground motions of the smoothed seismic sources, PS stochastic models are used, which are successful in representing small to moderate-sized magnitude earthquakes (M_w<7). Based on 2002 USGS hazard maps, Hashash et al. (2008) used four attenuation relationships to estimate ground motion parameters: Toro et al. (1997), Frankel et al. (1996), Atkinson and Boore (1995), and Campbell (2003), for smoothed seismic sources (Table 2.1). Hashash et al. (2008) also assigned the weights based on the following categories: Toro et al. (1997) (0.286w), Frankel et al. (1996) (0.286w), Atkinson and Boore (1995) (0.286w), and Campbell (2003) (0.142w). In this report, previous attenuation relationships and the weights are updated based on 2008 USGS hazard maps: (1) Frankel et al. (1996) (0.333w), (2) Campbell (2003) (0.333w), and (3) Tavakoli and Pezeshk (2005) (0.333w).

The stochastic model SMSIM [version 3.1, Boore (2005)] is used for simulating ground motions for the three attenuation relationships mentioned. The PS model for SMSIM is simulated using the effective distance rather than the closest distance to avoid much higher response spectral accelerations at 1 and 10 km. The corresponding model parameters for SMSIM to represent each attenuation relationship as presented in Table 3.3. The model parameters of shear-wave velocity, density, quality factor (Q), and stress drop are based on the values recommended by respective simulated models, and geometric spreading values are adjusted to match simulated ground motions for each attenuation relationship. Figure 3.3-

Figure 3.5 show PS simulations used to represent attenuation relationships of Frankel et al. (1996), Campbell (2003), and Tavakoli and Pezeshk (2005), at six selected epicentral distances (1, 10, 30, 70, 100, 200km) for NEHRP B/C boundary and hard rock. The calibrated PS models are able to represent well the respective attenuation relationships.

2.2.2 Finite Fault sources/Characteristic earthquakes

In order to generate the ground motions for the characteristic sources, a finite fault source model, which successfully represents large magnitude earthquakes, is adopted instead of a PS model. The finite fault model is capable of considering rupture propagation, directivity, and source-site geometry. It models fault rupture in a more realistic way and avoids the limitations of PS models where released energy is concentrated at one point. The fault geometry including length, width, strike, dip and depth, rupture propagation velocity, and slip velocity (energy release) should be defined in an FF model. The fault plane is divided into several subfaults considered as individual single-corner point sources. The delay between triggers is of a random nature depending on subfault rise time. The resulting ground motion time history is a combination of waveforms from different subfaults accounting for differences in triggered time (from hypocenter to the subsource on the fault plane) and path time (from subfault to observation site). Hashash et al. (2008) used the computer program FINSIM, the stochastic finite fault approach, to simulate ground motion time histories from finite faults, developed by Beresnev and Atkinson (1998). In this report, the simulations are implemented with EXSIM (Extended Finite-Fault Simulation; Motazedian and Atkinson (2005), which is an updated version of FINSIM stochastic finite fault simulation. This updated model incorporates the independence of results from subfault size, conservation of radiated energy, and the ability to have only a portion of the fault active at any time during the rupture (Heaton 1990).

In 2008 USGS hazard map, five attenuation relationships are implemented: Toro et al. (1997), Atkinson and Boore (2006) with 140 bar, Atkinson and Boore (2006) with 200 bar, Silva et al. (2002), and Somerville et al. (2001), to estimate the seismic hazard caused by characteristic earthquakes of Mw≥7.5 (with an average value of Mw 7.7 corresponding to an earthquake of 500 yr return period) as listed in Table 3.3

In this report, the dimensions of the fault representing this characteristic source are 125 × 26 km (length by width) based on empirical relations of magnitude and fault geometry (Wells and Coppersmith 1994). The hypothetical fault traces are assumed to be five rather than three used in 2002 USGS hazard map to explain spatial variability, and the fault is assumed to be dipping 38° to the southwest instead of vertical with the hypocenter located at the center of the fault plane based on 2002 USGS hazard map. In order to represent each of the five attenuation relationships for an M_w 7.7 event, geometric spreading parameters are modified to vary the rate of attenuation at different distances and represent the five attenuation relationships used in the 2008 USGS hazard maps for an M_w 7.7 event. As shown in Table 3.4, the stress drop is used as a parameter to reproduce each attenuation relationship for EXSIM, instead of the radiation-strength factor for FINSIM simulation of energy releases.

Figure 3.6 shows finite fault simulations using EXSIM to duplicate the Toro et al. (1997) attenuation relationship for an M_w 7.7 event at NEHRP B/C site condition as well as for a hard rock condition. The response spectra simulated by EXSIM compare well with the spectral accelerations suggested by Toro et al. (1997) for selected epicentral distances (1, 10, 30, 70, 100, 200km). The FF model provides reasonable spectral accelerations near the fault compared with the PS model. Similar comparisons are presented in Figure 3.7 to Figure 3.10 for the four other attenuation relationships.

2.2.3 Evaluation of resulting UHRS at B/C boundary

In order to verify that the proposed PSHA-NL(FF)(2011) procedure computes hazard levels consistent with 2008 USGS hazard maps without a consideration of site effect, the UHRS of the generated ground motions at the NEHRP B/C boundary are compared with spectral accelerations corresponding to PGA, 0.2 and 1.0 sec with a probability of exceedance of 2% in 50 years, and the selected nine sites.

Figure 3.11 shows the comparison of simulated UHRS of PSHA-NL(FF)(2011) and 2008 USGS hazard map corresponding to NEHRP B/C boundary and hard rock for sites 1 to 9. The UHRS is simulated by considering both the smoothed seismic source and finite-fault source methodologies. The UHRS via current proposed PSHA-NL(FF)(2011) procedure match well with 2008 USGS hazard maps at NEHRP site-class B/C and hard rock. Figure 3.12 shows the two sets of comparisons: simulated UHRS (PSHA-NL(FF)(2011) and PSHA-NL(FF)(2008)), and USGS hazard maps (2008 and 2002) at NEHRP B/C for sites 1 to 6. The simulated UHRS of PSHA-NL(FF)(2011) and Hashash et al. (2008) at the NEHRP B/C are representative of the hazard maps. Thus, this proposed method can generate ground motion time histories consistent with USGS hazard map regardless of seismic intensity for site response analysis.

2.3 Site response analysis

The generated ground motions at hard rock (NEHRP site-class A) representing Paleozoic bedrock are propagated to the ground surface to account for the effects of Mississippi embayment deposits. The seismic-wave propagation is simulated using the 1-D site response analysis code DEEPSOIL (version 4.0, Hashash and Park (2001); Hashash (2011)). The site response analysis requires information regarding dynamic soil properties including (1) the shear wave velocity profile and (2) the modulus reduction and damping curves. In order to

consider the uncertainty in the site response analysis due to variability in dynamic soil properties, two sets of randomized shear-wave velocity profiles representing the upland and lowland profiles are used in combination with two sets of normalized modulus reduction damping curves as shown in Table 3.6. The limitation of available computer resources and the computational cost to perform nonlinear site response analysis cause the determination of an appropriate number of randomized shear wave velocity profiles and dynamic soil properties.

The thickness of soil-column profile at each nine site is considered to be 30, 100, 200, 300, 500, and 1000m to represent the effect of deep soil deposit at each depth performed by site response analysis. Romero and Rix (2001) assumed that the shear-wave velocity of Paleozoic rock located at the bottom of the soil-column profiles is 3000 m/sec. The seismic-wave propagation is simulated via the one dimensional site response program, DEEPSOIL, used in order to consider equivalent-linear and nonlinear time domain site response. The results of site response analyses, which are the response spectra of the propagated ground motions on the surface, are used to develop UHRS.

2.3.1. Randomization of shear wave velocities

The shear wave velocity profiles corresponding to NEHRP site-class C, D, and E are randomized for uplands and lowlands, where Romero and Rix (2001) classified the UME based on geologic age as shown in Figure 3.2. Two shear-wave velocity profiles corresponding to the upland and the lowland regions are considered as input profiles in the site response analyses for different site-classes. The shear wave velocity profiles of upland and lowland regions corresponding to NEHRP site class C, D, and E show variation up until 200m from the top. As shown in Table 3.5, the V_{s30} of the upland is generally higher than that of the lowland in the NEHRP site-class C, D, and E due to loose Holocene-age deposits of the alluvial plains, and is identical at deeper thicknesses. The V_{s30} values (Upland: 275m/s,

Lowland: 234m/s) of the upland and the lowland within NEHRP site-class D are lower than those (Upland: 314m/s, Lowland: 249m/s) from Hashash et al. (2008) because the database of the shear wave velocity is updated based on the additional results from field tests.

The randomization methodology proposed by Toro and Silva (2001) and Wong et al. (2004) is used to generate 30 randomized shear wave velocity profiles for each of the upland and lowland profiles, and three site class (C, D, E), are shown in Figure 3.13 - Figure 3.15 under the following constraints:

1. Lognormal distribution of shear-wave velocity with σ_{ln}=0.15 (Romero and Rix 2001)
2. Correlation coefficient of the lognormal mean of adjacent layers is 0.5 (Romero and Rix 2001); and
3. The variation of shear-wave velocity is constrained within on standard deviation to avoid unrealistic velocity profiles.

2.3.2. Selection of the modulus reduction and damping curves

As shown in Figure 3.16-Figure 3.18, three sets of dynamic soil properties: (1) Mississippi embayment (ME; Park and Hashash (2005a)), (2) Electric Power Research Institute (EPRI; EPRI (1993)), and (3) Darendeli & Menq (Darendeli (2001), Menq (2003)), are considered to describe depth dependent nonlinear soil behavior for the thick deposits in both the upland and the lowland. The modulus reduction curves of EPRI have lower small-strain damping than that of ME. The modulus reduction and damping curves of Darendeli are used for cohesive soils and Menq are used for cohesionless soils.

The range of shear strain (γ) is extended from 0-1% to 0-10% in order to consider the effect of hysteretic damping, compared to the limited range of shear strain suggested by Park and Hashash (2005a). Thus, both small strain damping and hysteretic damping can be taken into account for nonlinear site response analysis.

Three sets of developed modulus reduction and damping curves are modified by the fitting procedures using the reduction factor (MRDF) proposed by Phillips and Hashash (2009) to match measured modulus reduction and damping curves over a wide range of shear strain simultaneously. Using MRDF fitting method, overestimation of hysteretic damping using Masing rules of ME and EPRI is reduced (Figure 3.16 (b) and Figure 3.17 (b)), and a reasonable match is obtained between developed dynamic soil properties before and after MRDF fitting method with relation to Darendel & Menq (Figure 3.18 (a) and (b)).

As shown in Table 3.6, the weight factors corresponding to ME, EPRI, and Darendeli & Menq curves, are selected based on engineering judgment, which is a commonly accepted way of accounting for epistemic uncertainty.

Table 3.1 Point source and finite fault models, calibrated to selected attenuation relationships, used in PSHA-NL(FF) to generate ground motions for smoothed sources and finite-fault sources.

Hashash et. al (2008)	Current study
Smoothed sources/Gridded sources (Point source models)	
Single corner model Toro et al. (1997) (0.286*w*) Frankel et al. (1996) (0.286*w*) Campbell (2003) (0.142*w*) *Double corner model* Atkinson and Boore (1995) (0.286*w*)	*Single-corner model* Frankel et al. (1996) (0.333*w*) *Hybrid model* Campbell (2003) (0.333*w*) Tavakoli and Pezeshk (2005) (0.333*w*)
Fault sources/Characteristic sources (Finite fault models)	
Toro et al. (1997) (0.25*w*) Frankel et al. (1996) (0.25*w*) Atkinson and Boore (1995) (0.25*w*) Campbell (2003) (0.125*w*) Somerville et al. (2001) (0.125*w*)	Toro et al. (1997) (0.25*w*) Atkinson and Boore (2006) (140 bar) (0.125*w*) Atkinson and Boore (2006) (200 bar) (0.125*w*) Silva et al. (2002) (0.25*w*) Somerville et al. (2001) (0.25*w*)

w is the weight which is the proportional of total number of generated ground-motion time histories.

Table 3.2 Selected locations at which simulations are made to develop UHRS and corresponding 2008 USGS spectral accelerations and NEHRP site coefficients.

Site no	Latitude	Longitude	S_s (g)	S_1 (g)	PGA (g)	F_a	F_v
1	34.70	-89.50	0.537	0.213	0.282	1.37	1.97
2	35.50	-88.60	0.655	0.247	0.350	1.28	1.91
3	35.50	-89.20	0.878	0.309	0.495	1.15	1.78
4	36.00	-90.90	0.967	0.337	0.557	1.13	1.73
5	36.20	-90.50	1.127	0.390	0.600	1.05	1.62
6	36.80	-88.80	1.311	0.452	0.606	1.00	1.55
7	36.18	-90.26	1.484	0.517	0.757	1.00	1.50
8	36.00	-89.60	2.572	0.966	1.683	1.00	1.50
9	34.00	-93.00	0.238	0.111	0.119	1.60	2.36

Table 3.3 PS models and revised parameters based on 2008 USGS attenuation relationships

Simulated Model	Type of point source model	β-shear wave velocity (km/s)	ρ-density (g/cm^3)	Q_s- quality factor	Stress drop (bar)	Geometric spreading
Frankel et al. (1996)	Single corner	3.8	2.8	$680f^{0.36}$	150	$D_g(R) = R^{-1.0} \quad if \quad R < 70km$ $D_g(R) = R^{0} \quad if \quad 70 < R < 130km$ $D_g(R) = R^{-1.0} \quad if \quad R > 130km$
Campbell (2003)	Single corner	3.6	2.8	$680f^{0.36}$	150	$D_g(R) = R^{-0.85} \quad if \quad R < 70km$ $D_g(R) = R^{0} \quad if \quad 70 < R < 130km$ $D_g(R) = R^{-0.5} \quad if \quad R > 130km$
Tavakoli and Pezeshk (2005)	Double corner	3.6	2.8	$680f^{0.36}$	150	$D_g(R) = R^{-0.78} \quad if \quad R < 70km$ $D_g(R) = R^{-0.2} \quad if \quad 70 < R < 130km$ $D_g(R) = R^{-1.0} \quad if \quad R > 130km$

Table 3.4 FF models and revised parameters based on 2008 USGS attenuation relationships

Simulated Model	β-shear wave velocity(km/s)	ρ-density (g/cm^3)	Q_s- quality factor	Stress drop (bar)	Geometric spreading
Toro et al. (1997)	3.8	2.8	$680f^{0.36}$	140	$D_g(R) = R^{-1} \quad if \quad R < 100km$ $D_g(R) = R^{-0.7} \quad if \quad R > 100km$
Atkinson and Boore (2006)	3.7	2.8	$893f^{0.32}$	140	$D_g(R) = R^{-1.25} \quad if \quad R < 70km$ $D_g(R) = R^{0.2} \quad if \quad 70 < R < 140km$ $D_g(R) = R^{-0.5} \quad if \quad R > 140km$
	3.7	2.8	$893f^{0.32}$	200	$D_g(R) = R^{-1.35} \quad if \quad R < 70km$ $D_g(R) = R^{0.2} \quad if \quad 70 < R < 140km$ $D_g(R) = R^{-0.5} \quad if \quad R > 140km$
Silva et al. (2002)	3.8	2.8	$351f^{0.84}$	120	$D_g(R) = R^{-0.95} \quad if \quad R \leq 80km$ $D_g(R) = R^{-0.8} \quad if \quad R > 80km$
Somerville et al. (2001)	3.8	2.8	$680f^{0.36}$	140	$D_g(R) = R^{-0.95} \quad if \quad R < 70km$ $D_g(R) = R^{0.2} \quad if \quad 70 < R < 130km$ $D_g(R) = R^{-0.9} \quad if \quad R > 130km$

Table 3.5 Average 30m shear wave velocities (V_{s30}) corresponding to site classes

Site	V_{s30}		
	NEHRP site-class C	NEHRP site-class D	NEHRP site-class E
Upland	533	275	166
Lowland	482	234	141

Table 3.6 Weights assigned to dyamic soil properties for each profile

Shear-Wave Velocity Profiles	Dynamic Soil Properties	Weight (Number of Simulations)
Uplands	ME	0.3 (9)
	EPRI	0.3 (9)
	Darendeli & Menq	0.4 (12)
Lowlands	ME	0.3 (9)
	EPRI	0.3 (9)
	Darendeli & Menq	0.4 (12)

Table 3.7 Matrix for PSHA-NL(FF)(2011)

NEHRP site-class	Shear-Wave Velocity Profiles	Sites	Soil column depth (m)
C, D, E	Uplands	1,2,3,4,5,6,7,8,9	30, 100, 200, 300, 500, 1000
	Lowlands		

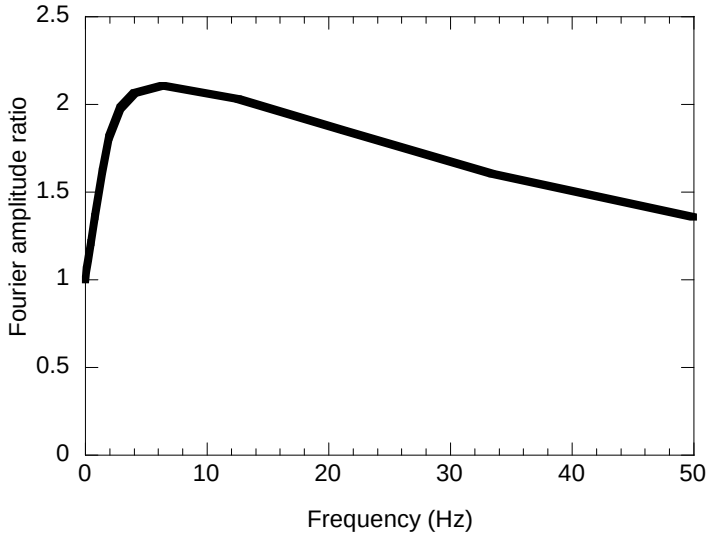

Figure 3.1 Transfer function to convert a motion from site class A to site class B (B/C boundary)

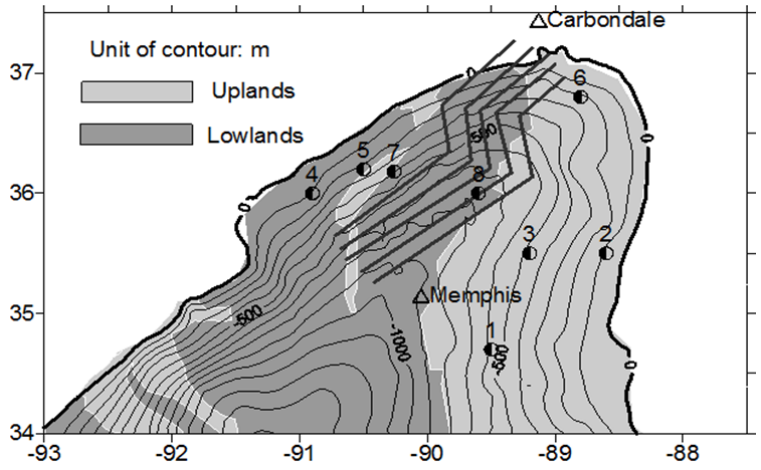

Figure 3.2 Fictitious faults in NMSZ and selected locations for PSHA-NL analysis

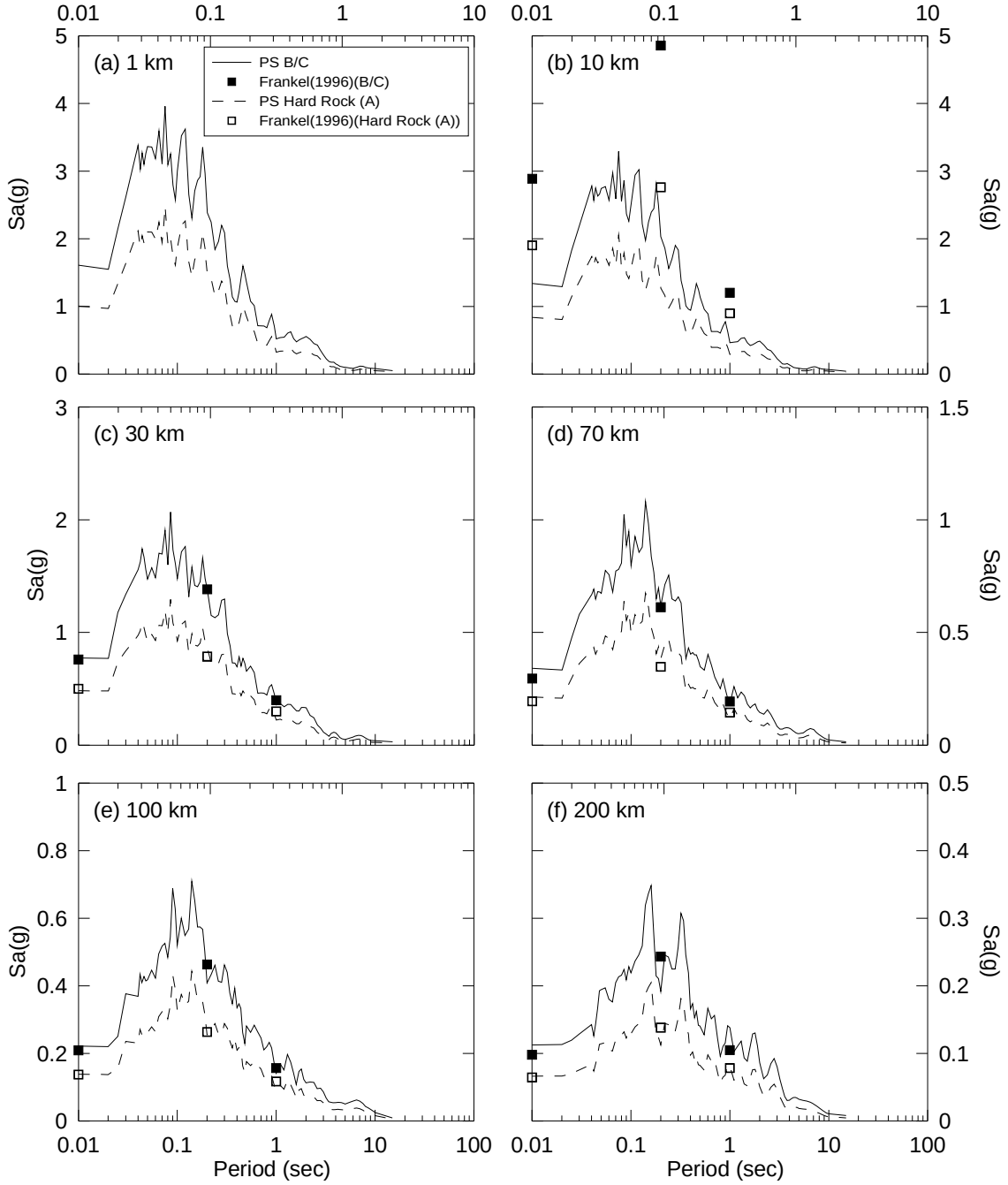

Figure 3.3 Comparison of calibrated PS simulation (SMSIM) and Frankel (1996) attenuation relationship at selected epicentral distances for NEHRP B/C and hard rock boundary.

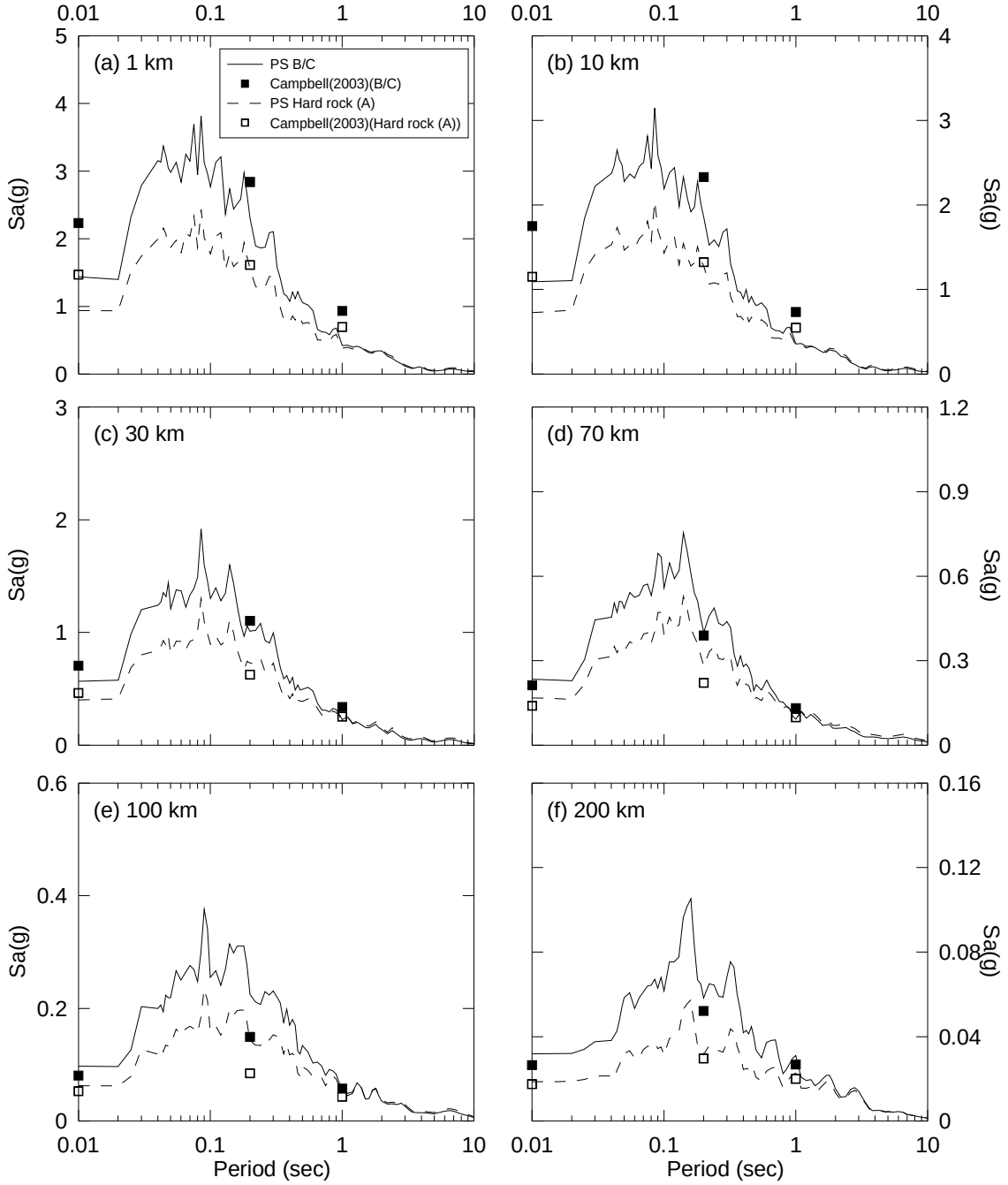

Figure 3.4 Comparison of calibrated PS simulation (SMSIM) and Campbell (2003) attenuation relationship at selected epicentral distances for NEHRP B/C and hard rock boundary.

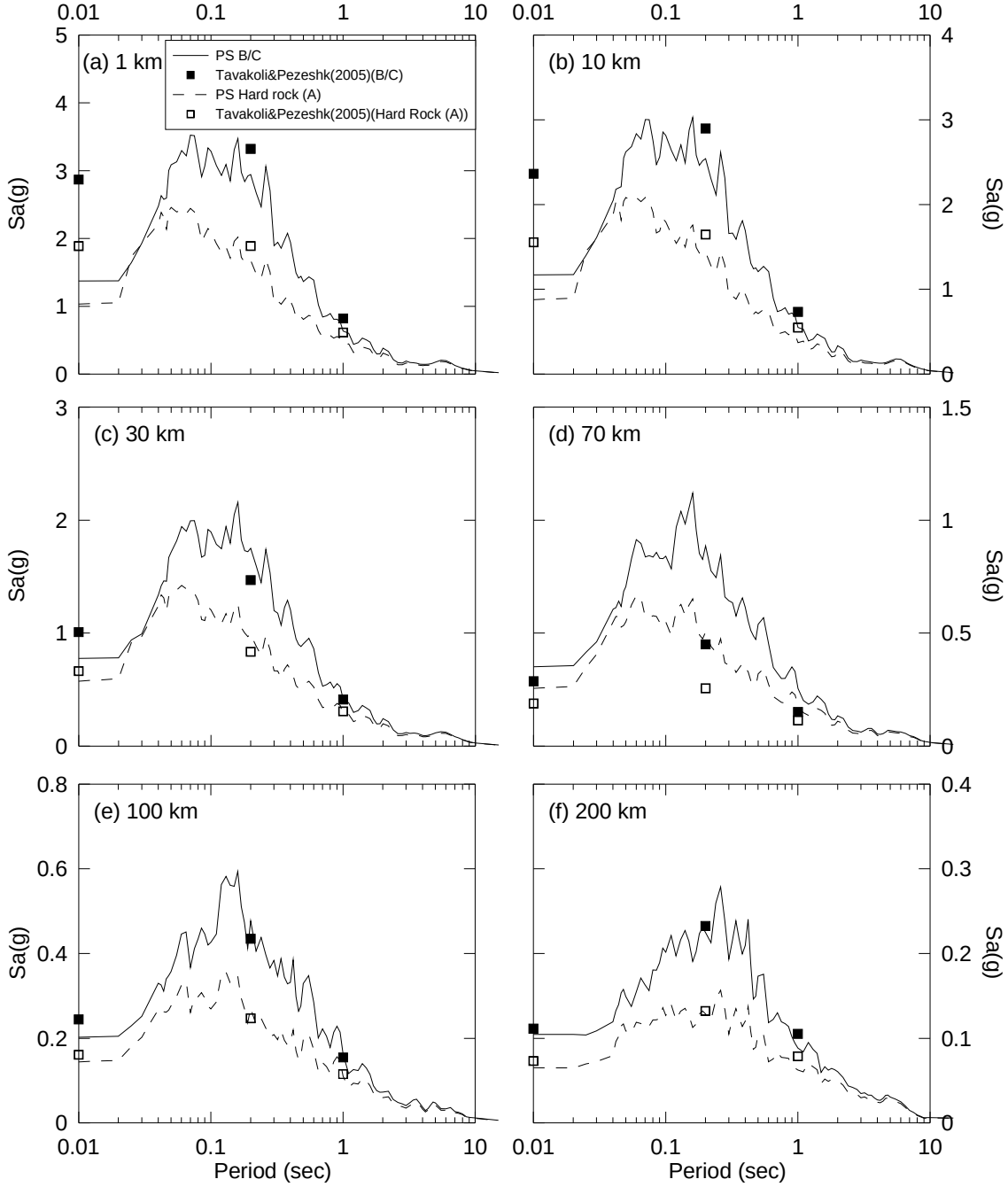

Figure 3.5 Comparison of calibrated PS simulation (SMSIM) and Tavakoli & Pezeshk (2003) attenuation relationship at selected epicentral distances for NEHRP B/C and hard rock boundary.

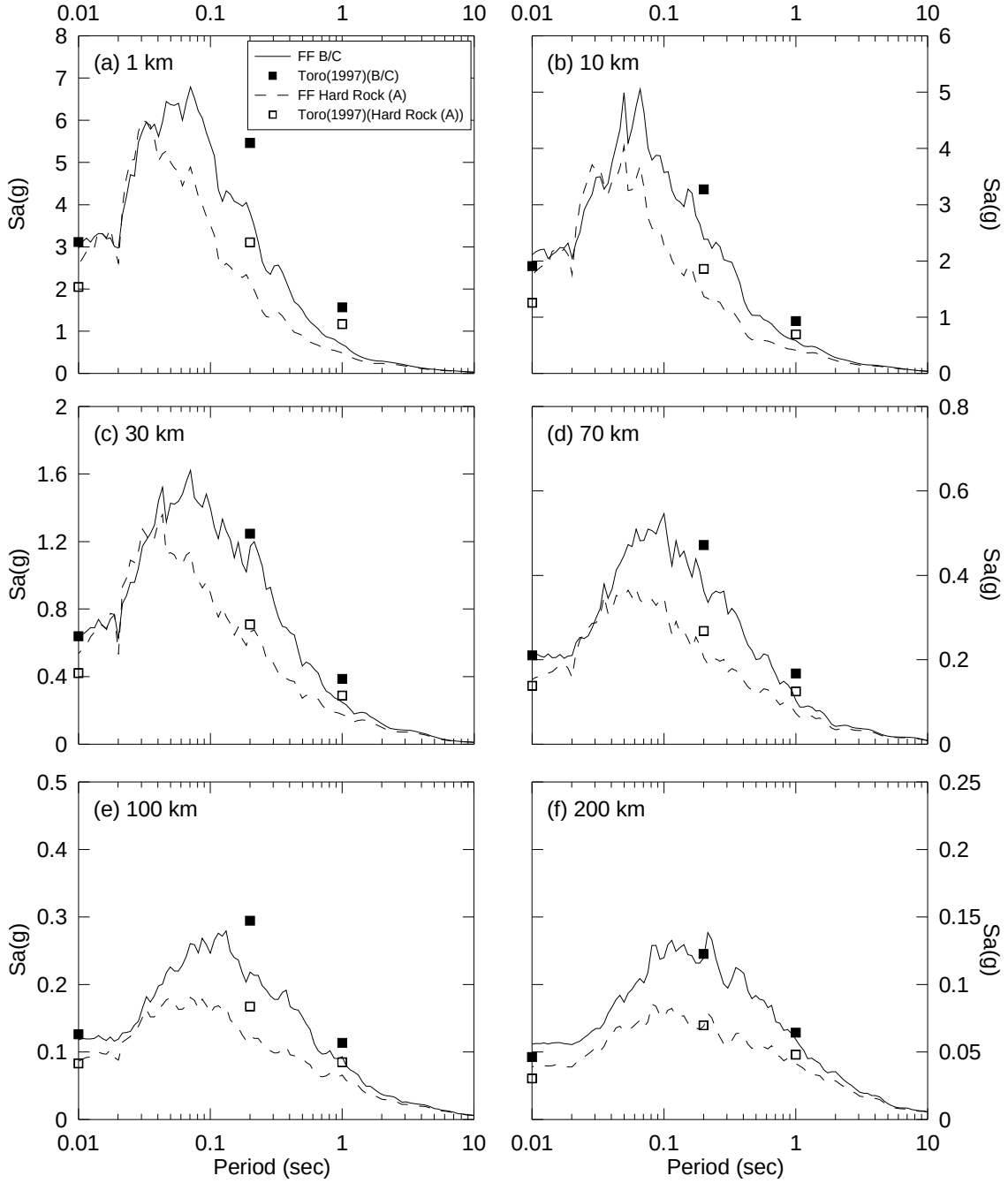

Figure 3.6 Comparison of calibrated FF simulation (EXSIM) and Toro (1997) attenuation relationship at selected epicentral distances for NEHRP B/C and hard rock boundary.

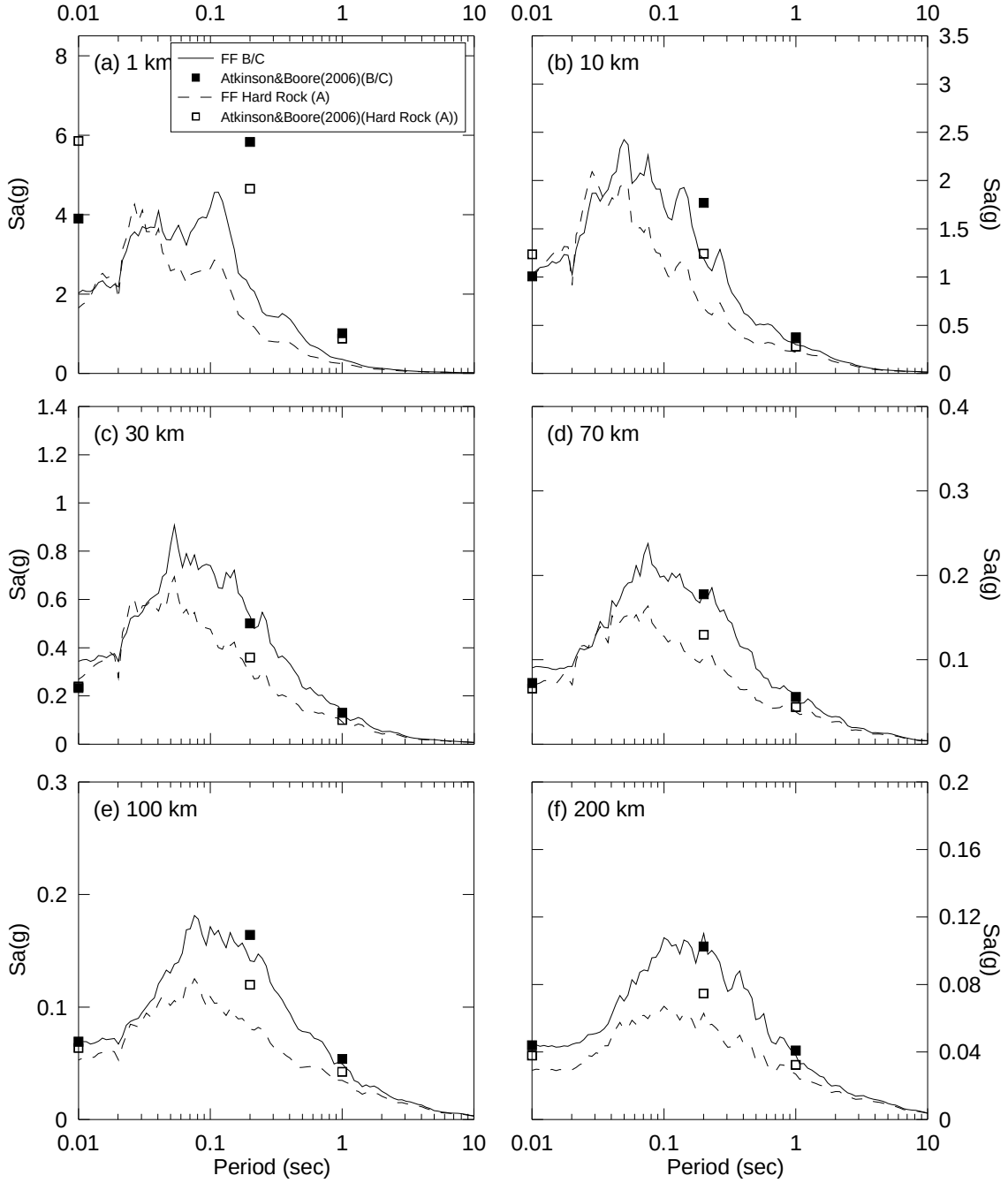

Figure 3.7 Comparison of calibrated FF simulation (EXSIM) and Atkinson & Boore (2006) with stress drop 140 attenuation relationship at selected epicentral distances for NEHRP B/C and hard rock boundary.

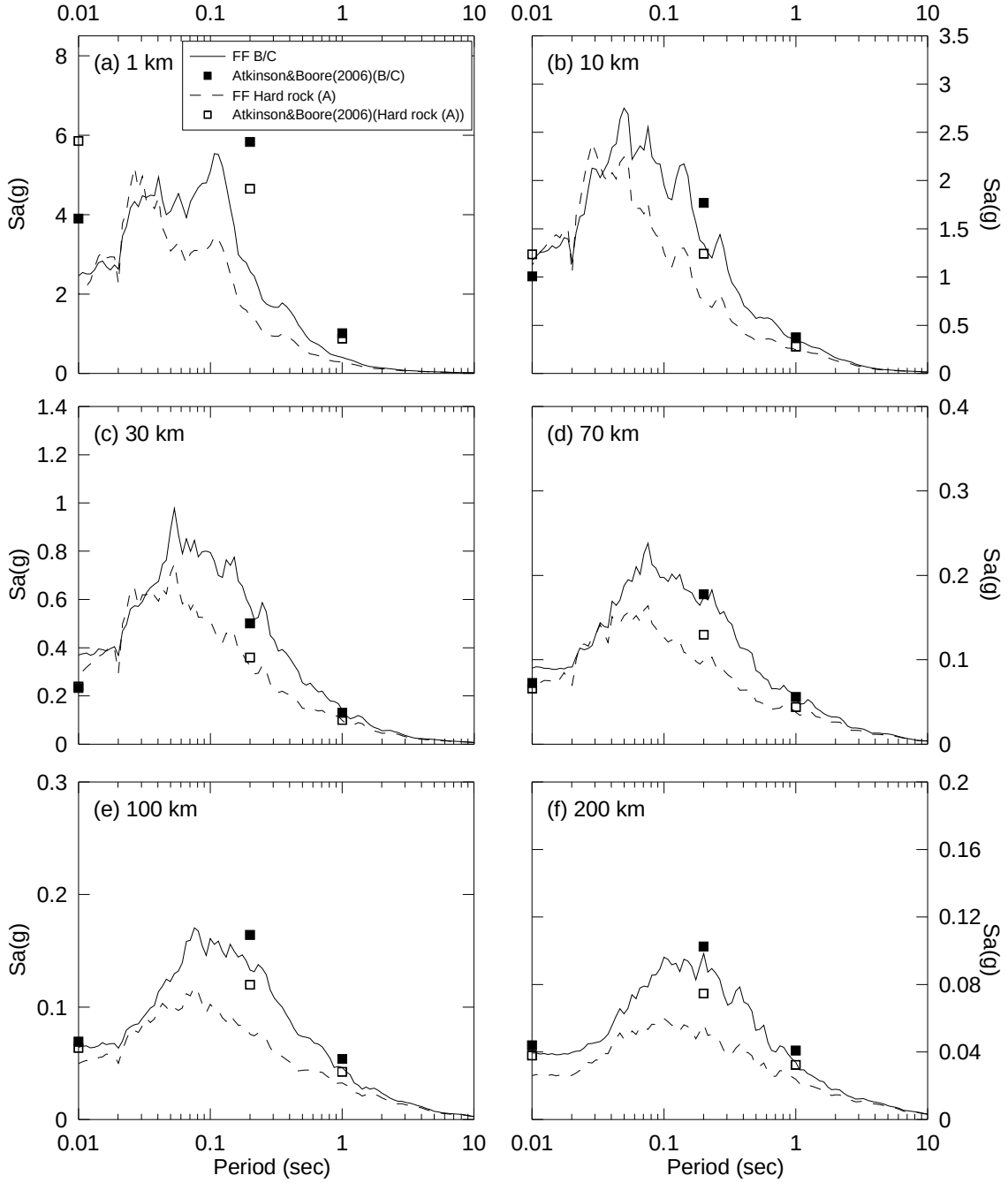

Figure 3.8 Comparison of calibrated FF simulation (EXSIM) and Atkinson & Boore (2006) with stress drop 200 attenuation relationship at selected epicentral distances for NEHRP B/C and hard rock boundary.

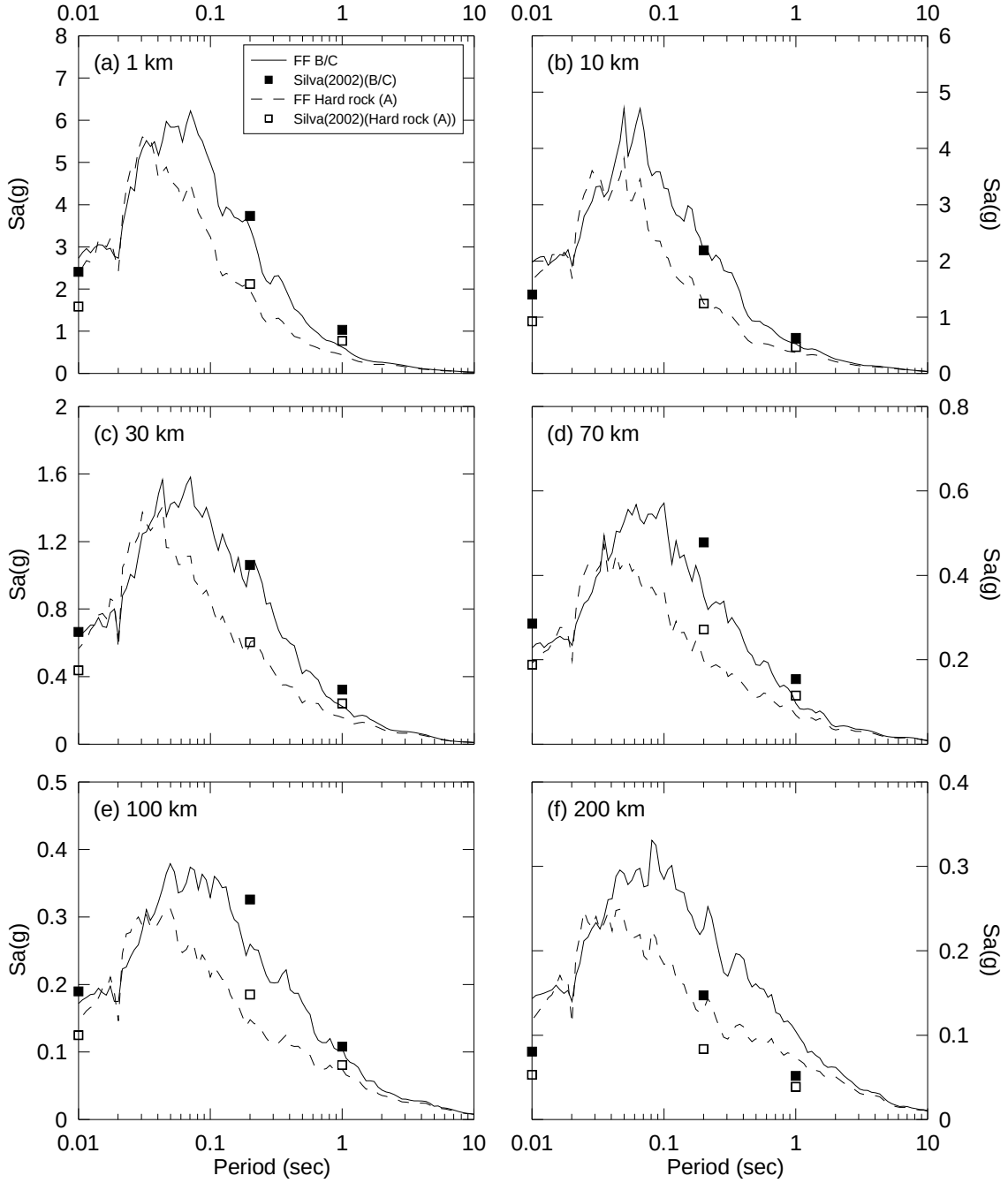

Figure 3.9 Comparison of calibrated FF simulation (EXSIM) and Silva (2002) attenuation relationship at selected epicentral distances for NEHRP B/C and hard rock boundary.

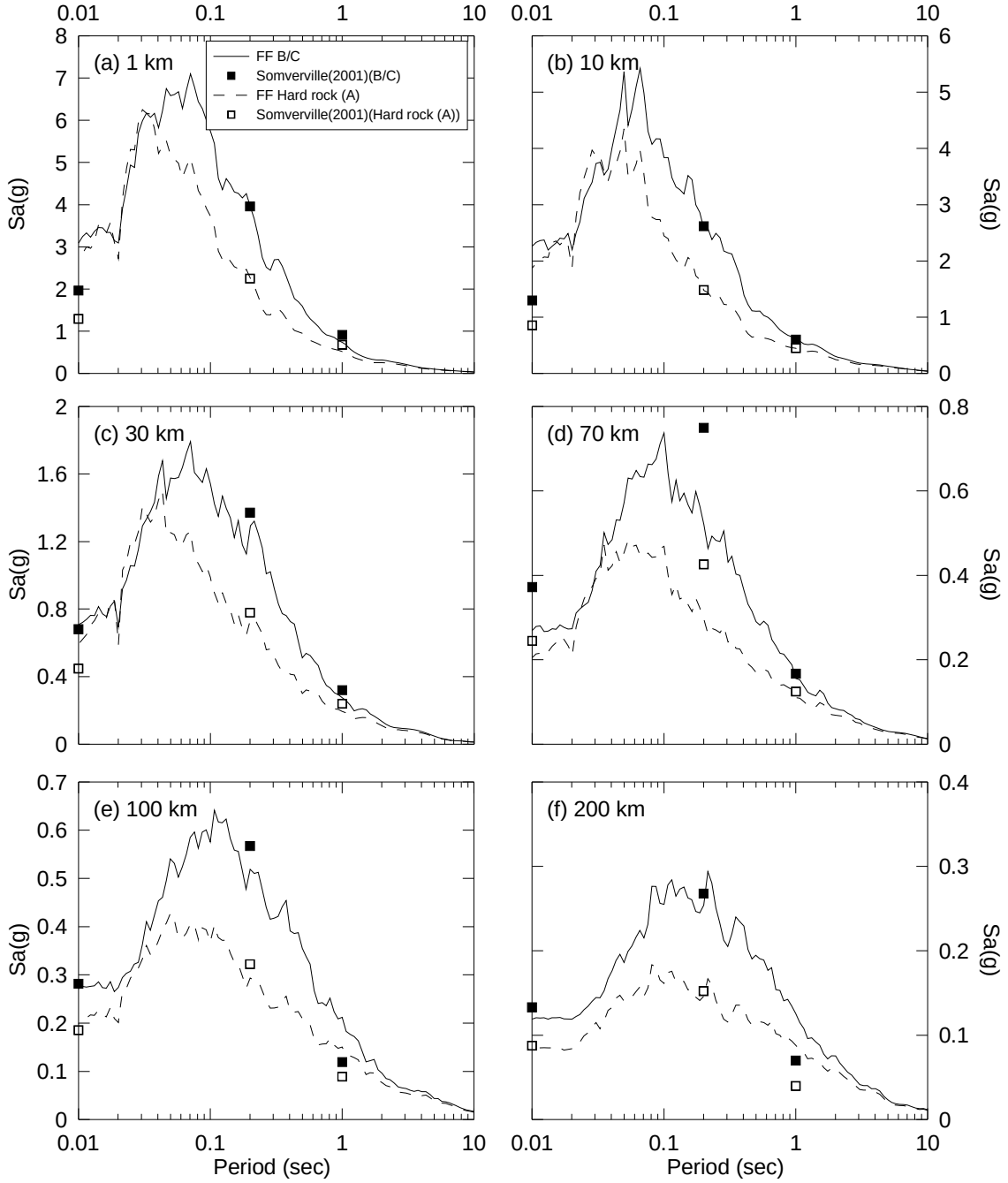

Figure 3.10 Comparison of calibrated FF simulation (EXSIM) and Somerville (2001) attenuation relationship at selected epicentral distances for NEHRP B/C and hard rock boundary.

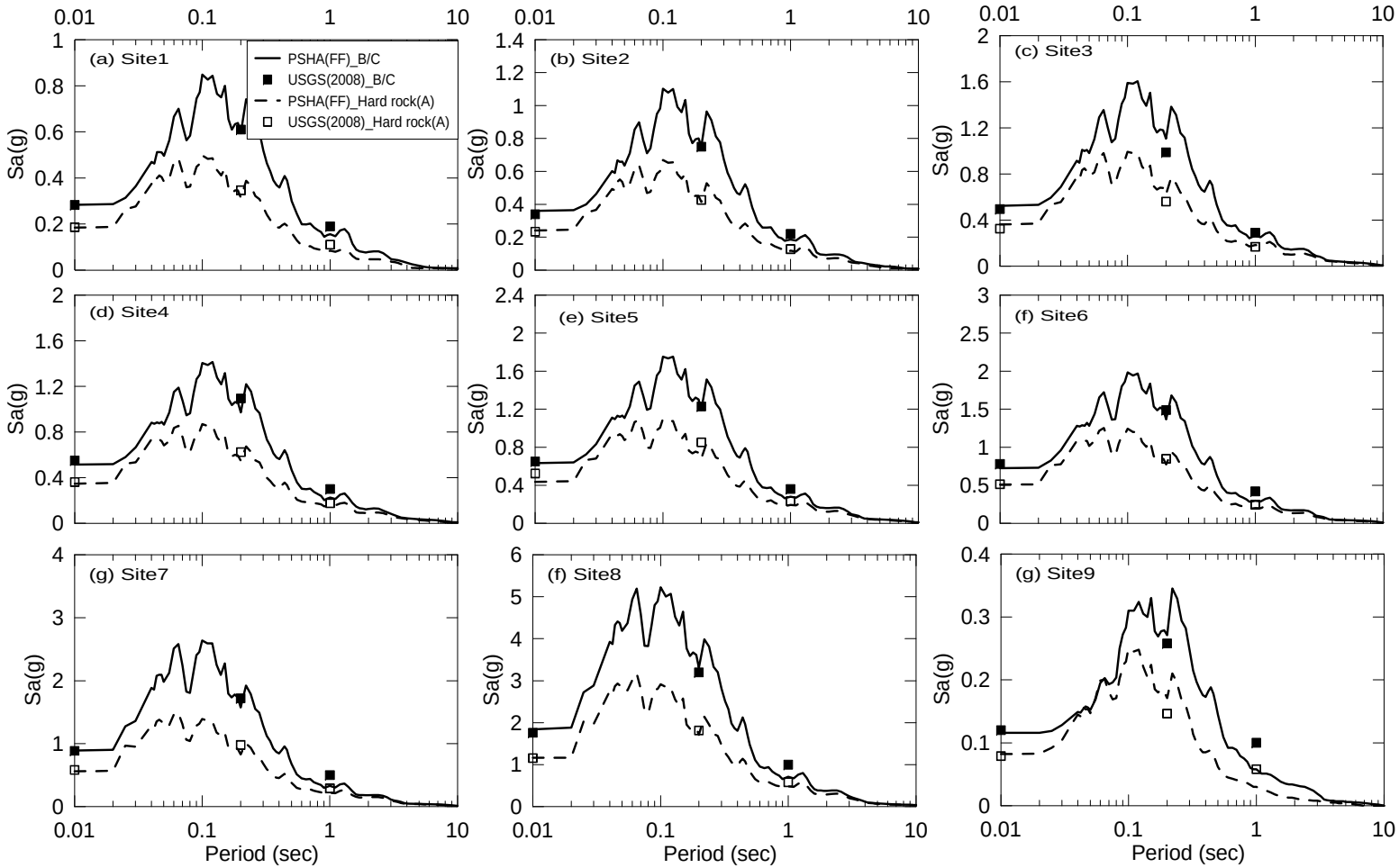

Figure 3.11 Comparison of simulated UHRS (PSHA-NL(FF)(2011)) and spectral acceleration taken from 2008 USGS hazard maps at PGA, 0.2, and 1 sec.

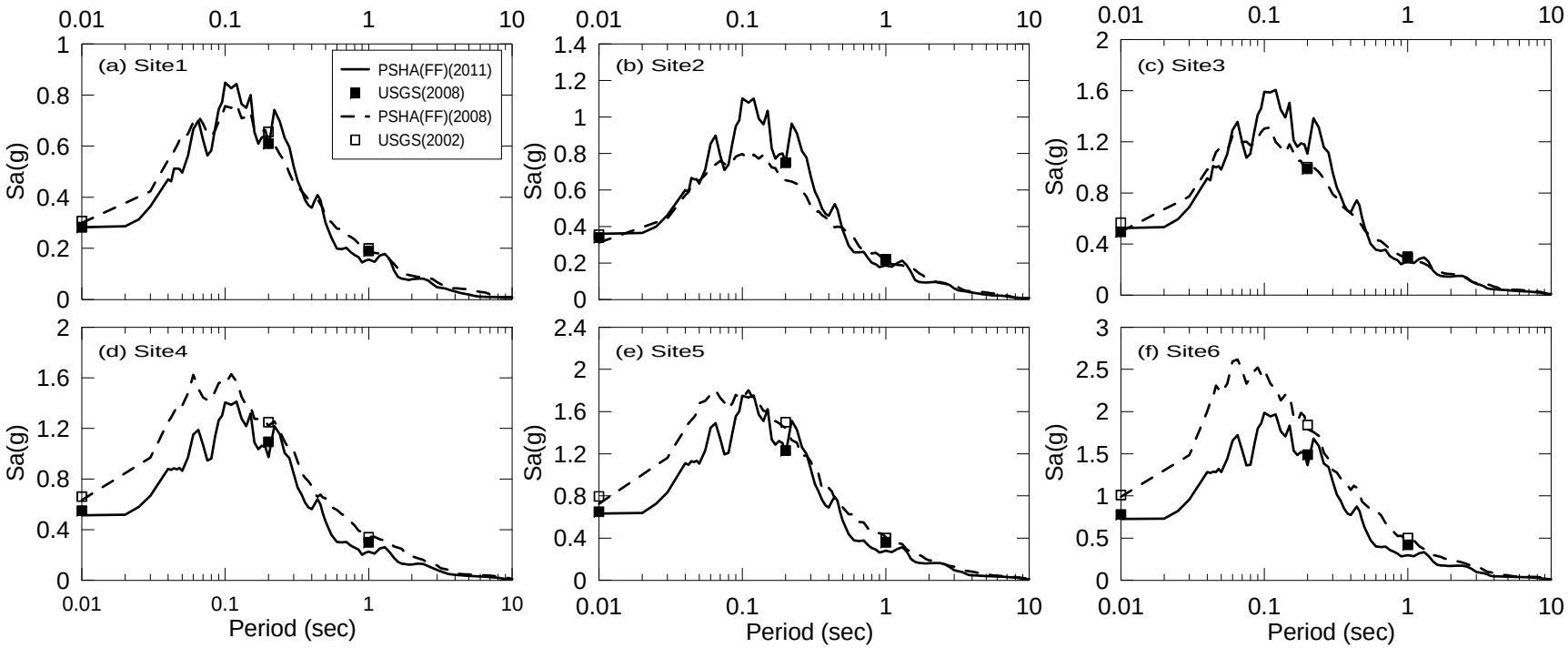

Figure 3.12 Comparison of simulated UHRS (PSHA-NL(FF)(2011) and PSHA-NL(FF)(2008)) and PGA, 0.2 and 1 sec spectral acceleration taken from 2002 and 2008 USGS hazard maps at NEHRP B/C boundary

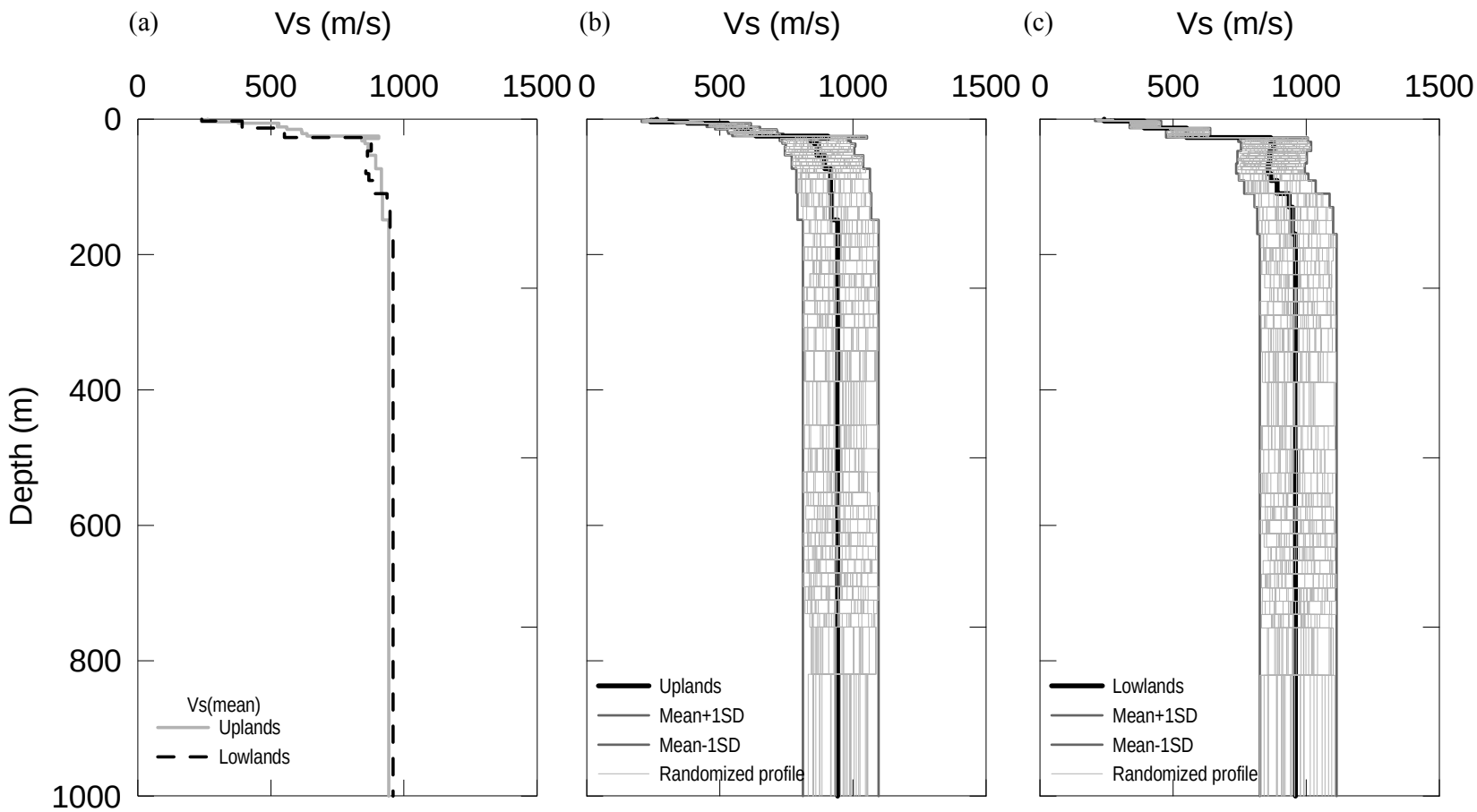

Figure 3.13 Shear wave velocity profiles for upland and lowland at site class C (a) mean values (b) 30 randomized profiles at upland (c) 30 randomized profiles at lowland

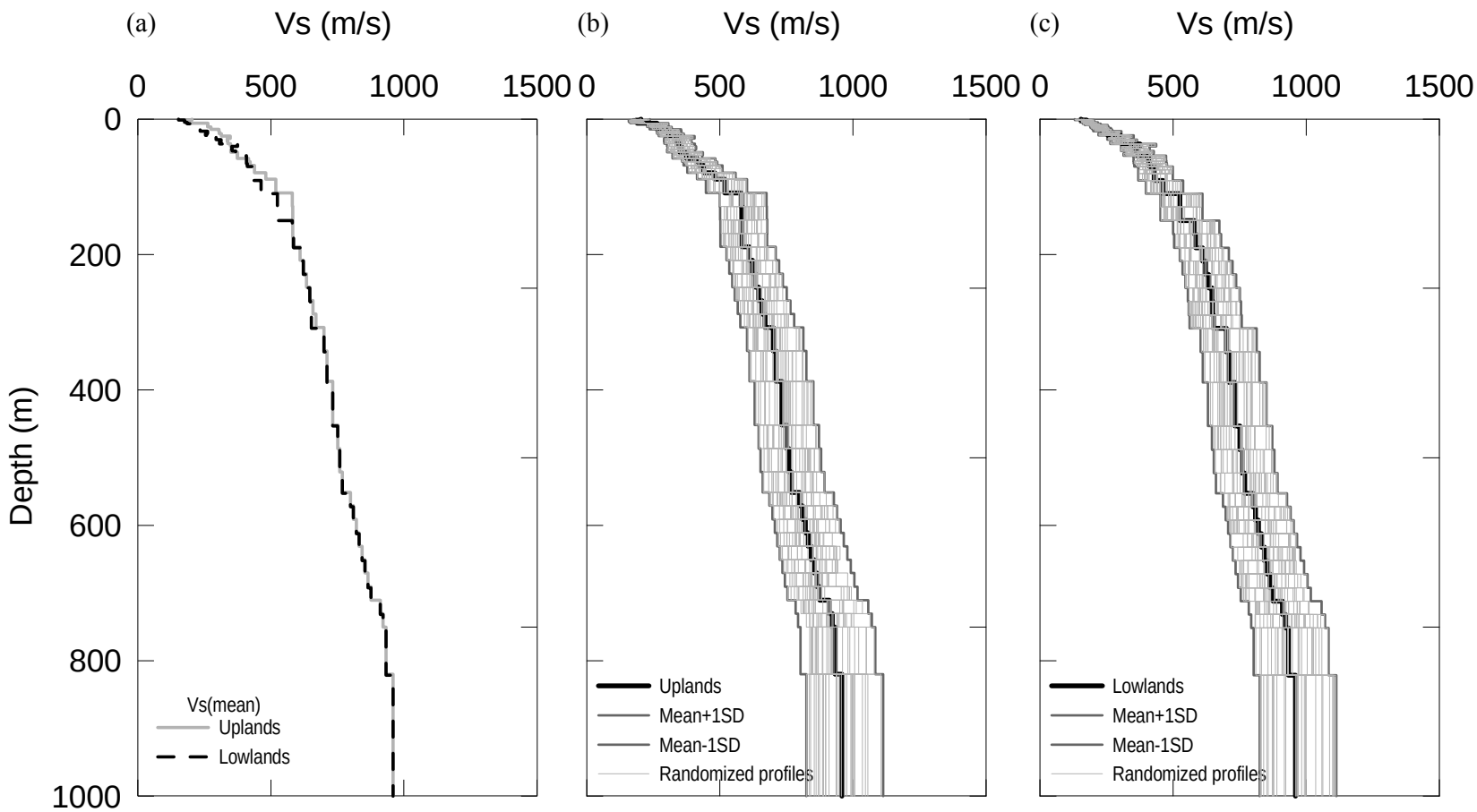

Figure 3.14 Shear wave velocity profiles for upland and lowland at site class D (a) mean values (b) 30 randomized profiles at upland (c) 30 randomized profiles at lowland

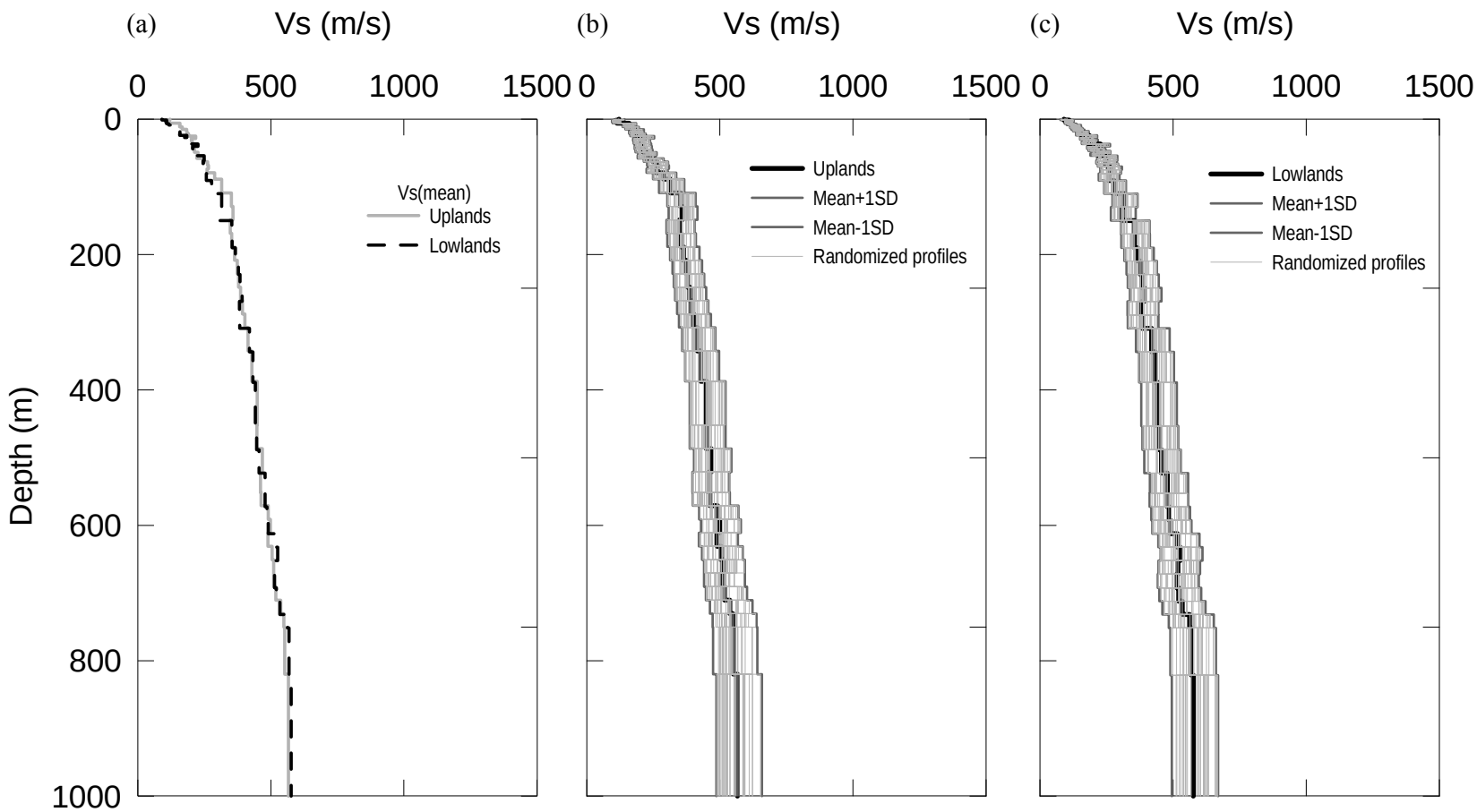

Figure 3.15 Shear wave velocity profiles for upland and lowland at site class E (a) mean values (b) 30 randomized profiles at upland (c) 30 randomized profiles at lowland

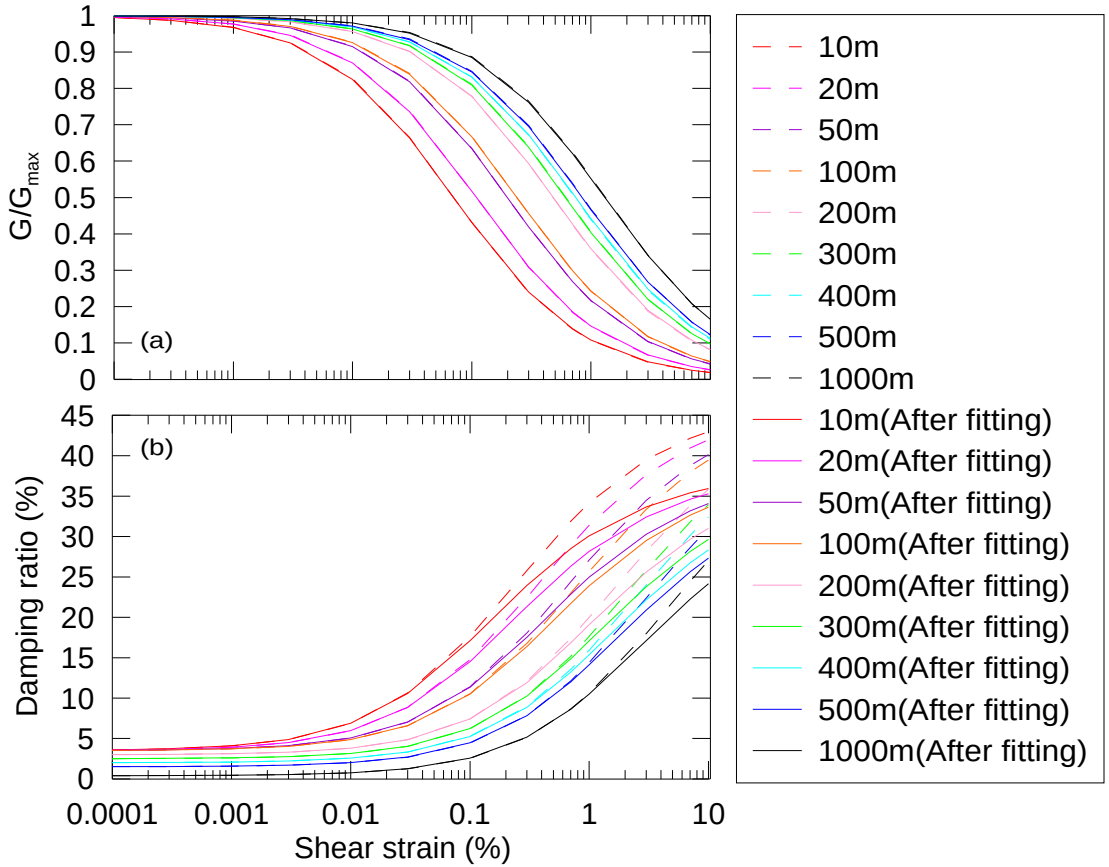

Figure 3.16 Dynamic soil properties of ME (a) Modulus reduction curves and (b) damping curves

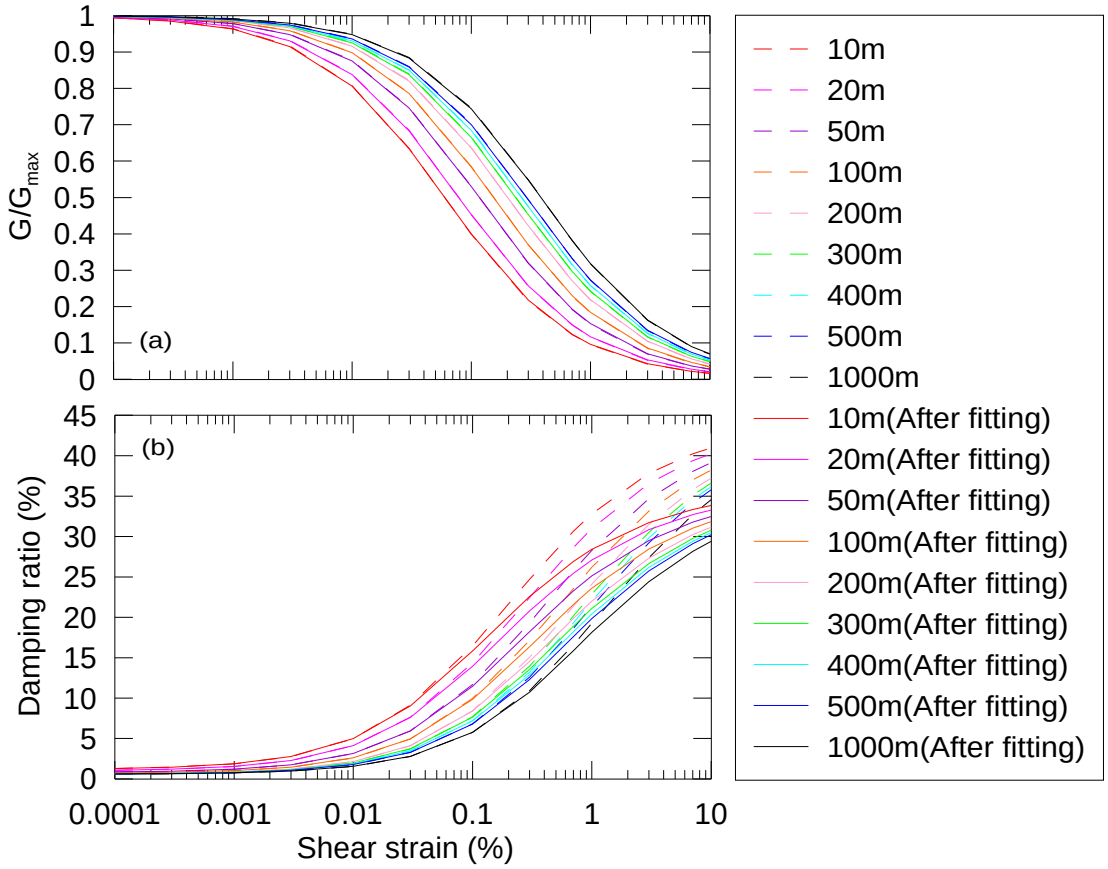

Figure 3.17 Dynamic soil properties of EPRI (a) Modulus reduction curves and (b) damping curves

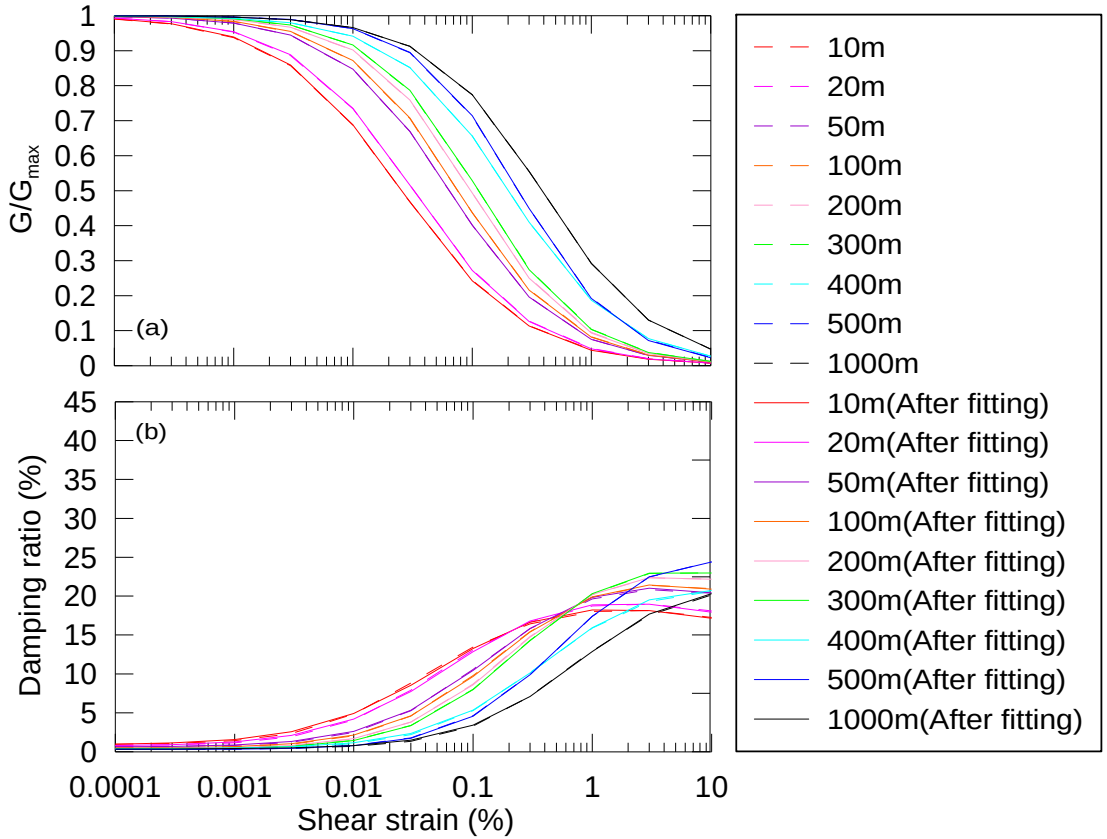

Figure 3.18 Dynamic soil properties of Darendeli&Menq (a) Modulus reduction curves and (b) damping curves

4. Evaluation of developed UHRS and site coefficients

The generated ground motions at NEHRP site-class A, hard rock, are propagated through the thickness of soil-column profiles at nine sites, which are considered to be 30, 100, 200, 300, 500, and 1000m thick to represent the effect of deep soil deposits at each depth. Romero and Rix (2001) assumed that the shear-wave velocity of Paleozoic rock located at the bottom of the soil-column profiles is 3000 m/sec. The seismic-wave propagation is simulated via the 1-D site response program, DEEPSOIL. The equivalent-linear analysis procedure is applied to the smoothed seismic sources and the nonlinear time domain analysis procedure is used for the finite-fault sources.

3.1 UHRS and site coefficients for 30m depth profiles

The generated ground motions at hard rock are propagated to the ground surface through a 30m deep soil-column used in NEHRP site classification within the PSHA-NL procedure described earlier for both = upland and lowland conditions corresponding to NEHRP site-classes C, D, and E. Figure 4.1 to Figure 4.3 show the comparison of the 2% in 50 yr UHRS for the 30m soil column and NEHRP design spectra, developed by using S_s and S_l of each of the nine sites.

The UHRS at a 30m depth for both the upland and the lowland at all sites generally match well with the developed site class D NEHRP design response spectra, as shown in Figure 4.1.

The UHRS at 30m depth for both the upland and the lowland at all sites are generally higher at short periods and lower at long periods relative to site class C NEHRP design spectra, as shown in Figure 4.2.

The UHRS at 30m depth for both the upland and the lowland at all sites are generally lower than site class E NEHRP design spectra, as shown in Figure 4.3.

Figure 4.4 shows the comparison of site coefficients (F_a, F_v) obtained from PSHA-

NL(FF)(2011) analyses and empirical studies, suggested by Power et al. (2004), for 30m thick soil column. Power et al. (2004) compared site coefficients which are in terms of the site ground motion spectral amplification for NEHRP site classes C, D, and E. In this figure, the relationship of site coefficients versus PGA is presented for short and long periods where F_a corresponds to the short-period amplification site coefficient, and F_v corresponds to the long period amplification site coefficient. This figure shows wide ranges of site coefficients provided by empirical studies, and moderately consistent trends of nonlinearity. The nonlinearity in site coefficients for site classes C, D, and E, increases as the soil becomes softer. The site coefficients calculated from PSHA-NL(FF)(2011) show the same trends with respect to the nonlinearity according to site classes. The calculated F_a for the upland and the lowland are located in the upper part within the range of empirical studies for site class C, in the middle part within the range of empirical studies for site class D, and in the lower part within the range of empirical studies for site class E. The developed F_v for both the upland and the lowland are in the lower part of the range of these studies regardless of site classes.

3.2 Depth-dependent site coefficients

PSHA-NL(FF)(2011) analyses are performed at all nine sites that cover the range of spectral acceleration levels in NEHRP factors and also in six soil-columns corresponding to NEHRP site-class C, D, and E to develop depth-dependent site coefficients in terms of different site-classes. A total of 324,000 site response analyses are performed at each site (9000 simulations for each one of the six depths and two soil profiles, corresponding to each NEHRP site-class, Table 3.7). The UHRS are estimated using PSHA-NL(FF)(2011) analyses and NEHRP design response spectra are developed using NEHRP style site coefficients corresponding to different levels of ground motions.

Figure 4.5 to Figure 4.7 compare the NEHRP-style depth-dependent site coefficients obtained

from PSHA-NL(FF)(2011) with NEHRP Provisions regardless of the dependency on embayment thickness, in terms of NEHRP site class C, D, and E in which previously reported PSHA-NL(FF)(2008) coefficients for site class D are added for the comparison. The proposed site coefficients are summarized in Table 4.1 to Table 4.6. For the upland and the lowland corresponding to NEHRP site-classes C, D, and E, the developed site coefficients (F_a) shows more dependence on the embayment thickness and greater of reduction as the soil becomes stiffer. The developed site coefficients (F_v) shows more dependence on the embayment thickness as the soil becomes softer, and has a more noticeable rate of increase up to 300m thickness. The calculated site coefficients (F_a, F_v) for the upland and the lowland are lower at short periods and greater at long periods than the NEHRP site coefficients, with the exception of the F_a of site class C shown in Figure 4.5. Figure 4.6 shows that the updated site coefficient (F_a) at short periods for the upland and the lowland conditions from PSHA-NL(FF)(2011) become greater at $S_s \leq 0.75$ and slightly lower at $S_s \geq 1.0$ than those from PSHA-NL(FF)(2008). In long periods, the updated site coefficient (Fv) for the upland and the lowland from PSHA-NL(FF)(2011) become much greater at $S_l \leq 0.2$ and slightly lower or similar at $S_l \geq 0.3$ than those from PSHA-NL(FF)(2008).

Figure 4.8 to Figure 4.10 compare the depth-dependent site coefficients at six soil-columns (30, 100, 200, 300, 500, 1000m) for the upland and the lowland obtained from PSHA-NL(FF)(2011) with other studies corresponding to site classes C, D, and E. The depth-dependent site coefficients generally cover the full range from empirical studies and extend beyond the reported ranges for site classes D and E. The plotted site coefficients clearly demonstrate the dependency on thickness on the embayment.

Table 4.1 Recommended site coefficients at site class C, Fa corresponding to soil column thickness and 0.2 sec period spectral acceleration based on 2008 USGS hazard map

Thickness (m)	S_s=0.25g			S_s=0.50g			S_s=0.75g			S_s=1.0g			S_s≥1.25g		
	NEHRP	Upland	Lowland	NEHRP	Upland	Lowland	NEHRP	Upland	Lowland	NEHRP	Upland	Lowland	NEHRP	Upland	Lowland
30	1.2	1.80	1.72	1.2	1.75	1.68	1.1	1.66	1.62	1	1.57	1.49	1	1.54	1.47
100	1.2	1.73	1.69	1.2	1.68	1.65	1.1	1.59	1.57	1	1.51	1.46	1	1.48	1.43
200	1.2	1.67	1.63	1.2	1.61	1.59	1.1	1.53	1.51	1	1.46	1.40	1	1.42	1.37
300	1.2	1.62	1.58	1.2	1.56	1.53	1.1	1.48	1.45	1	1.40	1.34	1	1.37	1.31
500	1.2	1.54	1.52	1.2	1.49	1.46	1.1	1.40	1.35	1	1.31	1.24	1	1.28	1.21
1000	1.2	1.39	1.38	1.2	1.32	1.29	1.1	1.24	1.17	1	1.14	1.07	1	1.11	1.05

Table 4.2 Recommended site coefficients at site class C, Fv corresponding to soil column thickness and 1.0 sec period spectral accelelration bsed on 2008 USGS hazard map

Thickness (m)	S_l=0.10g			S_l=0.20g			S_l=0.30g			S_l=0.40g			S_l≥0.50g		
	NEHRP	Upland	Lowland	NEHRP	Upland	Lowland	NEHRP	Upland	Lowland	NEHRP	Upland	Lowland	NEHRP	Upland	Lowland
30	1.7	1.42	1.40	1.6	1.40	1.39	1.5	1.36	1.38	1.4	1.35	1.29	1.3	1.34	1.24
100	1.7	1.59	1.76	1.6	1.53	1.73	1.5	1.48	1.71	1.4	1.44	1.55	1.3	1.41	1.51
200	1.7	1.82	2.00	1.6	1.72	1.91	1.5	1.61	1.80	1.4	1.55	1.66	1.3	1.54	1.65
300	1.7	1.98	2.22	1.6	1.83	2.03	1.5	1.67	1.81	1.4	1.55	1.66	1.3	1.54	1.65
500	1.7	1.98	2.22	1.6	1.83	2.03	1.5	1.67	1.81	1.4	1.55	1.66	1.3	1.54	1.65
1000	1.7	1.98	2.22	1.6	1.83	2.03	1.5	1.67	1.81	1.4	1.55	1.66	1.3	1.54	1.65

Table 4.3 Recommended site coefficients at site class D, F_a corresponding to soil column thickness and 0.2 sec period spectral acceleration based on 2008 USGS hazard map

Thickness (m)	S_s=0.25g			S_s=0.50g			S_s=0.75g			S_s=1.0g			S_s≥1.25g		
	NEHRP	Upland	Lowland	NEHRP	Upland	Lowland	NEHRP	Upland	Lowland	NEHRP	Upland	Lowland	NEHRP	Upland	Lowland
30	1.6	1.65	1.45	1.4	1.48	1.34	1.2	1.21	1.07	1.1	1.06	0.94	1.0	0.97	0.84
100	1.6	1.54	1.35	1.4	1.42	1.24	1.2	1.14	0.97	1.1	1.00	0.84	1.0	0.91	0.75
200	1.6	1.49	1.28	1.4	1.39	1.19	1.2	1.12	0.92	1.1	0.98	0.79	1.0	0.88	0.69
300	1.6	1.48	1.25	1.4	1.37	1.14	1.2	1.09	0.87	1.1	0.96	0.75	1.0	0.86	0.66
500	1.6	1.46	1.20	1.4	1.33	1.09	1.2	1.05	0.82	1.1	0.92	0.70	1.0	0.83	0.64
1000	1.6	1.41	1.15	1.4	1.27	1.04	1.2	0.97	0.77	1.1	0.84	0.66	1.0	0.80	0.62

Table 4.4 Recommended site coefficients at site class D, F_v corresponding to soil column thickness and 1.0 sec period spectral acceleration based on 2008 USGS hazard map

Thickness (m)	S_l=0.10g			S_l=0.20g			S_l=0.30g			S_l=0.40g			S_l≥0.50g		
	NEHRP	Upland	Lowland	NEHRP	Upland	Lowland	NEHRP	Upland	Lowland	NEHRP	Upland	Lowland	NEHRP	Upland	Lowland
30	2.4	2.20	2.3	2.0	1.87	1.93	1.8	1.64	1.63	1.6	1.45	1.38	1.5	1.34	1.24
100	2.4	3.18	3.12	2.0	2.59	2.58	1.8	2.17	2.33	1.6	1.81	1.86	1.5	1.61	1.60
200	2.4	3.60	3.52	2.0	3.08	3.11	1.8	2.56	2.66	1.6	2.19	2.07	1.5	1.94	1.77
300	2.4	3.78	3.76	2.0	3.29	3.36	1.8	2.73	2.85	1.6	2.29	2.15	1.5	2.02	1.83
500	2.4	3.81	3.79	2.0	3.32	3.39	1.8	2.76	2.88	1.6	2.32	2.18	1.5	2.05	1.86
1000	2.4	3.83	3.81	2.0	3.34	3.41	1.8	2.78	2.90	1.6	2.34	2.20	1.5	2.07	1.88

Table 4.5 Recommended site coefficients at site class E, F_a corresponding to soil column thickness and 0.2 sec period spectral acceleration based on 2008 USGS hazard map

Thickness (m)	S_s=0.25g			S_s=0.50g			S_s=0.75g			S_s=1.0g			S_s≥1.25g		
	NEHRP	Upland	Lowland	NEHRP	Upland	Lowland	NEHRP	Upland	Lowland	NEHRP	Upland	Lowland	NEHRP	Upland	Lowland
30	2.5	1.62	1.46	1.7	1.10	0.99	1.2	0.92	0.87	0.9	0.79	0.74	0.9	0.69	0.64
100	2.5	1.56	1.44	1.7	1.05	0.95	1.2	0.87	0.81	0.9	0.75	0.69	0.9	0.66	0.58
200	2.5	1.52	1.44	1.7	1.03	0.95	1.2	0.87	0.81	0.9	0.75	0.69	0.9	0.66	0.58
300	2.5	1.48	1.42	1.7	1.03	0.95	1.2	0.86	0.81	0.9	0.75	0.69	0.9	0.66	0.58
500	2.5	1.44	1.40	1.7	1.00	0.95	1.2	0.83	0.81	0.9	0.72	0.68	0.9	0.64	0.58
1000	2.5	1.38	1.34	1.7	0.94	0.91	1.2	0.79	0.76	0.9	0.69	0.63	0.9	0.62	0.58

Table 4.6 Recommended site coefficients at site class E, F_v corresponding to soil column thickness and 1.0 sec period spectral acceleration based on 2008 USGS hazard map

Thickness (m)	S_l=0.10g			S_l=0.20g			S_l=0.30g			S_l=0.40g			S_l≥0.50g		
	NEHRP	Upland	Lowland	NEHRP	Upland	Lowland	NEHRP	Upland	Lowland	NEHRP	Upland	Lowland	NEHRP	Upland	Lowland
30	3.5	3.00	3.06	3.2	2.58	2.36	2.8	2.15	1.78	2.4	1.85	1.33	2.4	1.64	1.08
100	3.5	3.90	4.4	3.2	3.38	3.48	2.8	2.58	2.77	2.4	2.27	2.26	2.4	1.95	1.82
200	3.5	4.90	4.8	3.2	4.06	3.74	2.8	3.14	3.17	2.4	2.82	2.63	2.4	2.32	2.13
300	3.5	5.26	5.06	3.2	4.11	3.93	2.8	3.14	3.35	2.4	2.82	2.68	2.4	2.42	2.33
500	3.5	5.26	5.5	3.2	4.21	4.40	2.8	3.14	3.48	2.4	2.84	2.83	2.4	2.45	2.54
1000	3.5	5.26	5.5	3.2	4.21	4.52	2.8	3.14	3.65	2.4	2.84	2.98	2.4	2.47	2.65

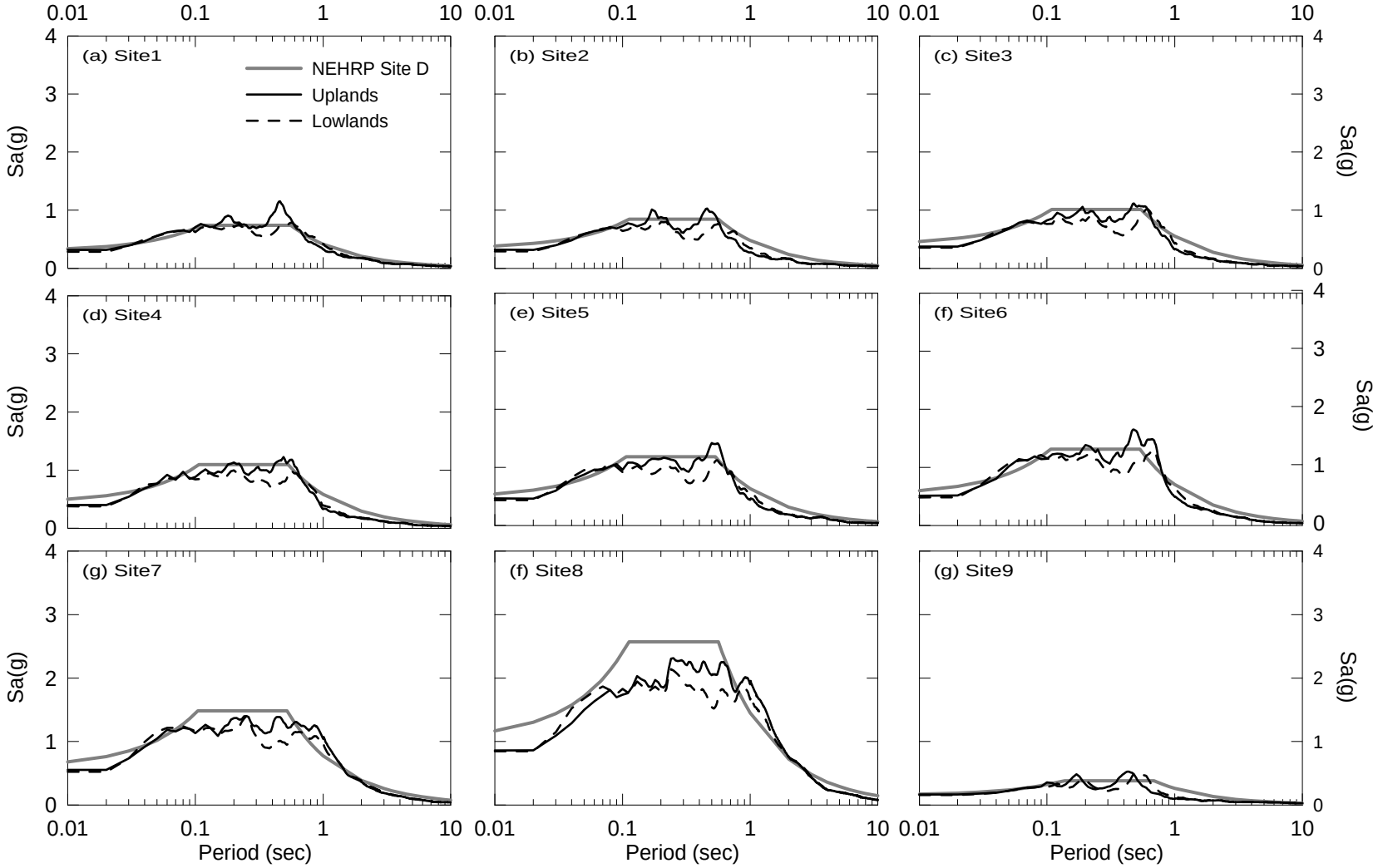

Figure 4.1 Comparison of PSHA(FF) (2011) UHRS at 30m depth soil-column and NEHRP design spectra at site class D

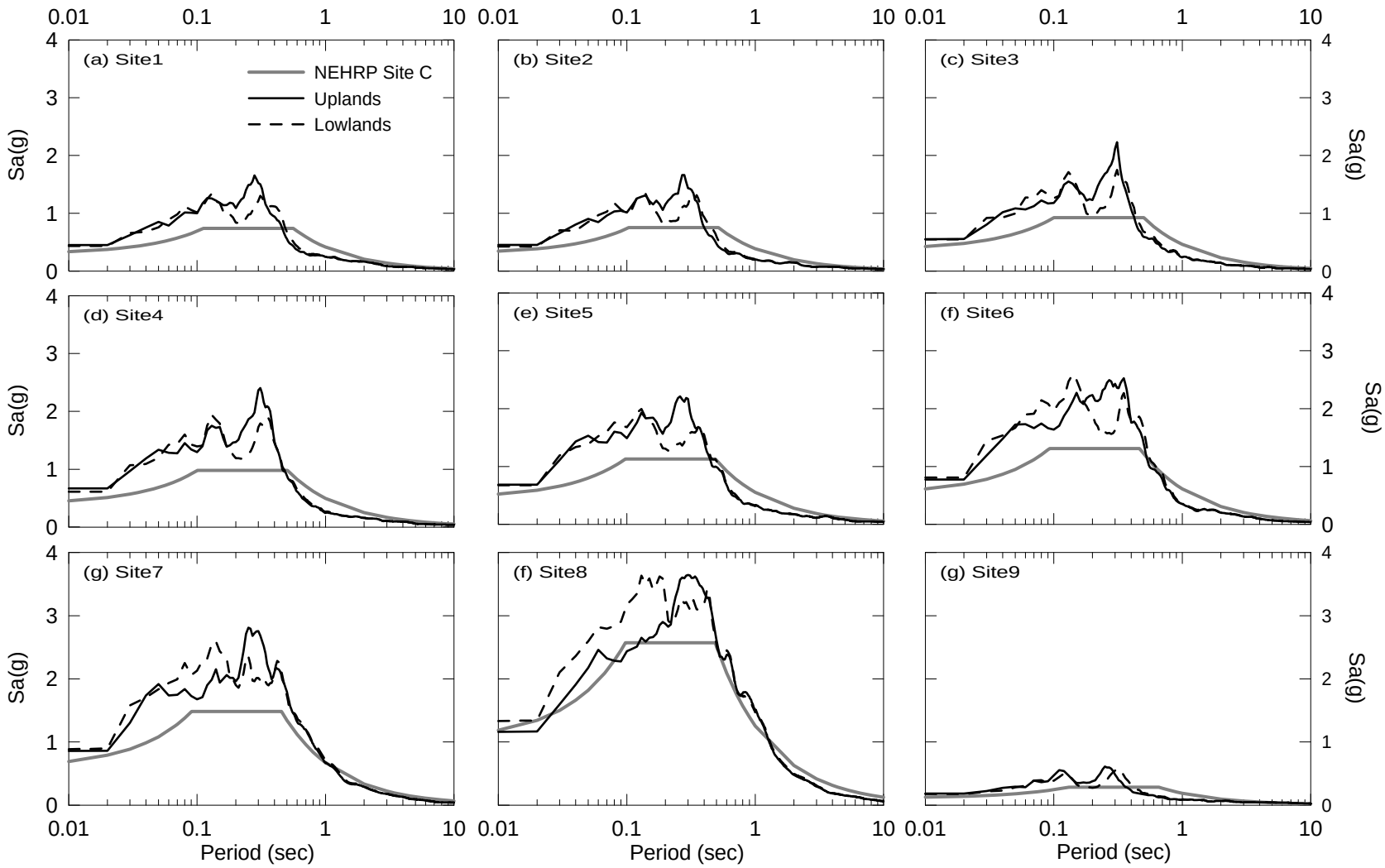

Figure 4.2 Comparison of PSHA(FF) (2011) UHRS at 30m depth soil-column and NEHRP design spectra at site class C

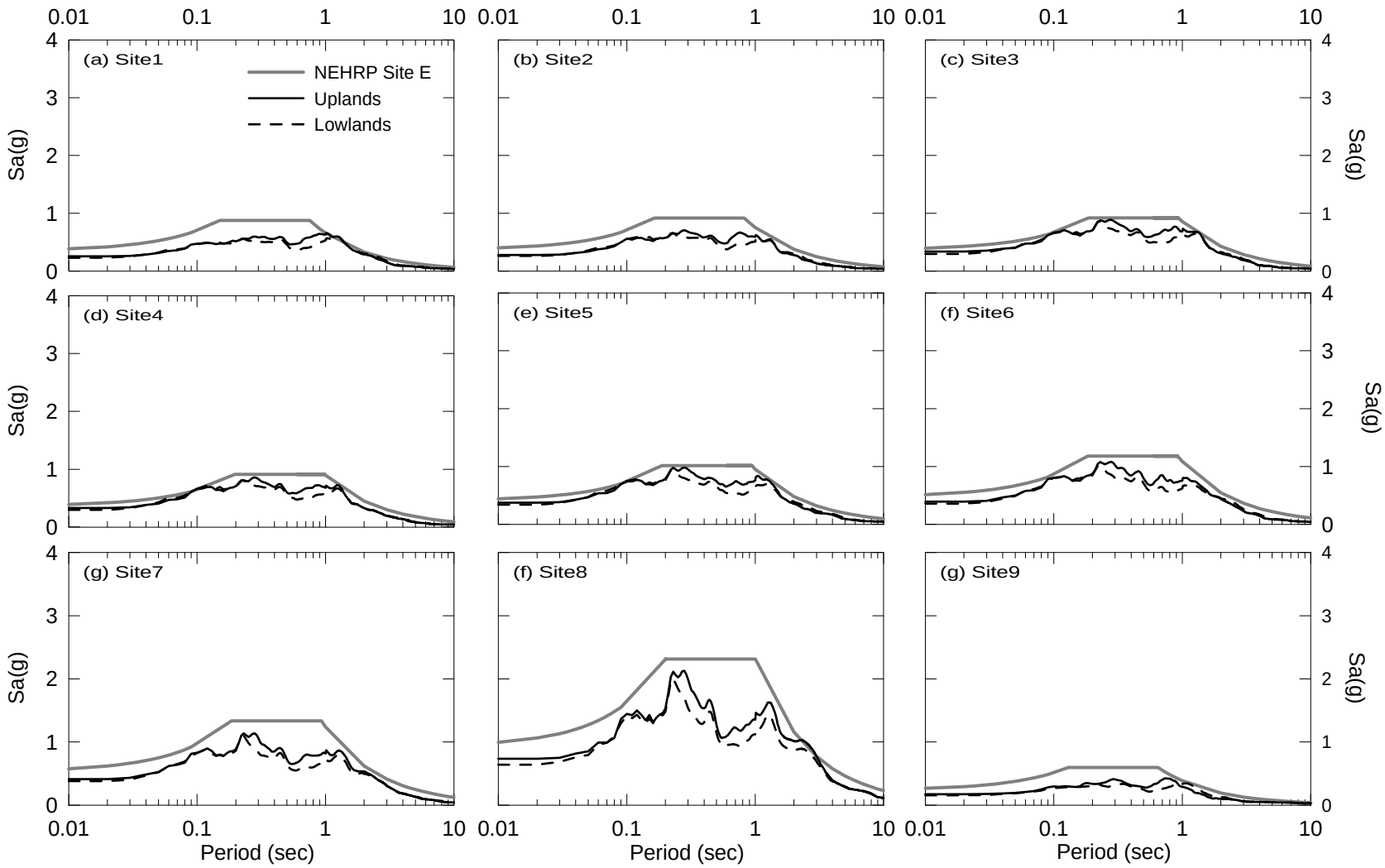

Figure 4.3 Comparison of PSHA(FF) (2011) UHRS at 30m depth soil-column and NEHRP design spectra at site class E

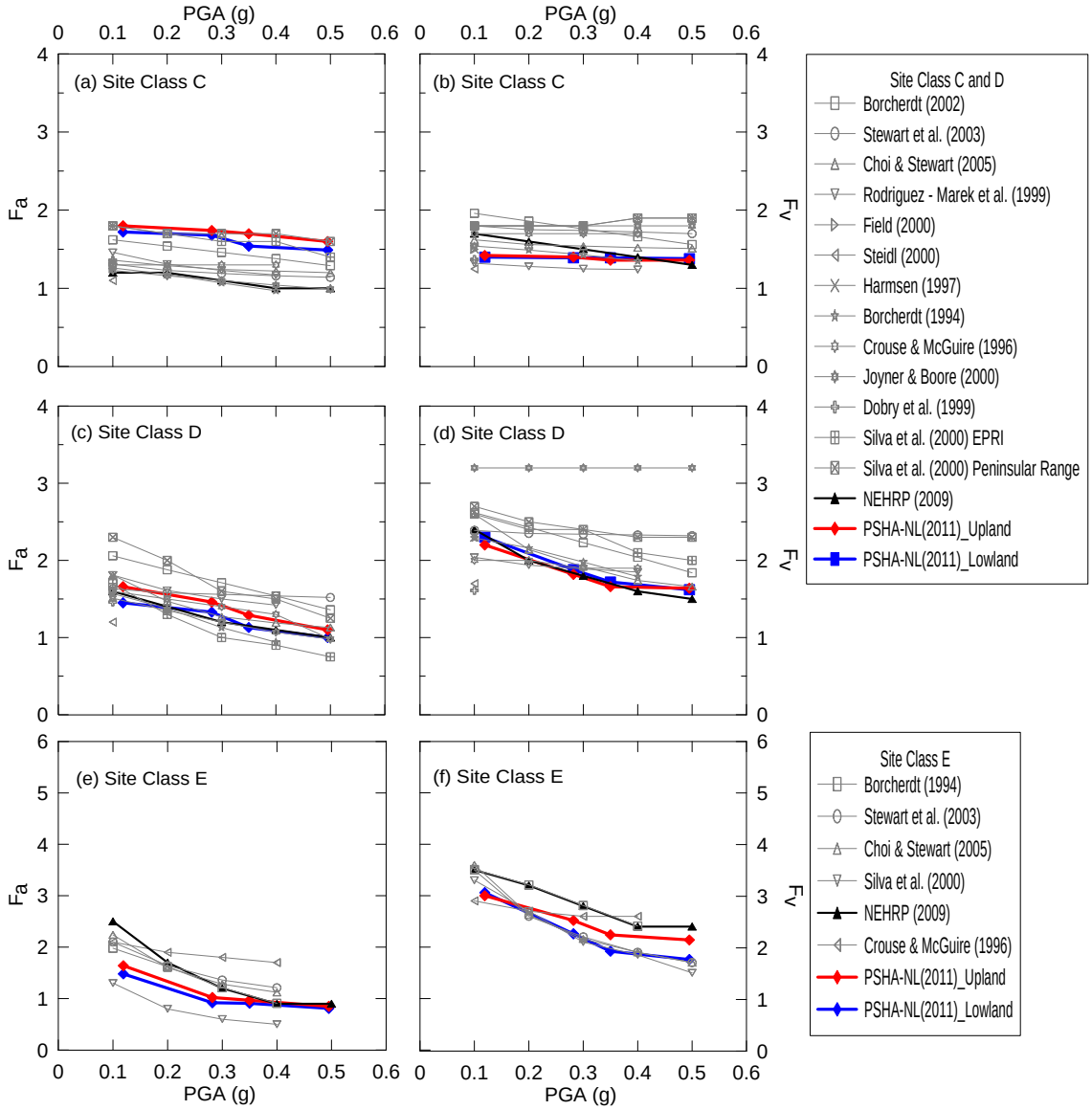

Figure 4.4 Comparison of site coefficients obtained from PSHA-NL(FF)(2011) and other studies for 30m thick soil column.

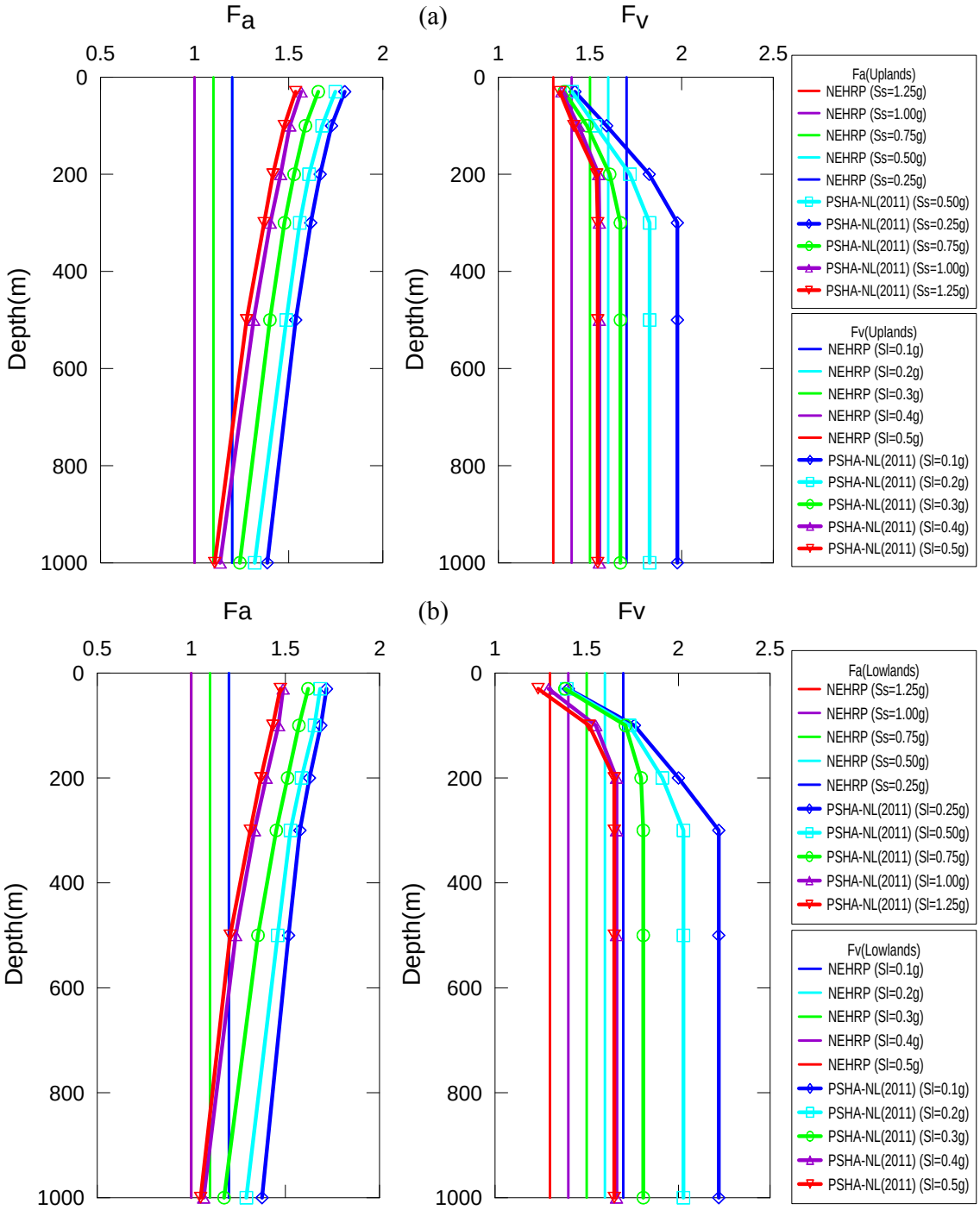

Figure 4.5 Comparison of depth-dependent site coefficients obtained from PSHA-NL(FF) and NEHRP site coefficients at site class C (a) Upland (b) Lowland

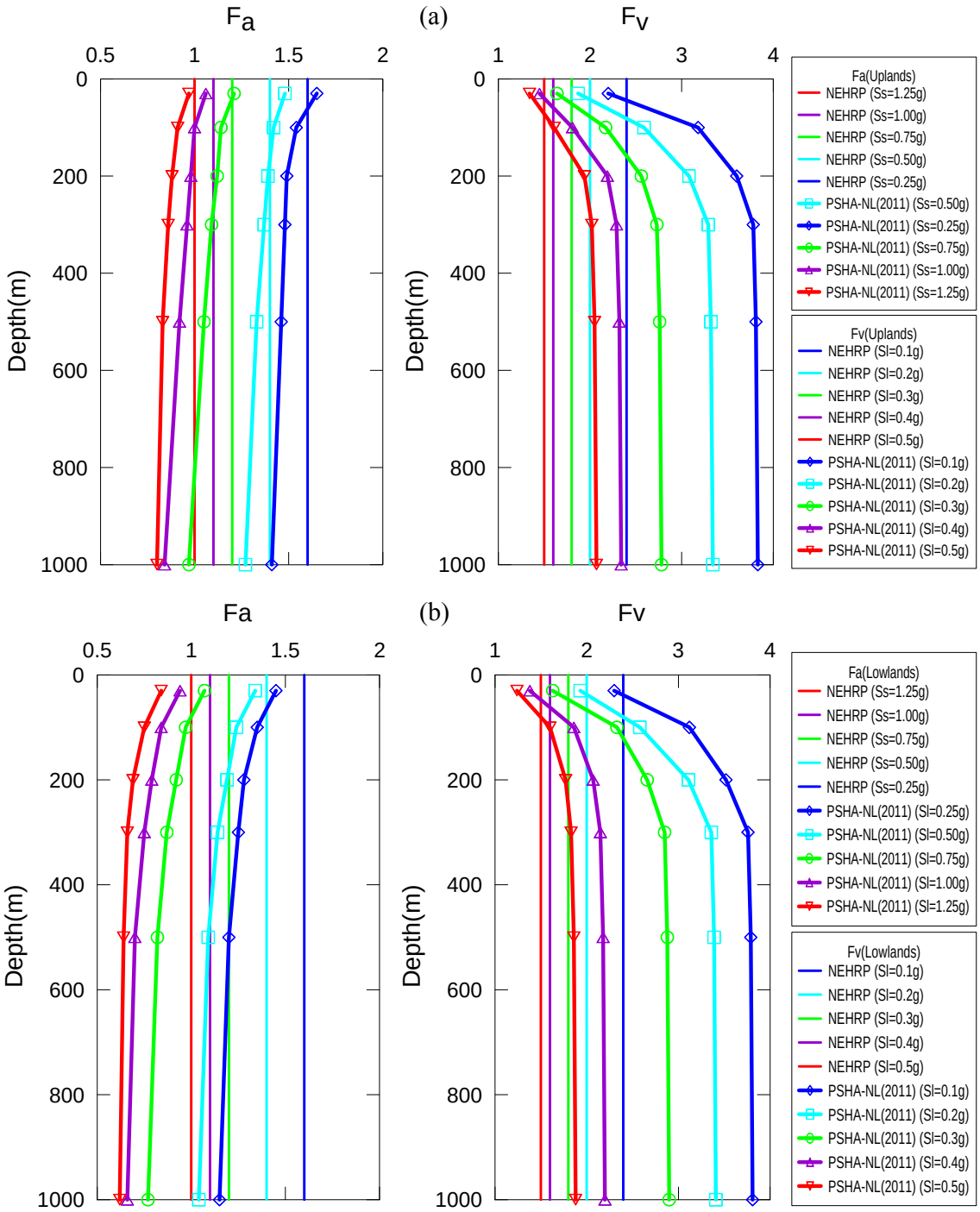

Figure 4.6 Comparison of depth-dependent site coefficients obtained from PSHA-NL(FF) and NEHRP site coefficients at site class D (a) Upland (b) Lowland

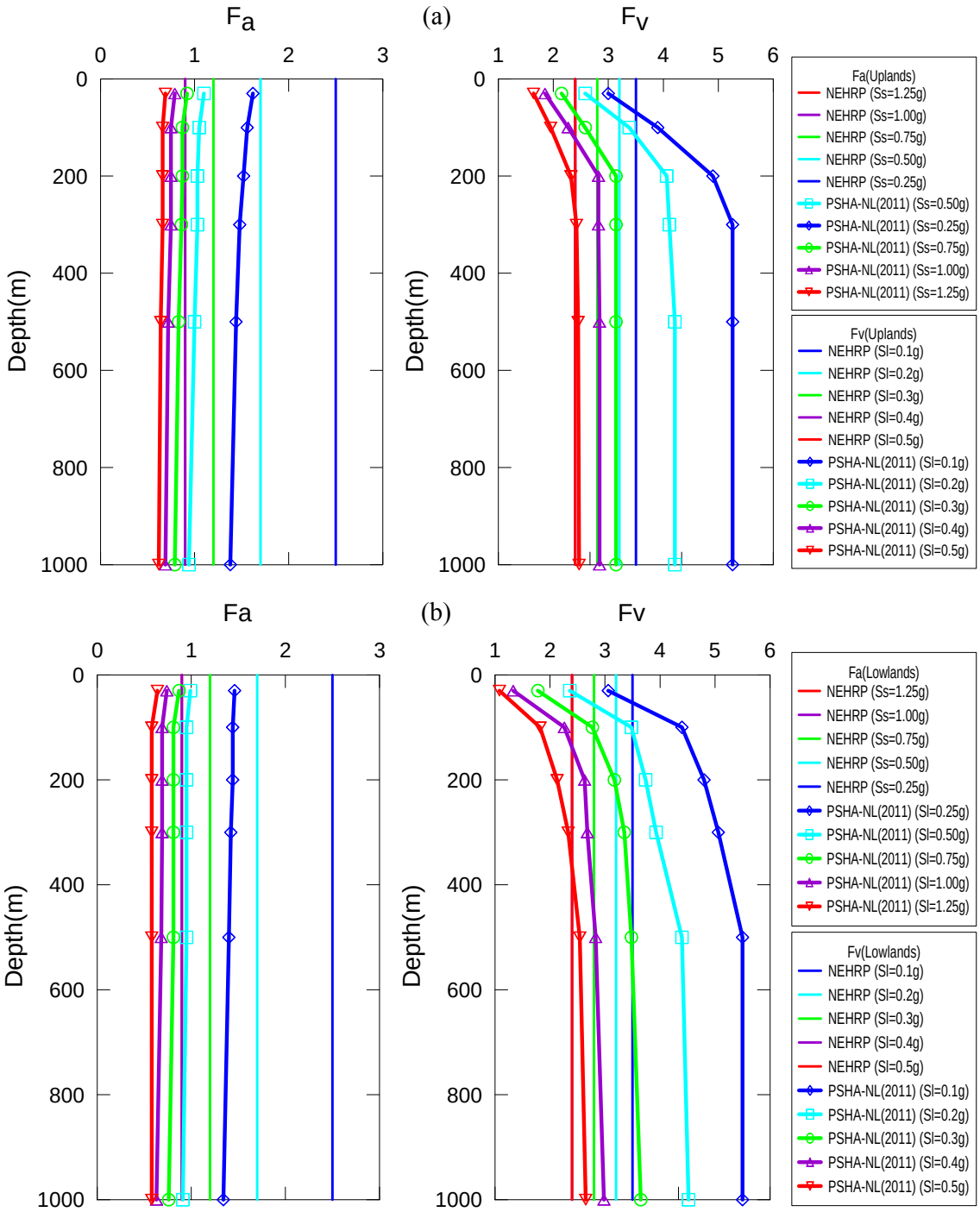

Figure 4.7 Comparison of depth-dependent site coefficients obtained from PSHA-NL(FF) and NEHRP site coefficients at site class E (a) Upland (b) Lowland

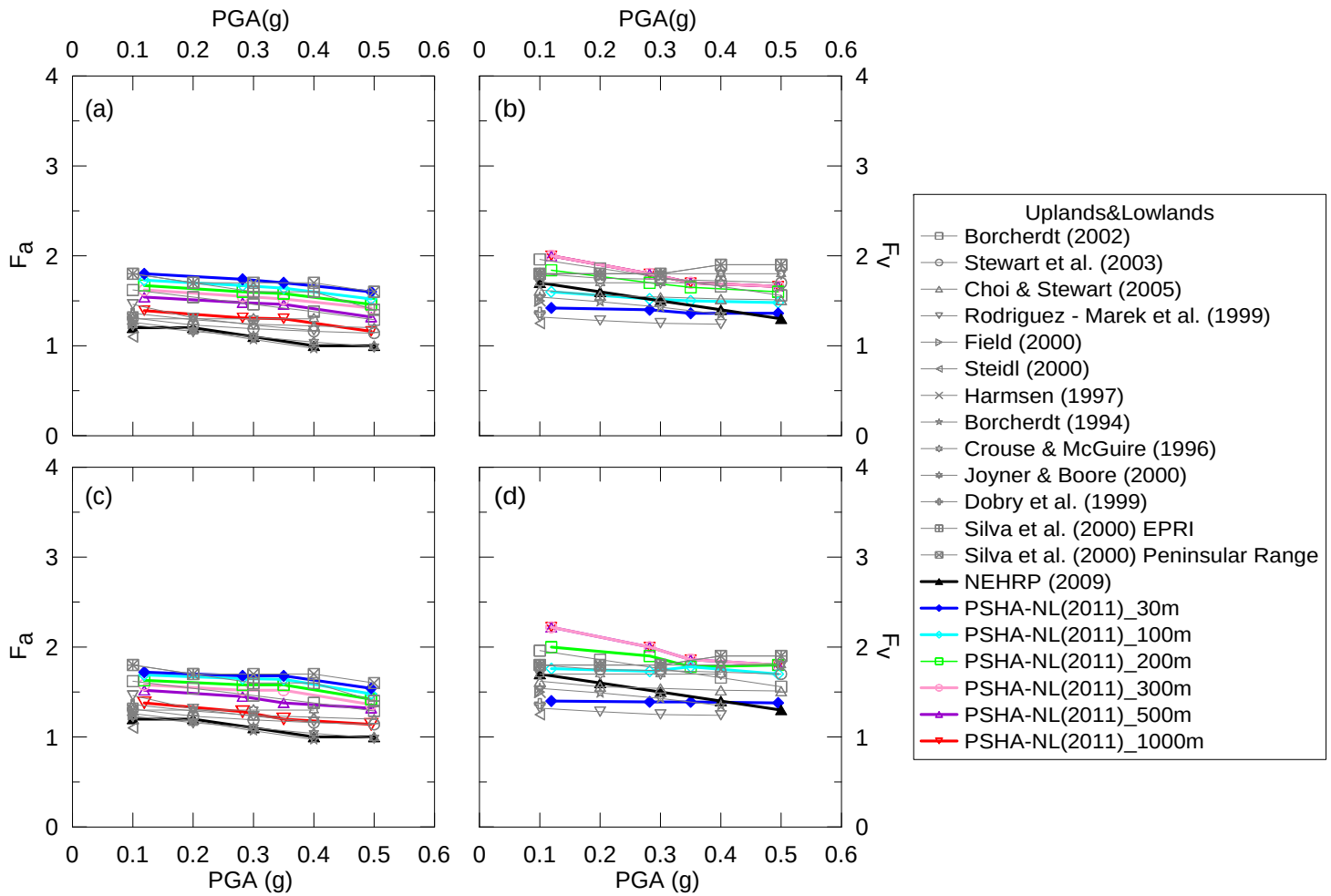

Figure 4.8 Comparison of depth-dependent site coefficients obtained from PSHA-NL(FF) and empirical studies at 30m,100m,200m,300m,500m,1000m depth soil column (a) and (b) Uplands, (c) and (d) Lowlands at site class C.

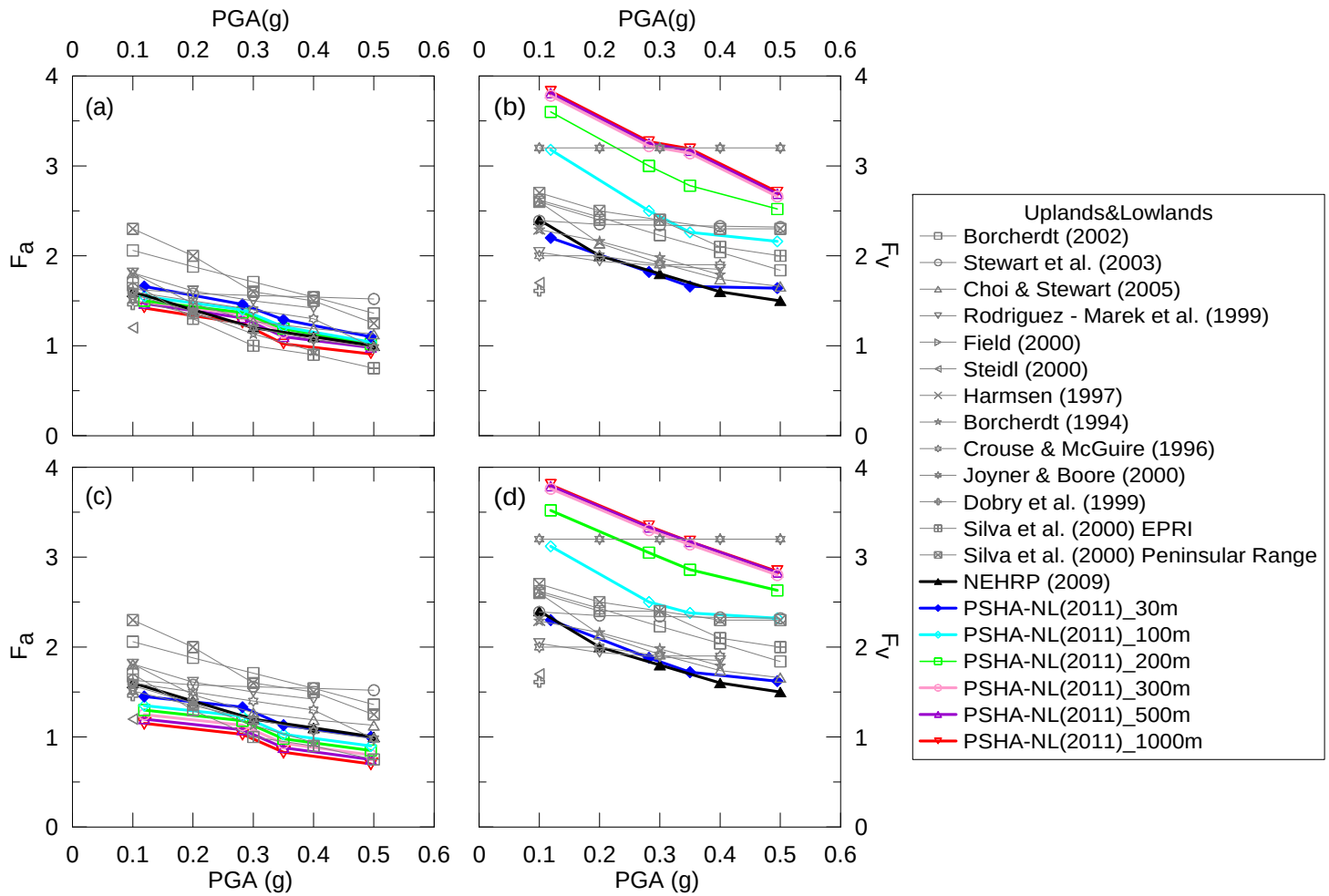

Figure 4.9 Comparison of depth-dependent site coefficients obtained from PSHA-NL(FF) and empirical studies at 30m,100m,200m,300m,500m,1000m depth soil column (a) and (b) Uplands, (c) and (d) Lowlands at site class D.

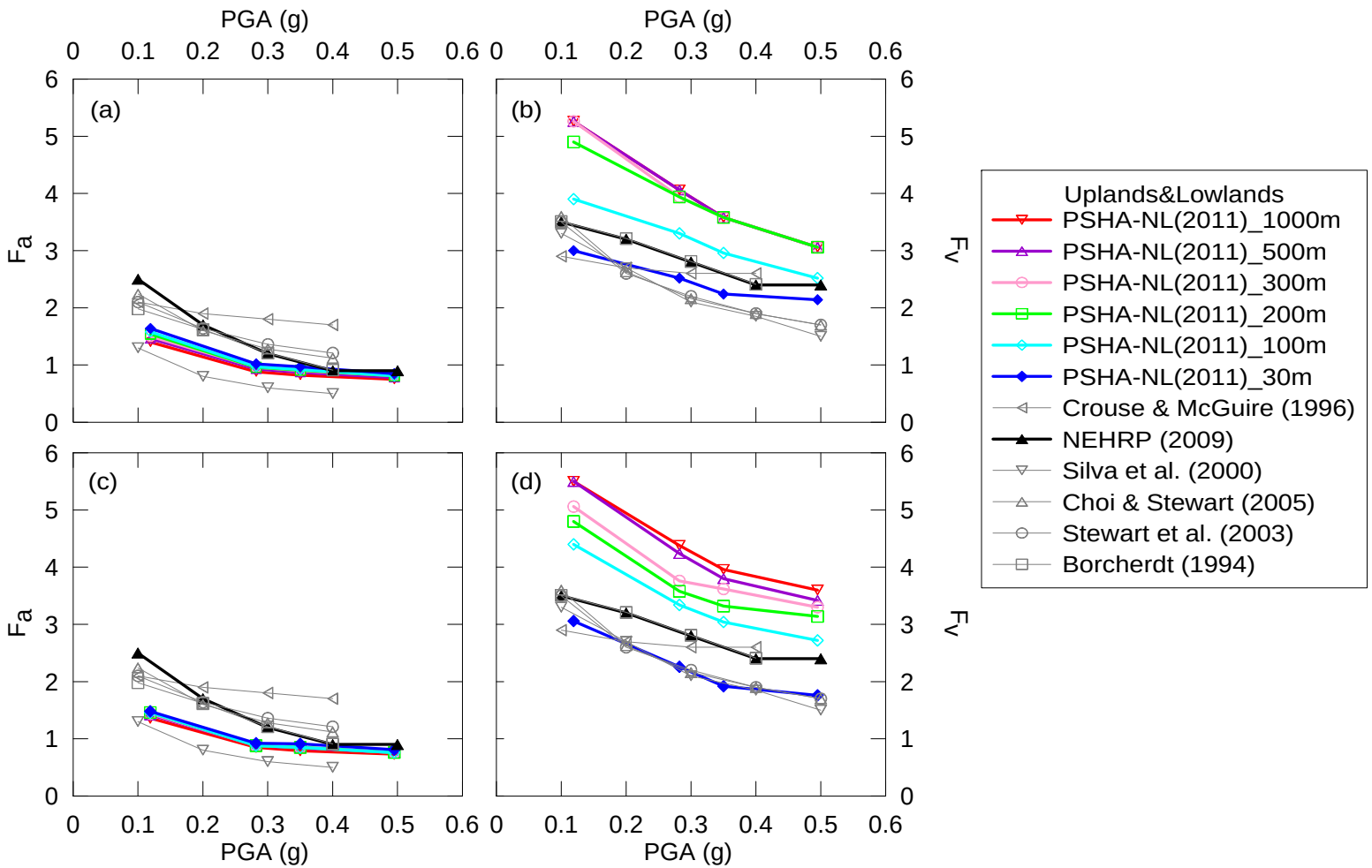

Figure 4.10 Comparison of depth-dependent site coefficients obtained from PSHA-NL(FF)(2011) and empirical studies at 30m,100m,200m,300m,500m,1000m depth soil column (a) and (b) Uplands, (c) and (d) Lowlands at site class E.

5. Summary and Conclusions

Sediment thickness plays a significant role in seismic hazard analysis and ground motion estimation. In order to consider its effect, the methodology (PSHA approach) proposed by Park and Hashash (2005b) and enhanced by Hashash et al. (2008) for nonlinear site effects is extend in the current study. The three significant improvements of this methodology are (1) use of 2008 USGS hazard map, (2) updated simulation programs for the stochastic finite-fault and point source models, and (3) fitting methods for new modulus reduction and damping curves. This enhanced PSHA approach, PSHA-NL(FF)(2011), is applied to NEHRP site-classes C, D, and E for evaluation of depth-dependent site coefficients.

The proposed procedure results in UHRS for 30m soil-column profiles that generally exceed site class C NEHRP design spectra, are consistent with site class D NEHRP design spectra, and lower than site class E NEHRP design spectra. For soil column thickness more than 30m, the proposed site coefficients are generally lower at short periods and greater at long periods than the NEHRP site coefficients, with the exception of site class C. The proposed site coefficients (F_a) of NEHRP site class D are higher at $S_s \leq 0.75$ than the site coefficients proposed by Hashash et al. (2008), and the gap between site coefficients gradually decreases as S_s becomes larger. Also, the proposed site coefficients (F_v) of NEHRP site class D are higher at $S_l \leq 0.2$ than the site coefficients by proposed Hashash et al. (2008), and the gap between site coefficients gradually decreases as Sl becomes larger. It is recommended that sediment thickness dependent site factors be used in lieu of the depth independent factors currently in use.

6. References

Atkinson, G., and Boore, D. (2006). "Earthquake ground-motion prediction equations for eastern North America." *Bulletin of the Seismological Society of America*, 96(6), 2181-2205.

Atkinson, G. M., and Boore, D. M. (1995). "Ground motions relations for eastern North America." *Bulletin of Seismological Society of America*, 85, 17-30.

Baker, J. W., and Cornell, C. A. (2006). "Spectral shape, epsilon and record selection." *Earthquake Engineering and Structural Dynamics*, 35(9), 1077-1095.

Beresnev, I. A., and Atkinson, G. M. (1998). "FINSIM - a FORTRAN Program for simulating stochastic acceleration time histories from finite faults." *Seismological Research Letters*, 69(1), 27-32.

Boore, D. M. (2002). "SMSIM Fortran programs for simulating ground motions from earthquakes: Version 2.16. A revision of OFR 96-80-A." US Geological Survey, Menlo Park.

Boore, D. M. (2005). "SMSIM Fortran programs for simulating ground motions from earthquakes, version 2.3." A revision of U.S.Geol.Surv.Open-File Rept. 96-80-A.

Campbell, K. W. (2003). "Prediction of strong ground motion using the hybrid empirical method and its use in the development of ground-motion (attenuation) relations in Eastern North America." *Bulletin of the Seismological Society of America*, 93(3), 1012-1033.

Cornell, A. C. (1968). "Engineering Seismic Risk Analysis." *Bulletin of the Seismological Society of America*, 58(5), 1583-1606.

Cramer, C. H. (2006). "Quantifying the uncertainty in site amplification modeling and its effects on site-specific seismic-hazard estimation in the upper Mississippi embayment and adjacent areas." *Bulletin of the Seismological Society of America*, 96(6), 2008-2020.

Darendeli, M. B. (2001). "Development of a new family of normalized modulus reduction and material damping curves," Ph. D., University of Texas at Austin, Austin.

EPRI. (1993). "Guidelines for determining design basis ground motions." *EPRI Tr-102293*, Electric Power Research Institute, Palo Alto, CA.

Field, E. H., Kramer, S., Elgamal, Bray, A.-W., J.D.,Matasovic, N. Johnson, P.A. Cramer, C. Roblee, C. Wald, D.J. Bonilla, L.F., Dimitriu, P.P., Anderson, J.G. (1998). "Nonlinear site response: Where we're at (A report from a SCEC/PEER seminar and workshop)." Seismological Research Letters, 230-234.

Frankel, A., Mueller, C., Perkins, D., Barnhard, T., Leyendecker, E., Safak, E., Hanson, S., Dickman, N., and Hopper, M. (1996). "New USGS seismic hazard maps for the United States." *The Conference on Natural Disaster Reduction 1996*, Washington, DC, USA, 173-174.

Frankel, A., Pertersen, M. D., Mueller, C. S., Haller, K. M., Wheeer, R. L., Leyendecker, E. V., Wesson, R. L., Harmsen, S. C., Cramer, C. H., Perkins, D. M., and Rukstales, K. S. (2002). "Documentation for the 2002 update of the national seismic hazard maps." *OFR 02-420*, US Geological Survey.

Hashash, Y. M. A. (2011). "DEEPSOIL V 4.0, Tutorial and User Manual. 2002-2011." University of Illinois at Urbana-Champaign, Urbana Illinois.

Hashash, Y. M. A., and Park, D. (2001). "Non-linear one-dimensional seismic ground motion propagation in the Mississippi embayment." *Engineering Geology*, 62(1-3), 185-206.

Hashash, Y. M. A., Tsai, C.-C., Phillips, C., and Park, D. (2008). "Soil column depth

dependent seismic site coefficients and hazard maps for the Upper Mississippi Embayment." *Bull. Seism. Soc. Am.*, 98(4), 2004-2021.

Heaton, T. H. (1990). "Evidence for and implications of self-healing pulses of slip in earthquake rupture." *Physics of the Earth and Planetary Interiors*, 64(1), 1-20.

Menq, F. Y. (2003). "Dynamic Properties of Sandy and Gravelly Soils," Ph.D, University of Texas at Austin, Austin.

Motazedian, D., and Atkinson, G. M. (2005). "Stochastic finite-fault modeling based on a dynamic corner frequency." *Bulletin of the Seismological Society of America*, 95(3), 995-1010.

Park, D. (2003). "Estimation of non-linear seismic site effects for deep deposits of the Mississippi Embayment," Ph.D., University of Illinois, Urbana.

Park, D., and Hashash, Y. M. A. (2005a). "Estimation of seismic factors in the Mississippi Embayment: I. Estimation of dynamic properties." *Soil Dynamics and Earthquake Engineering*, 25, pp. 133-144.

Park, D., and Hashash, Y. M. A. (2005b). "Estimation of seismic factors in the Mississippi Embayment: II. Probabilistic seismic hazard with nonlinear site effects." *Soil Dynamics and Earthquake Engineering*, 25, pp. 145-156.

Petersen, M. D., Frankel, A. D., Harmsen, S. C., Mueller, C. S., Haller, K. M., Wheeler, R. L., Wesson, R. L., Zeng, Y., Boyd, O. S., Perkins, D. M., Luco, N., Field, E. H., Wills, C. J., and Rukstales, K. S. (2008). "Documentation for the 2008 Update of the United States National Seismic Hazard Maps." USGS.

Phillips, C., and Hashash, Y. M. A. (2009). "Damping formulation for non-linear 1D site response analyses." *Soil Dynamics and Earthquake Engineering*, 29(7), Pages 1143-1158.

Power, M., Borcherdt, R. D., and Stewart, J. (2004). "Site amplification factors from empirical studies." NGA WORKING GROUP #5.

Romero, S. M., and Rix, G. J. (2001). "Ground motion amplification in the Upper Mississippi Embayment." *GIT-CEE/GEO-01-1*, National Science Foundation Mid America Center, Atlanta.

Silva, W., Gregor, N., and Darragh, R. (2002). "Development of hard rock attenuation relations for central and eastern North America, internal report from Pacific Engineering." http://www.pacificengineering.org/CEUS/Development%20of%20Regional%20Hard_ABC.pdf.

Silva, W. J., and Darragh, R. (1995). "Engineering characterization of earthquake strong ground motion recorded at rock sites." *TR-102261*, Electric Power Research Institute Palo Alto, Calif.

Somerville, P., Collins, N., Abrahamson, N., Graves, R., and Saikia, C. (2001). "Ground motion attenuation relations for the central and eastern United States." Final report to U.S. Geol. Survey, June 30, 2001, URS Group, Inc., Pasadena CA, USA.

Tavakoli, B., and Pezeshk, S. (2005). "Empirical-stochastic ground-motion prediction for eastern North America." *Bulletin of the Seismological Society of America*, 95(6), 2283-2296.

Toro, G., Abrahamson, N., and Schneider, J. (1997). "Model of strong ground motions from earthquakes in the central and eastern North America: best estimates and uncertainties." *Seismological Research Letters*, 68, 41-57.

Toro, G. R., and Silva, W. J. (2001). "Scenario earthquakes for Saint Louis, MO, and Memphis, TN, and seismic hazard mpas for the Centraul United States Region including the effect of site conditions." *USGS 1434-HQ-97-GR-02981*.

Wells, D. L., and Coppersmith, K. J. (1994). "New empirical relationships among magnitude, rupture length, rupture width, rupture area, and surface displacement." *Bulletin of teh Seismological Society of America*, 84(4), 974-1002.

Wen, Y. K., and Wu, C. L. (2001). "Uniform hazard ground motions for Mid-America Cities." *Earthquake spectra*, 17(2), 359-384.

Wong, I., Thomas, P., Silva, W., Quittmeyer, R., Toro, G., Dober, M., Pattanapong, C. L., Upadhyaya, S., Logeswaran, S., Olig, S., and Terra, F. (2004). "Development of Earthquake Ground Motion Input for Preclosure Seismic Design and Postclosure Performance Assessment of a Geologic Repository at Yucca Mountain." Bechtel SAIC Company, NV.

APPENDIX A - Site Class C

Computed PSHA(FF)(2011) UHRS for 30m, 100m, 200m, 300m, 500m, 1000m soil-columns and NEHRP design spectra for uplands and lowlands.

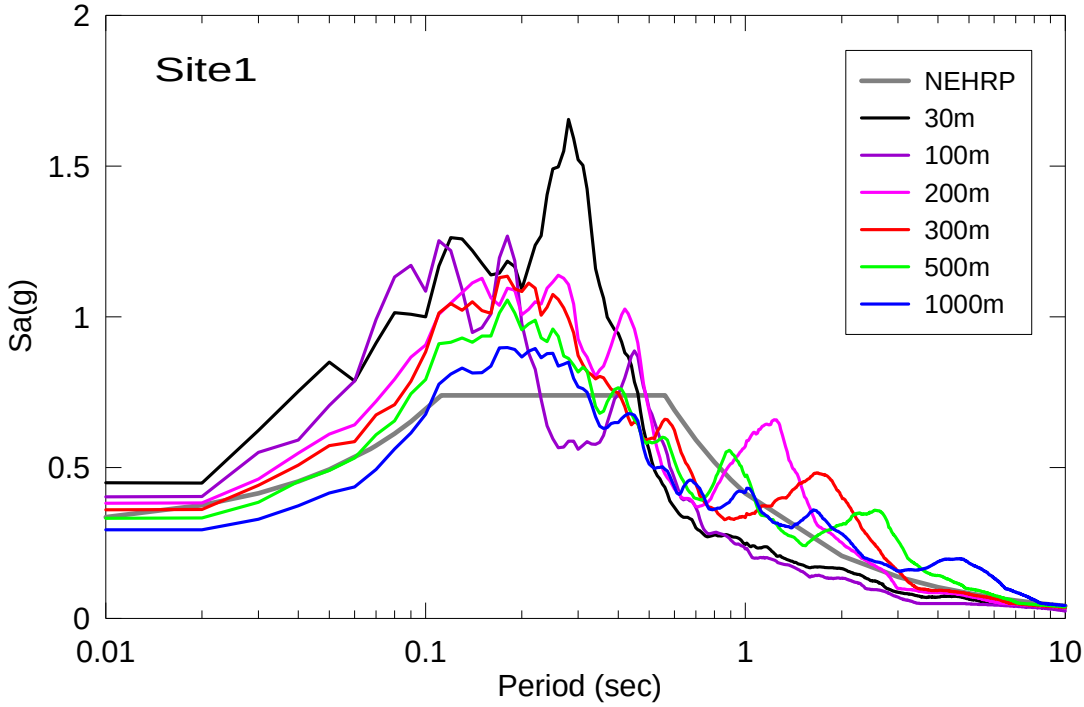

Figure A 1 Computed PSHA(FF)(2011) UHRS for 30m, 100m, 200m, 300m, 500m, 1000m soil-columns and NEHRP design spectra. Uplands, site 1.

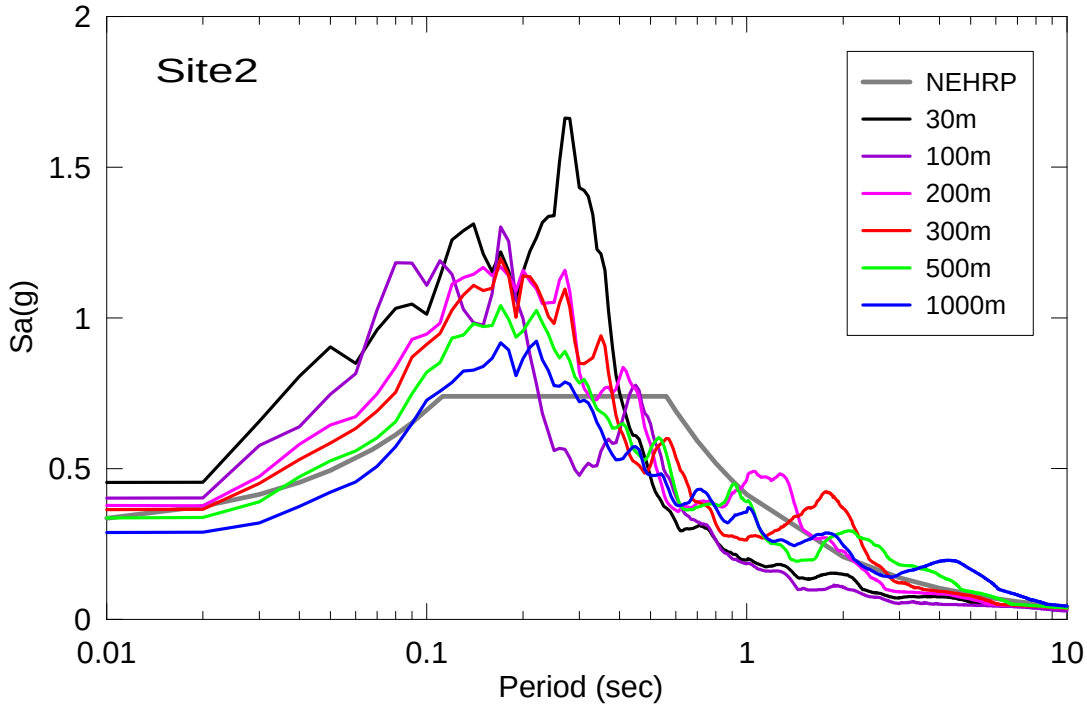

Figure A 2 Computed PSHA(FF)(2011) UHRS for 30m, 100m, 200m, 300m, 500m, 1000m soil-columns and NEHRP design spectra. Uplands, site 2.

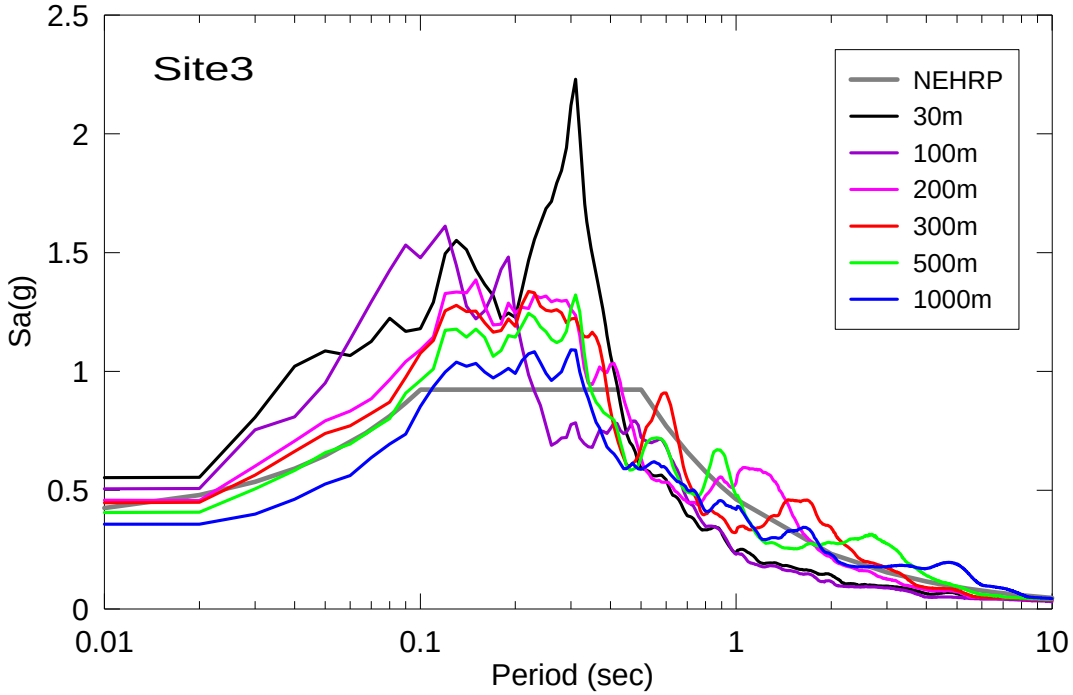

Figure A 3 Computed PSHA(FF)(2011) UHRS for 30m, 100m, 200m, 300m, 500m, 1000m soil-columns and NEHRP design spectra. Uplands, site 3.

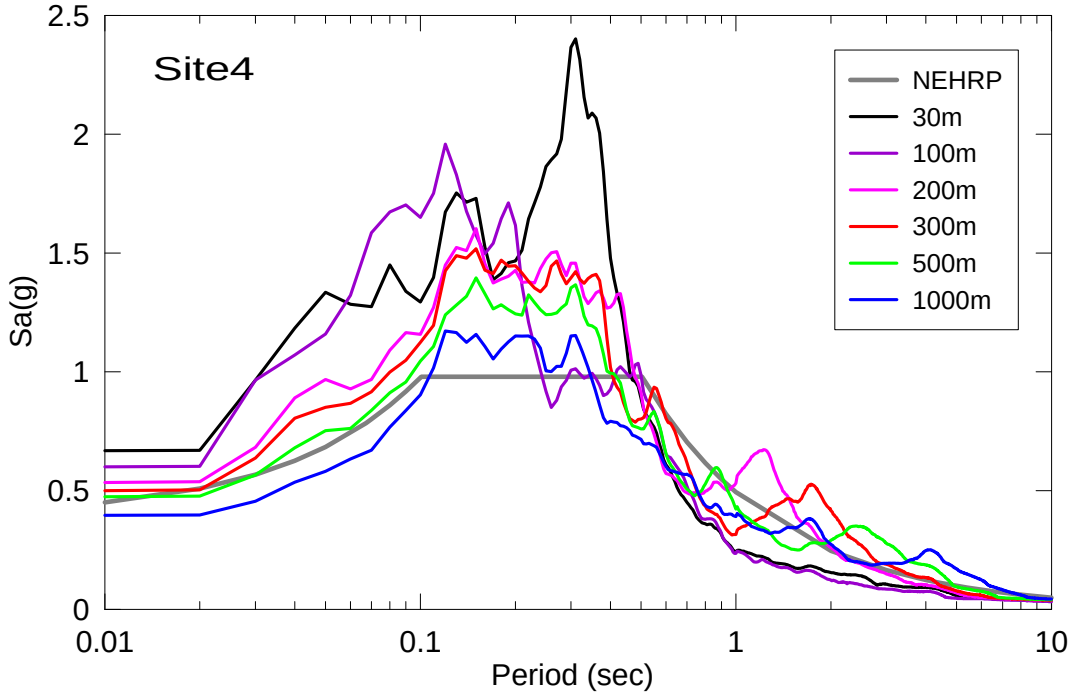

Figure A 4 Computed PSHA(FF)(2011) UHRS for 30m, 100m, 200m, 300m, 500m, 1000m soil-columns and NEHRP design spectra. Uplands, site 4.

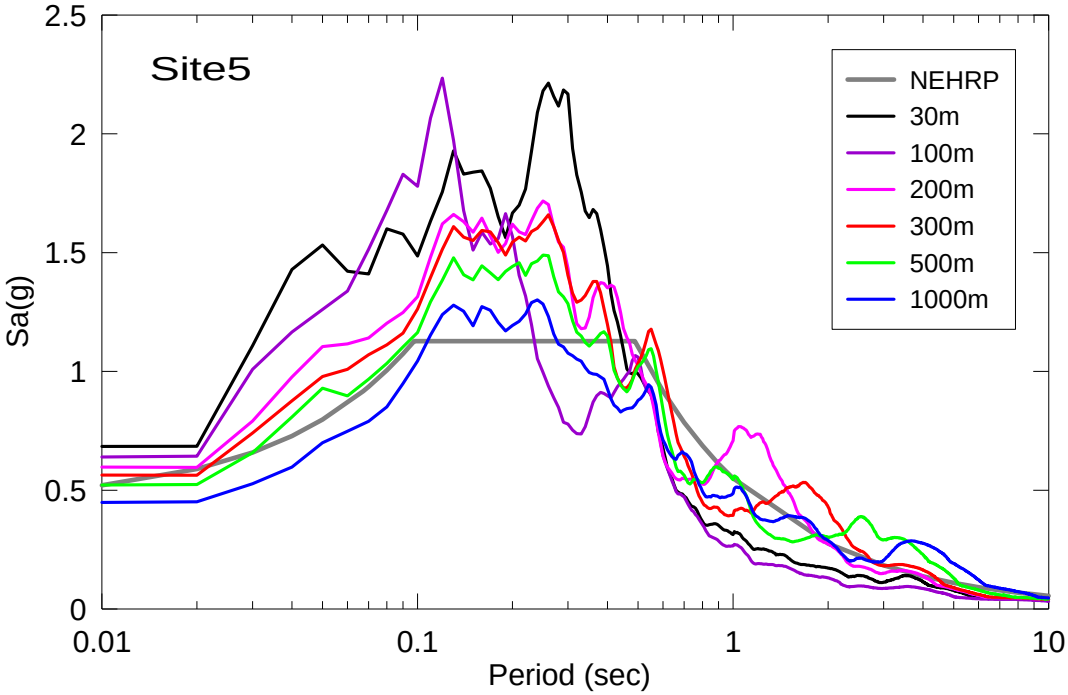

Figure A 5 Computed PSHA(FF)(2011) UHRS for 30m, 100m, 200m, 300m, 500m, 1000m soil-columns and NEHRP design spectra. Uplands, site 5.

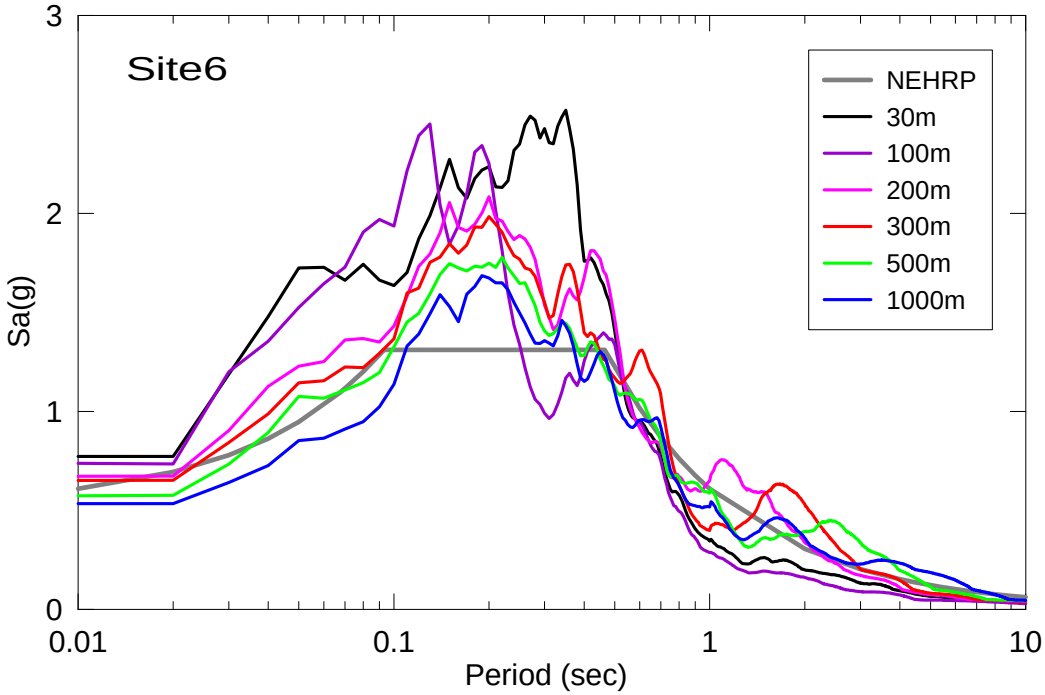

Figure A 6 Computed PSHA(FF)(2011) UHRS for 30m, 100m, 200m, 300m, 500m, 1000m soil-columns and NEHRP design spectra. Uplands, site 6.

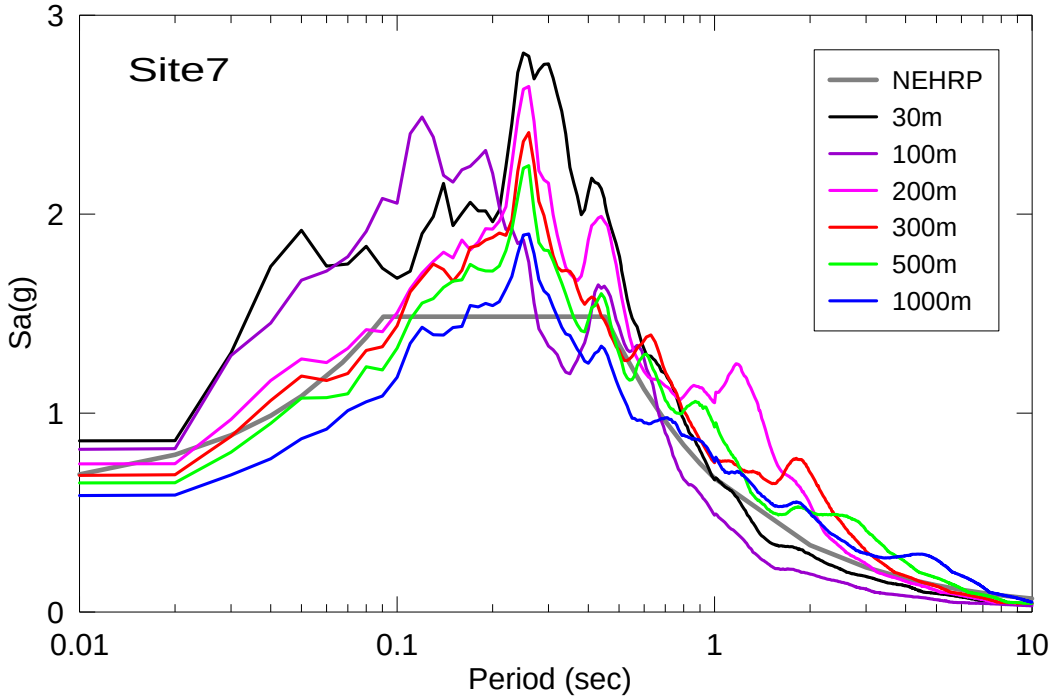

Figure A 7 Computed PSHA(FF)(2011) UHRS for 30m, 100m, 200m, 300m, 500m, 1000m soil-columns and NEHRP design spectra. Uplands, site 7.

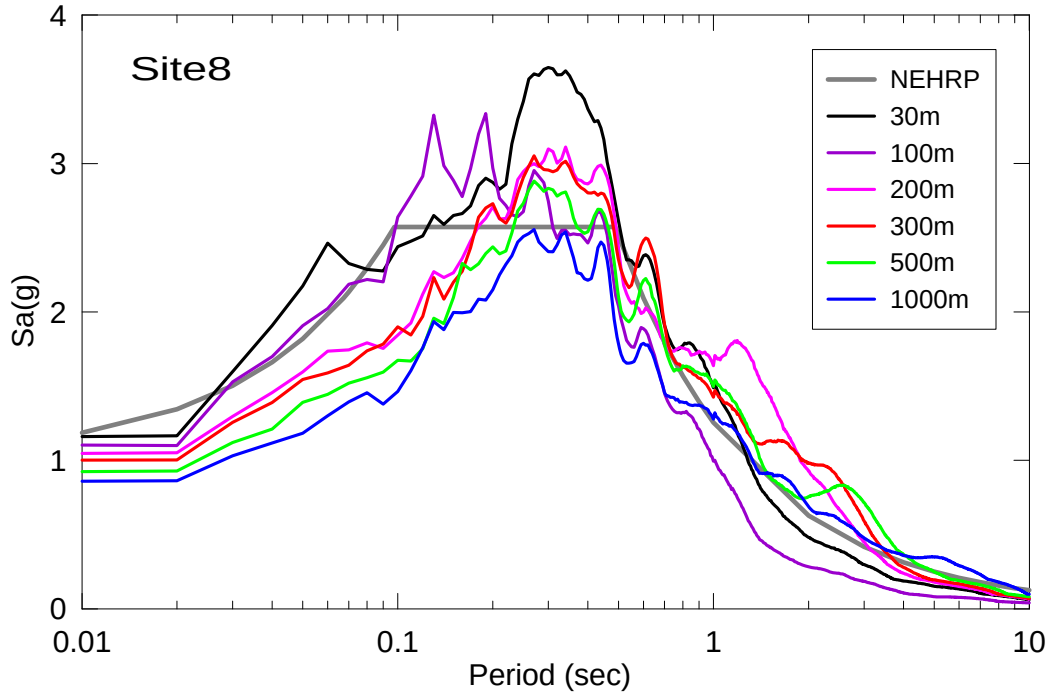

Figure A 8 Computed PSHA(FF)(2011) UHRS for 30m, 100m, 200m, 300m, 500m, 1000m soil-columns and NEHRP design spectra. Uplands, site 8.

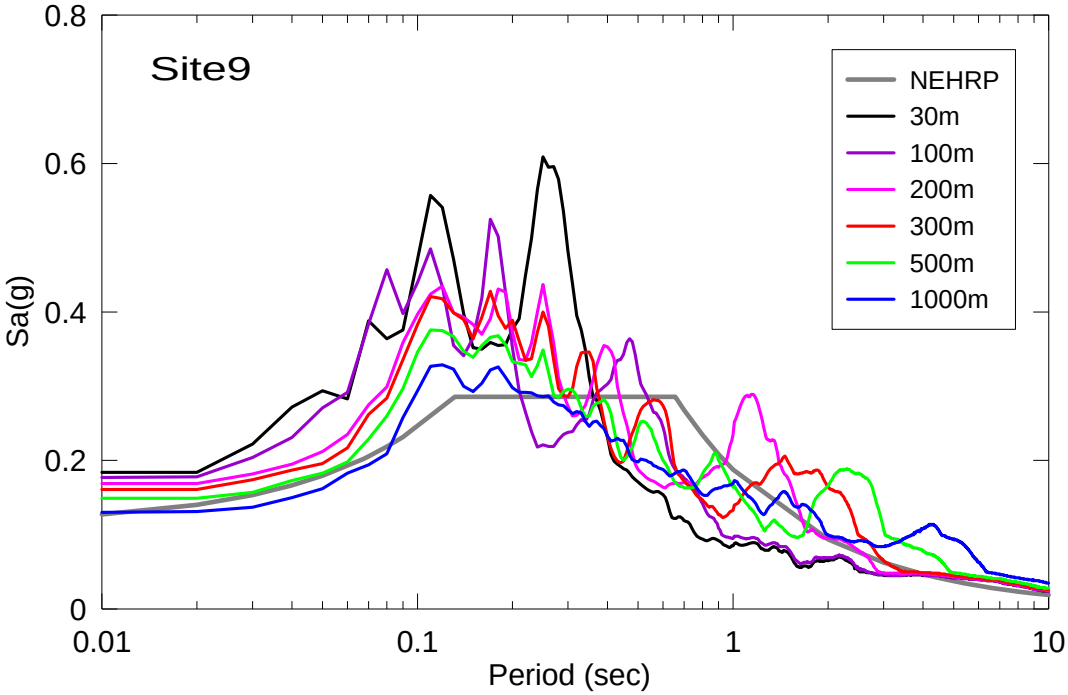

Figure A 9 Computed PSHA(FF)(2011) UHRS for 30m, 100m, 200m, 300m, 500m, 1000m soil-columns and NEHRP design spectra. Uplands, site 9.

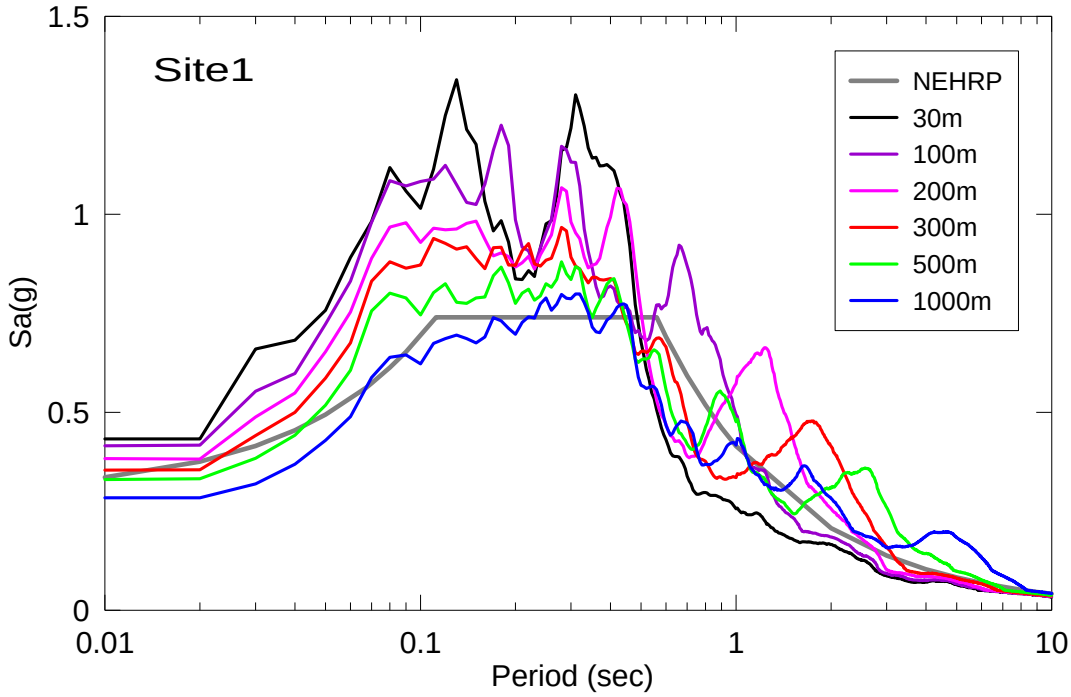

Figure A 10 Computed PSHA(FF)(2011) UHRS for 30m, 100m, 200m, 300m, 500m, 1000m soil-columns and NEHRP design spectra. Lowlands, site 1.

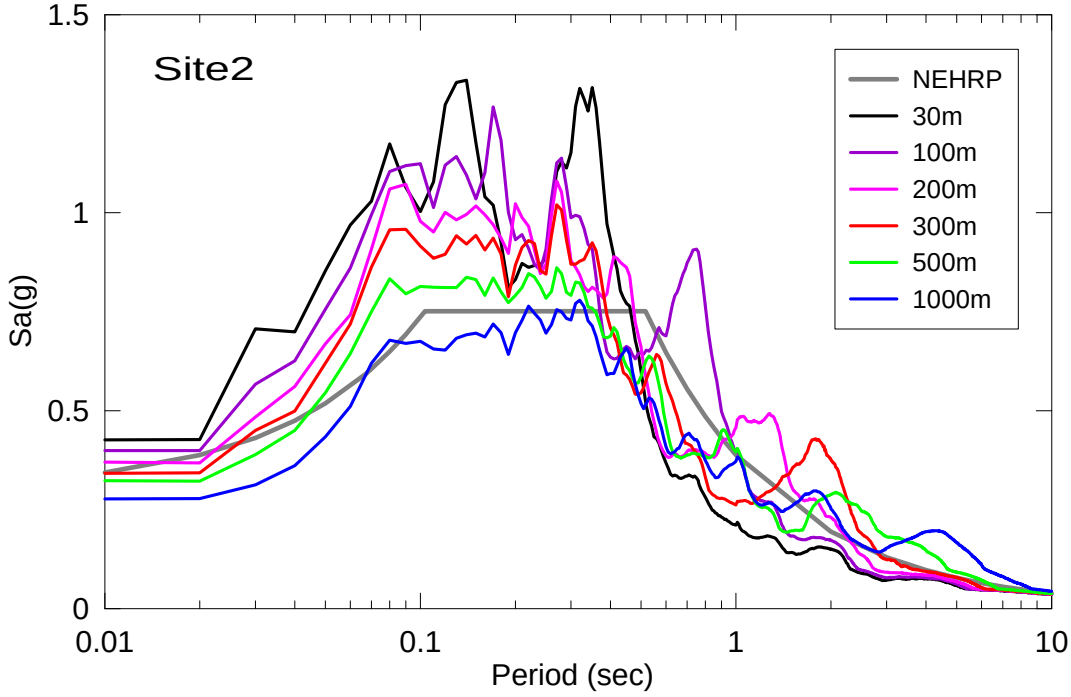

Figure A 11 Computed PSHA(FF)(2011) UHRS for 30m, 100m, 200m, 300m, 500m, 1000m

soil-columns and NEHRP design spectra. Lowlands, site 2.

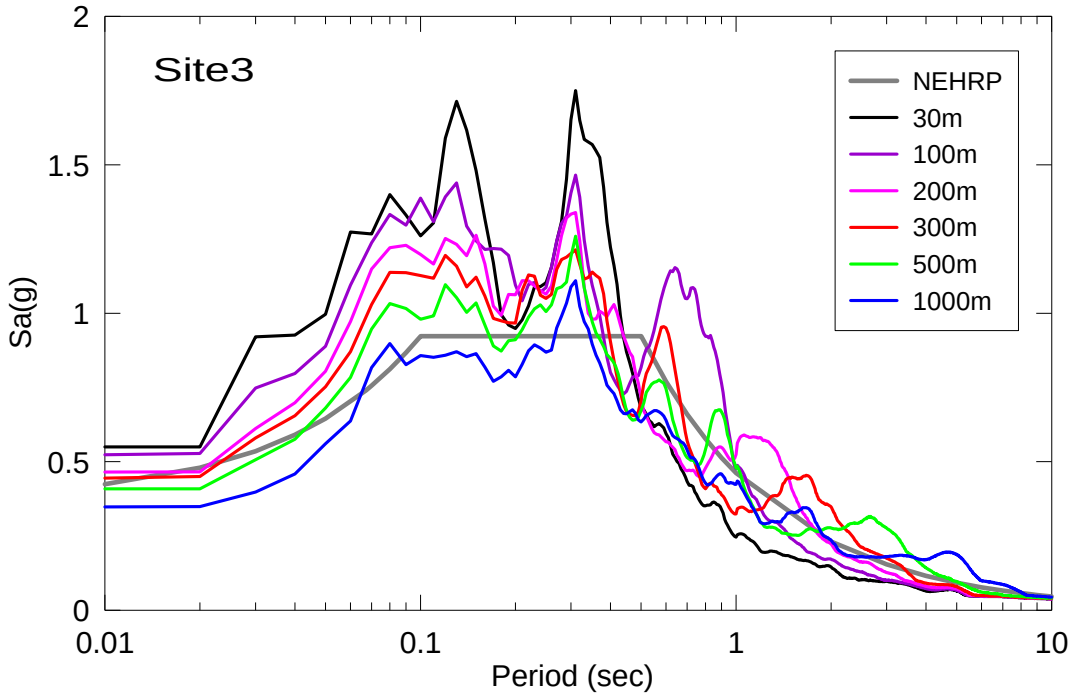

Figure A 12 Computed PSHA(FF)(2011) UHRS for 30m, 100m, 200m, 300m, 500m, 1000m soil-columns and NEHRP design spectra. Lowlands, site 3.

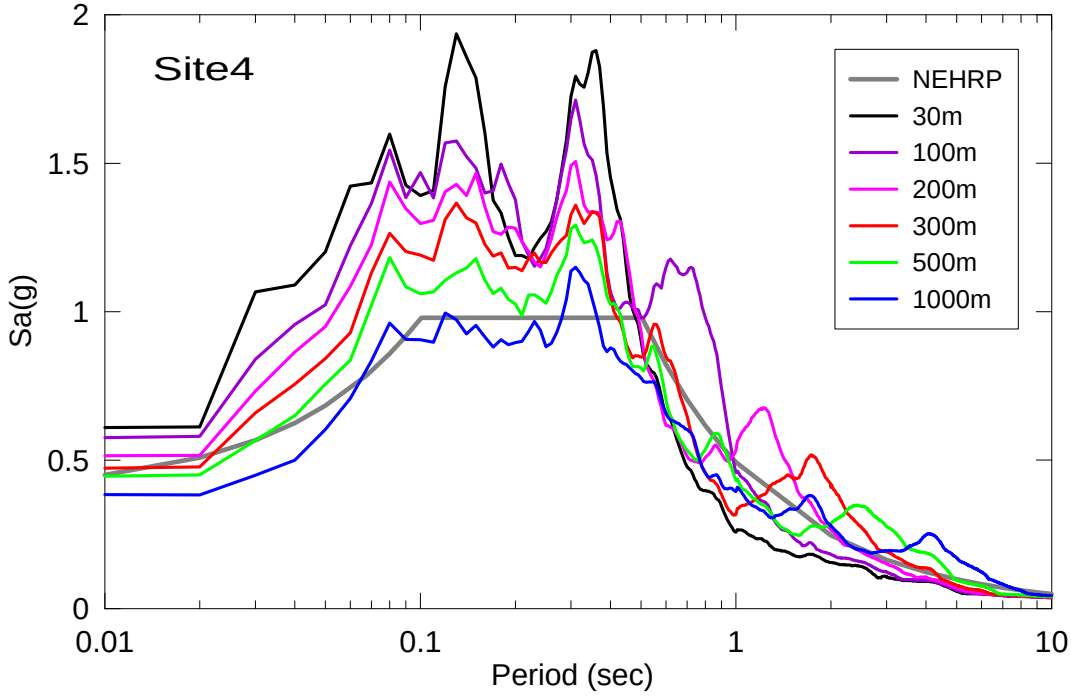

Figure A 13 Computed PSHA(FF)(2011) UHRS for 30m, 100m, 200m, 300m, 500m, 1000m

soil-columns and NEHRP design spectra. Lowlands, site 4.

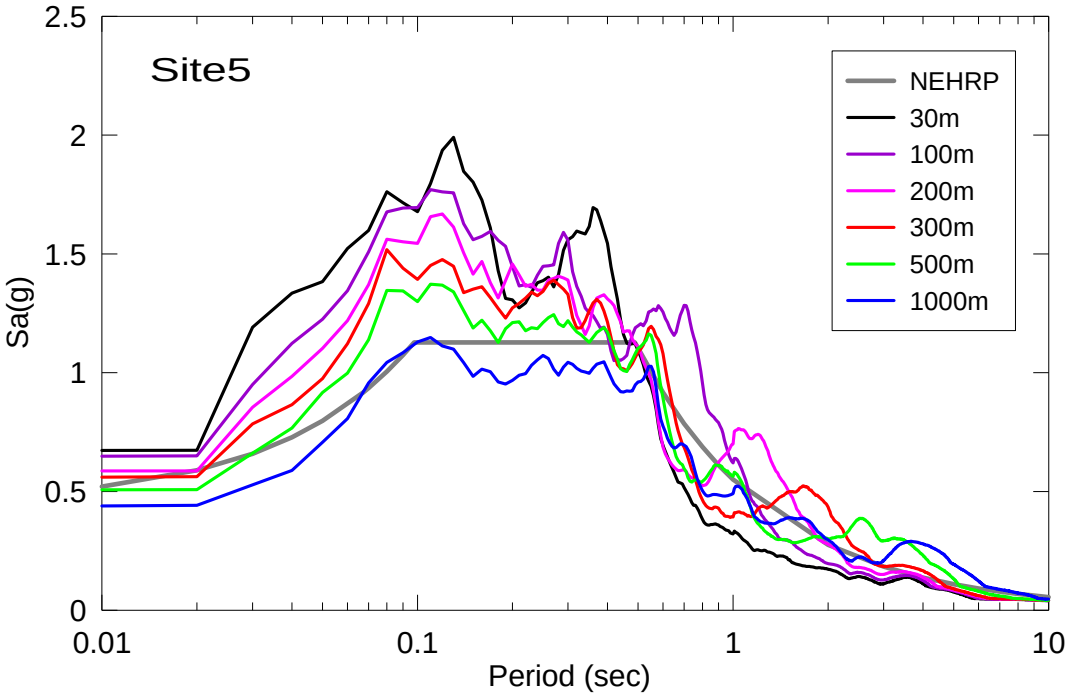

Figure A 14 Computed PSHA(FF)(2011) UHRS for 30m, 100m, 200m, 300m, 500m, 1000m soil-columns and NEHRP design spectra. Lowlands, site 5.

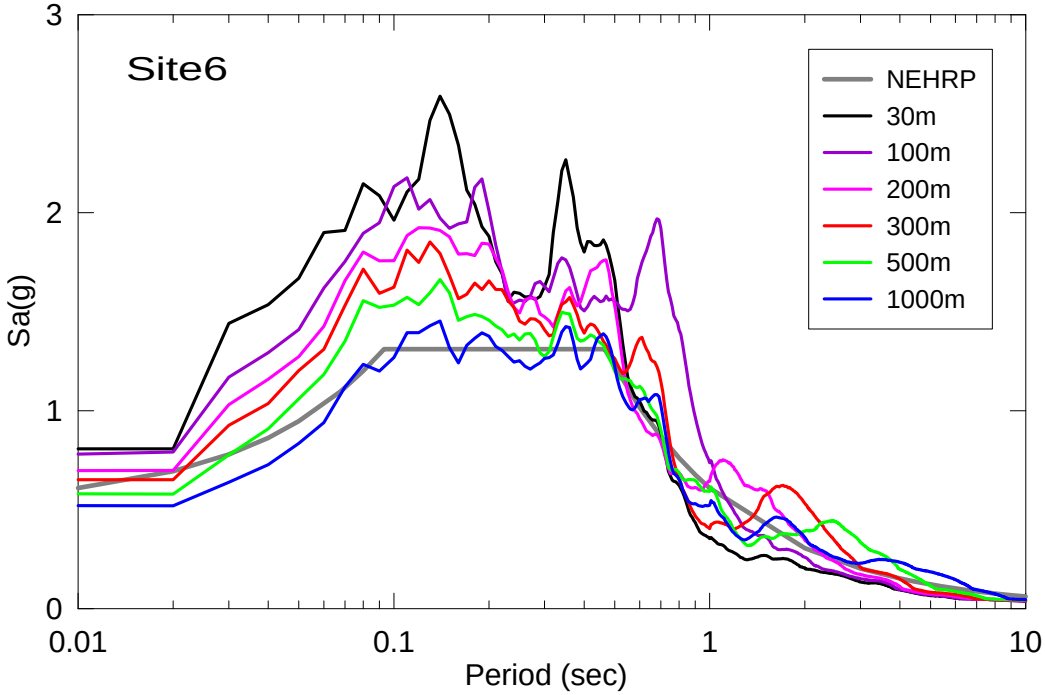

Figure A 15 Computed PSHA(FF)(2011) UHRS for 30m, 100m, 200m, 300m, 500m, 1000m

soil-columns and NEHRP design spectra. Lowlands, site 6.

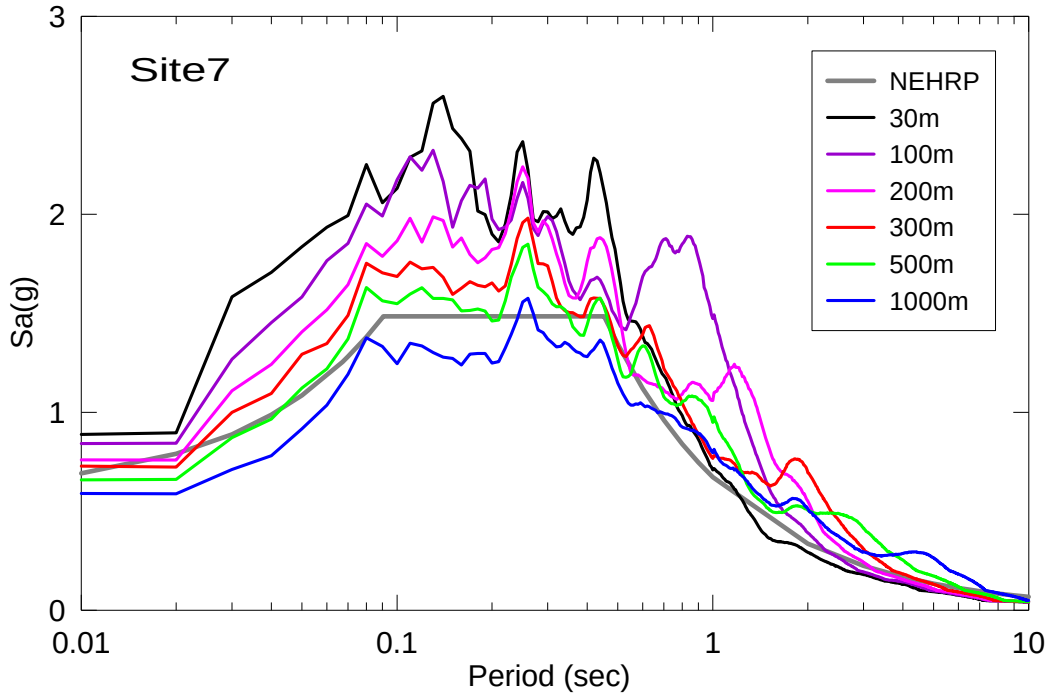

Figure A 16 Computed PSHA(FF)(2011) UHRS for 30m, 100m, 200m, 300m, 500m, 1000m soil-columns and NEHRP design spectra. Lowlands, site 7.

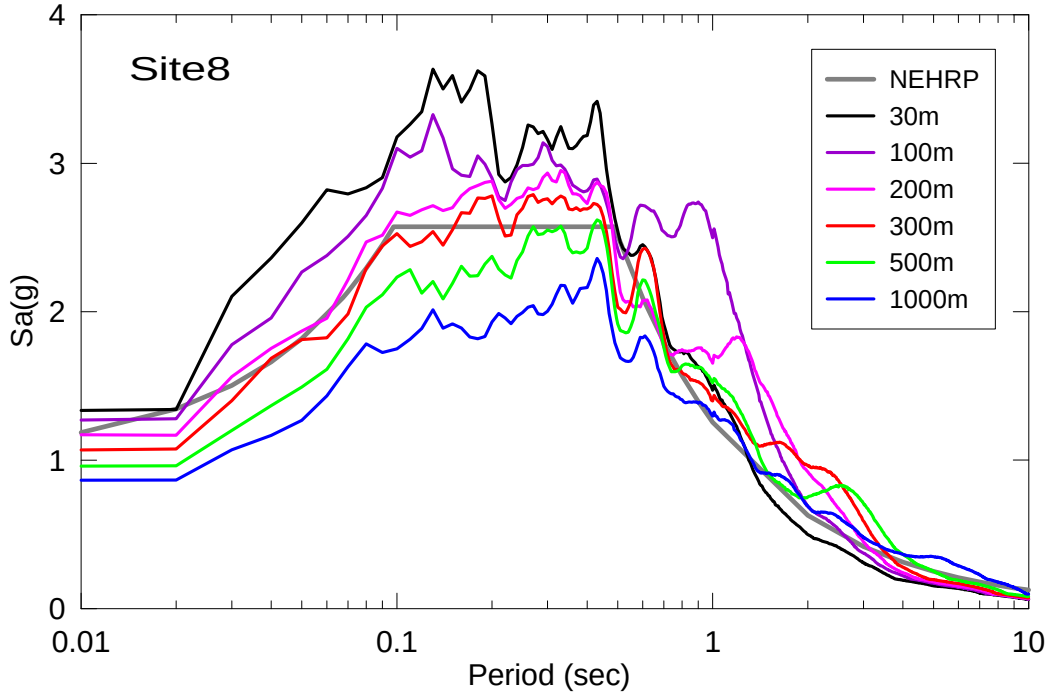

Figure A 17 Computed PSHA(FF)(2011) UHRS for 30m, 100m, 200m, 300m, 500m, 1000m

soil-columns and NEHRP design spectra. Lowlands, site 8.

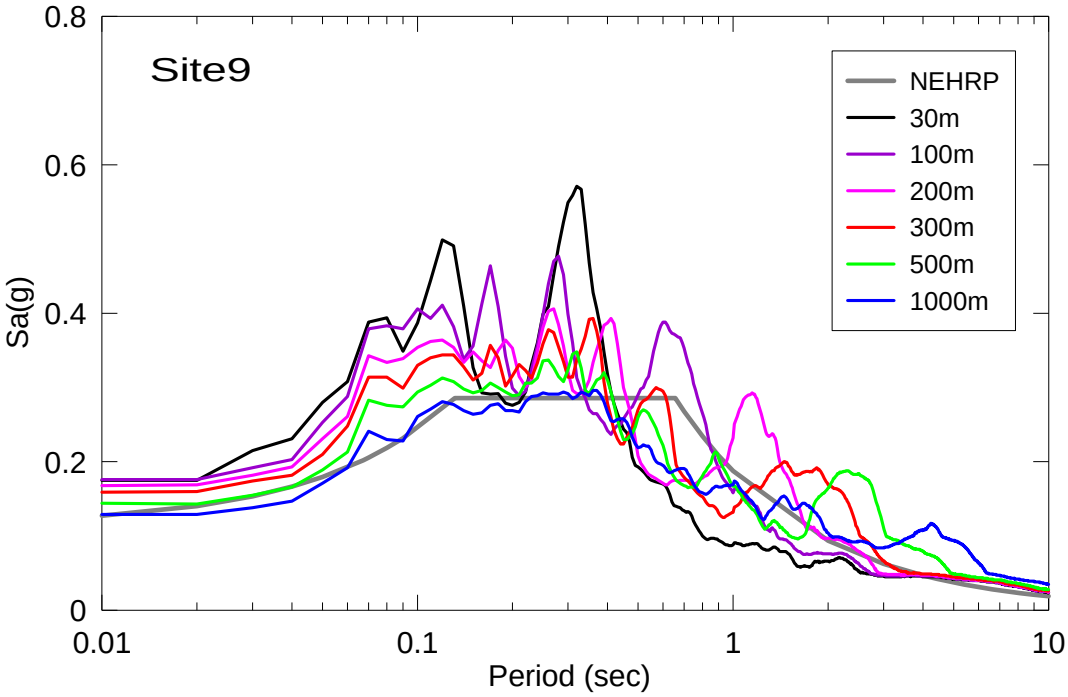

Figure A 18 Computed PSHA(FF)(2011) UHRS for 30m, 100m, 200m, 300m, 500m, 1000m soil-columns and NEHRP design spectra. Lowlands, site 9

APPENDIX B - Site Class D

Comparison of PSHA(FF)(2011) UHRS at different depth soil-columns (30m, 100m, 200m, 300m, 500m, 1000m) and NEHRP design spectra at uplands and lowlands

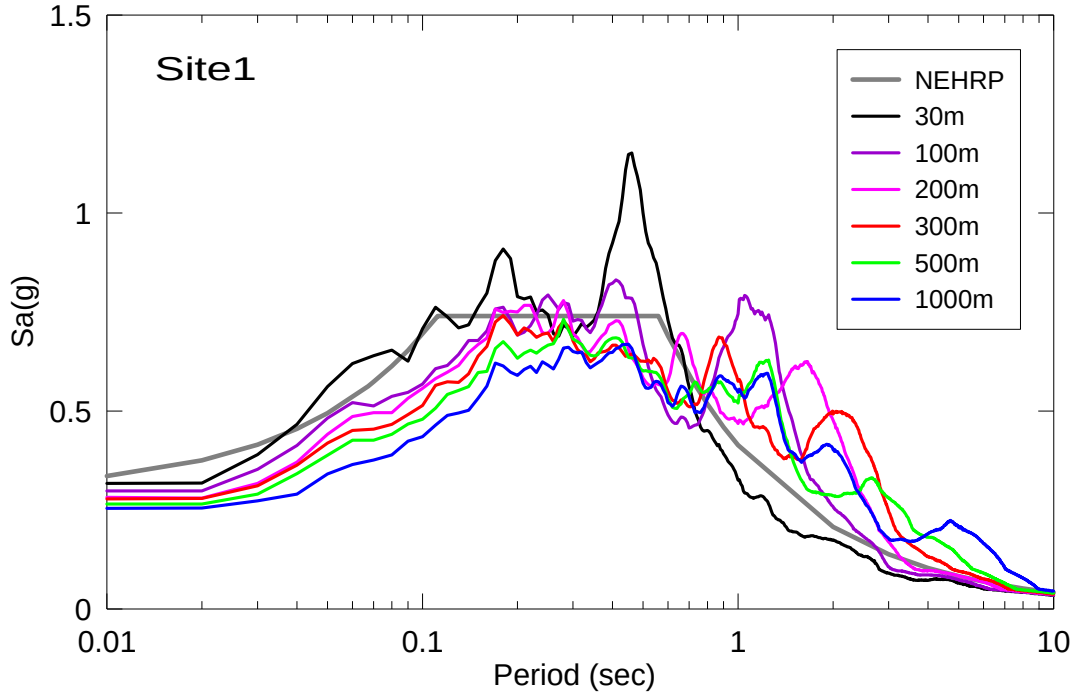

Figure B 1 Computed PSHA(FF)(2011) UHRS for 30m, 100m, 200m, 300m, 500m, 1000m soil-columns and NEHRP design spectra. Uplands, site 1.

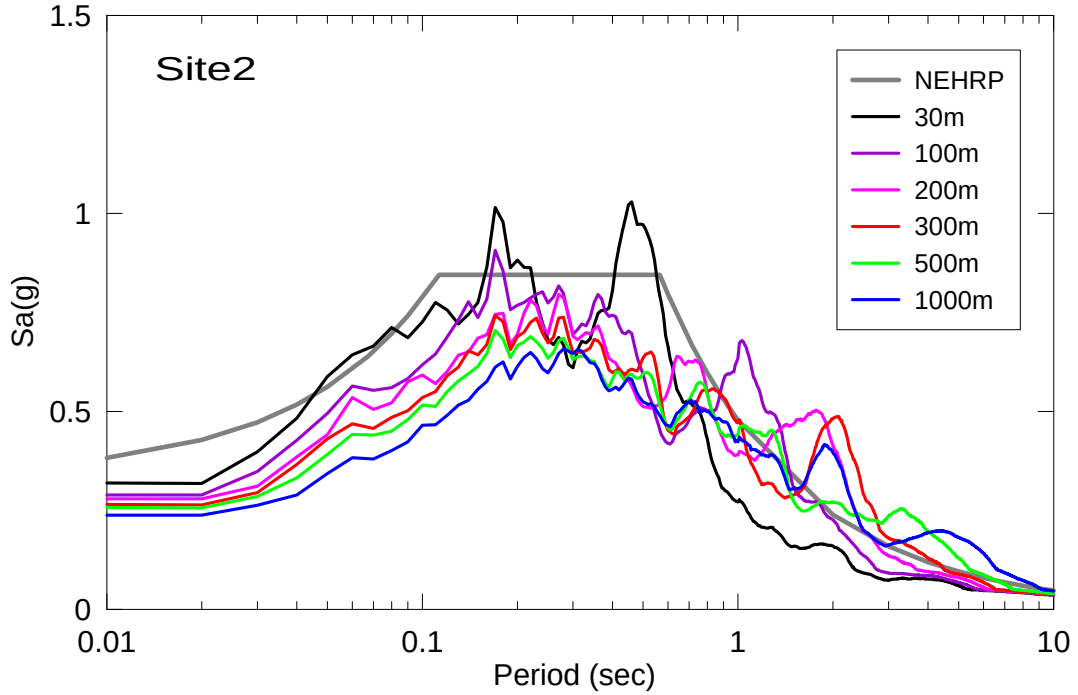

Figure B 2 Computed PSHA(FF)(2011) UHRS for 30m, 100m, 200m, 300m, 500m, 1000m soil-columns and NEHRP design spectra. Uplands, site 2.

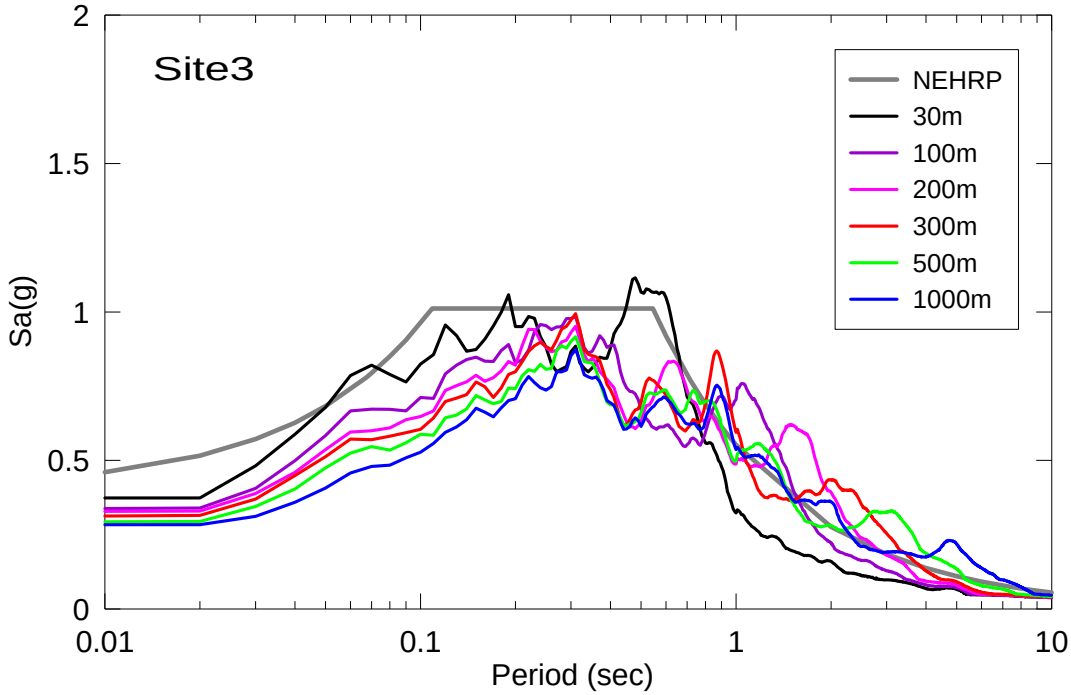

Figure B 3 Computed PSHA(FF)(2011) UHRS for 30m, 100m, 200m, 300m, 500m, 1000m soil-columns and NEHRP design spectra. Uplands, site 3.

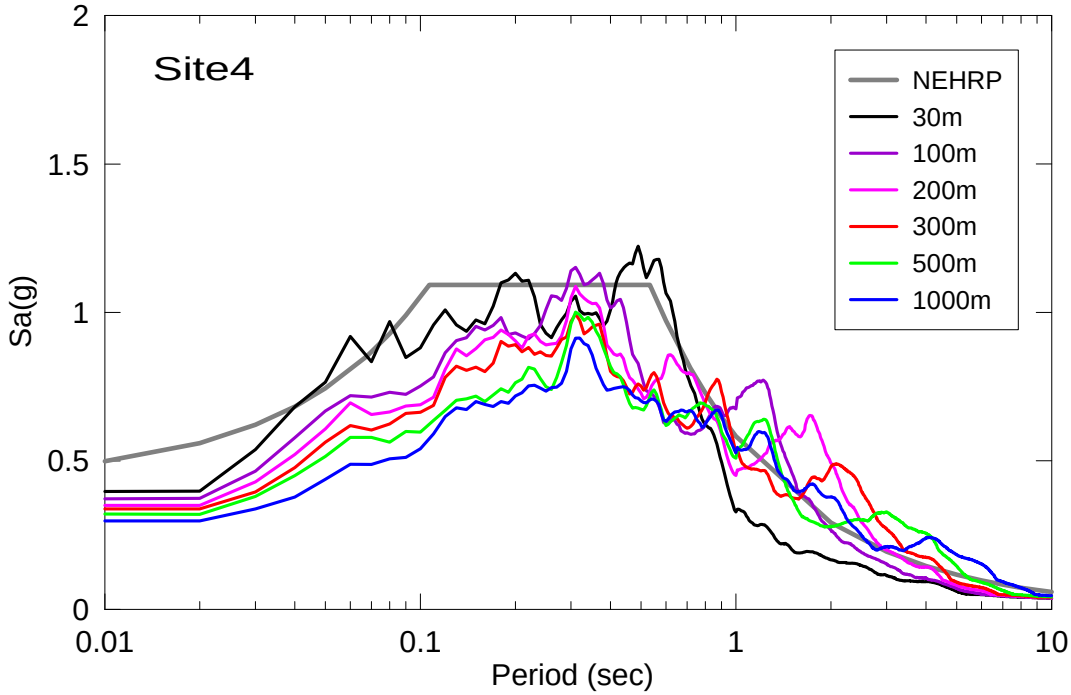

Figure B 4 Computed PSHA(FF)(2011) UHRS for 30m, 100m, 200m, 300m, 500m, 1000m soil-columns and NEHRP design spectra. Uplands, site 4.

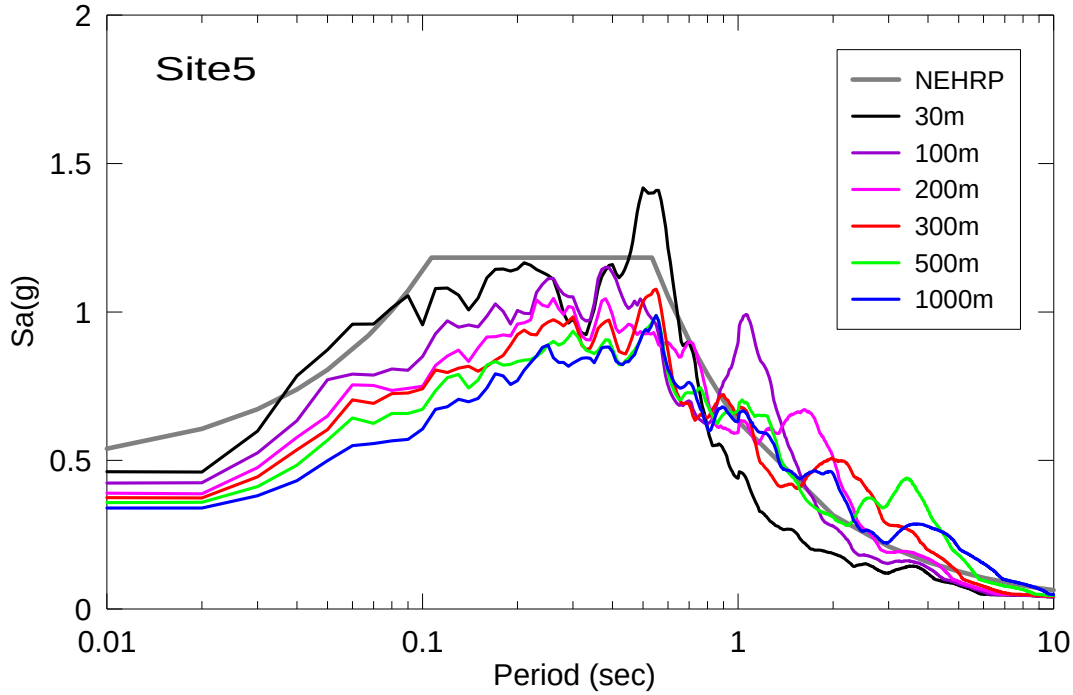

Figure B 5 Computed PSHA(FF)(2011) UHRS for 30m, 100m, 200m, 300m, 500m, 1000m soil-columns and NEHRP design spectra. Uplands, site 5.

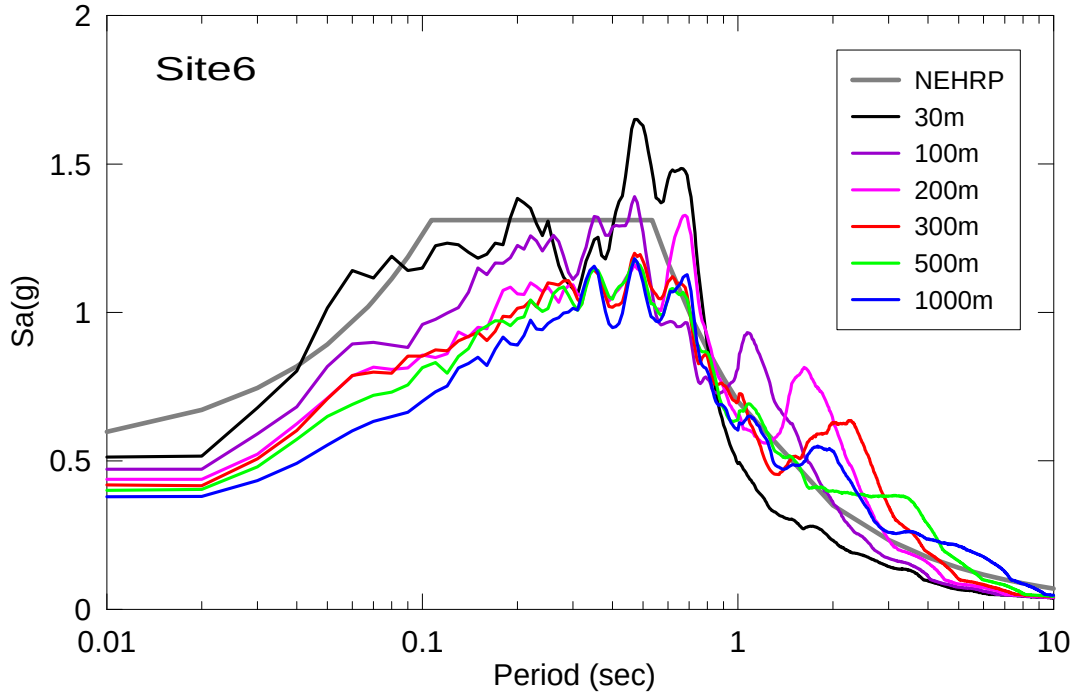

Figure B 6 Computed PSHA(FF)(2011) UHRS for 30m, 100m, 200m, 300m, 500m, 1000m soil-columns and NEHRP design spectra. Uplands, site 6.

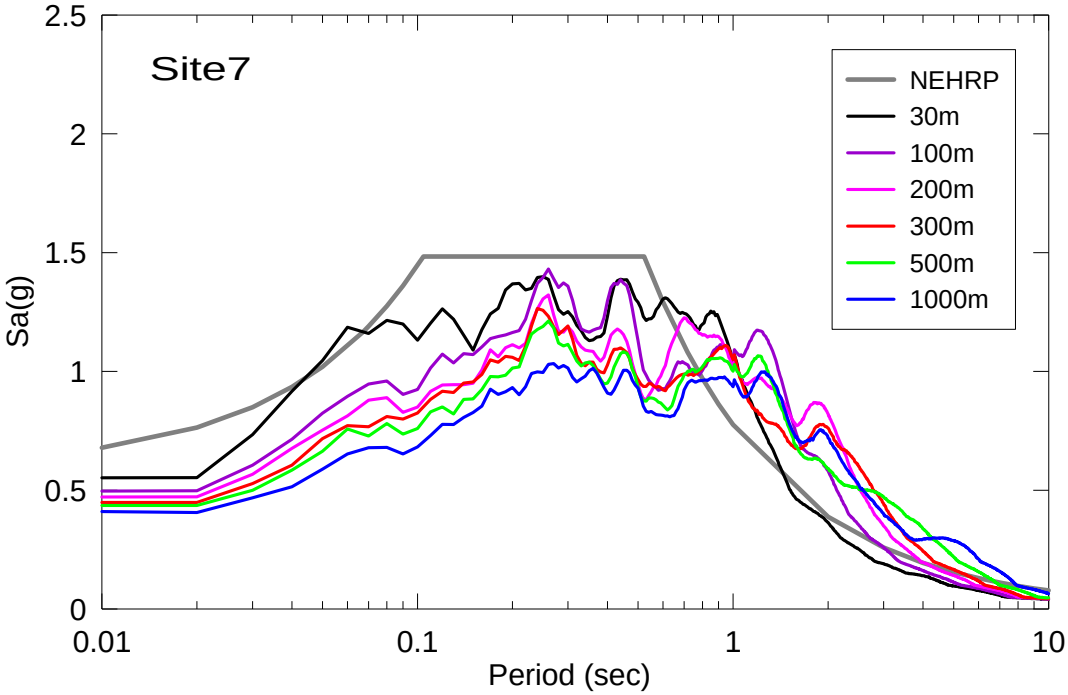

Figure B 7 Computed PSHA(FF)(2011) UHRS for 30m, 100m, 200m, 300m, 500m, 1000m soil-columns and NEHRP design spectra. Uplands, site 7.

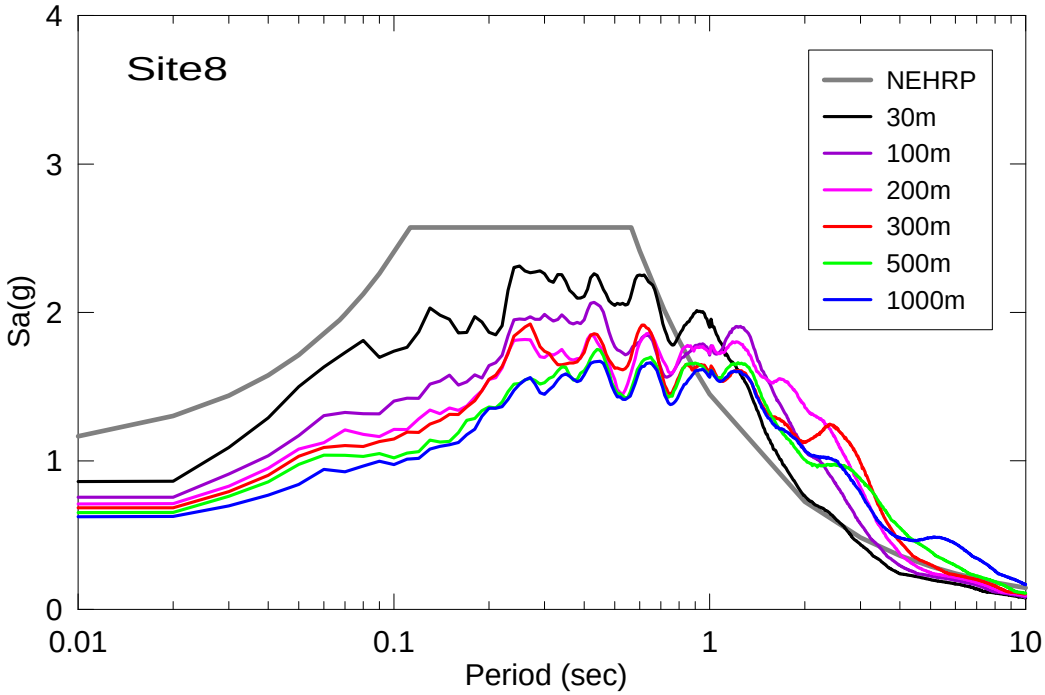

Figure B 8 Computed PSHA(FF)(2011) UHRS for 30m, 100m, 200m, 300m, 500m, 1000m soil-columns and NEHRP design spectra. Uplands, site 8.

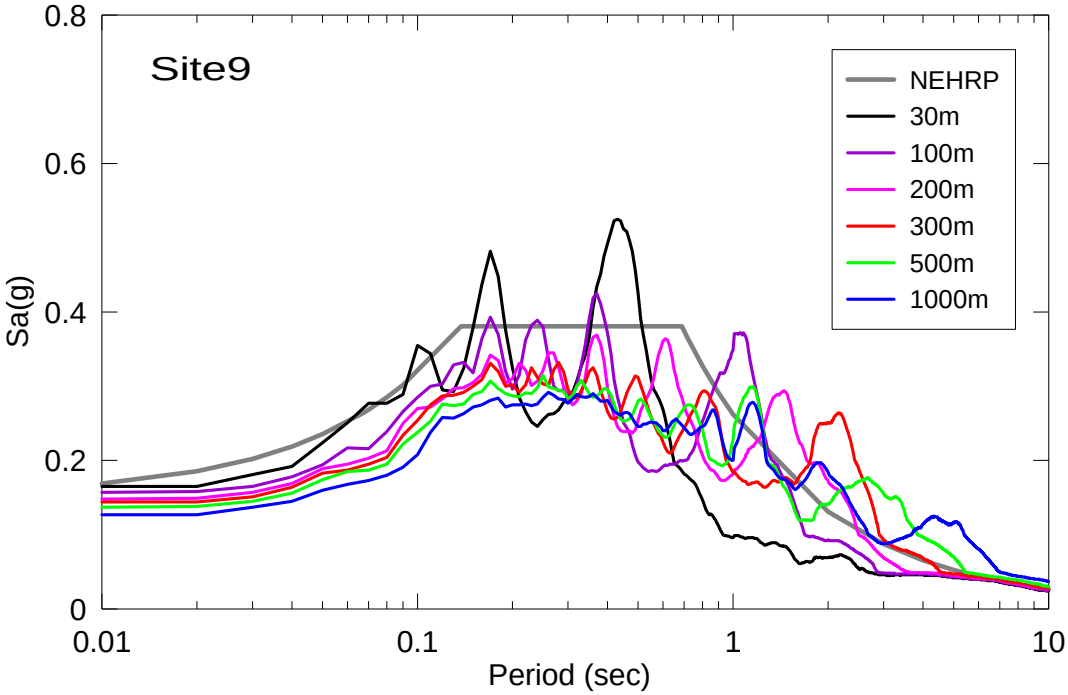

Figure B 9 Computed PSHA(FF)(2011) UHRS for 30m, 100m, 200m, 300m, 500m, 1000m soil-columns and NEHRP design spectra. Uplands, site 9.

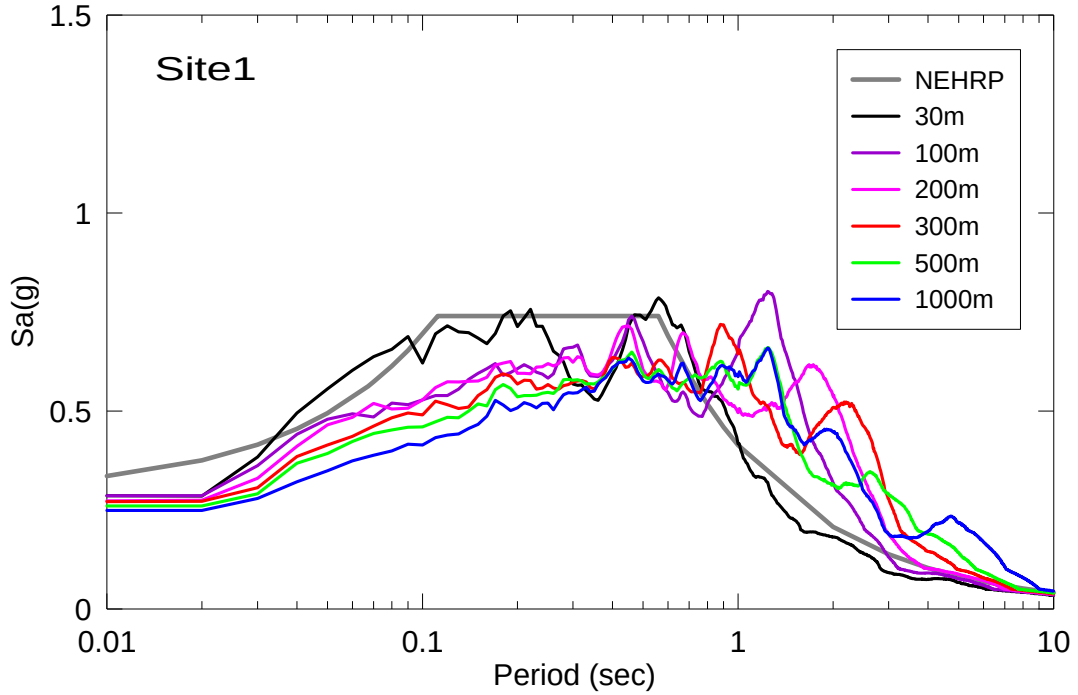

Figure B 10 Computed PSHA(FF)(2011) UHRS for 30m, 100m, 200m, 300m, 500m, 1000m soil-columns and NEHRP design spectra. Lowlands, site 1.

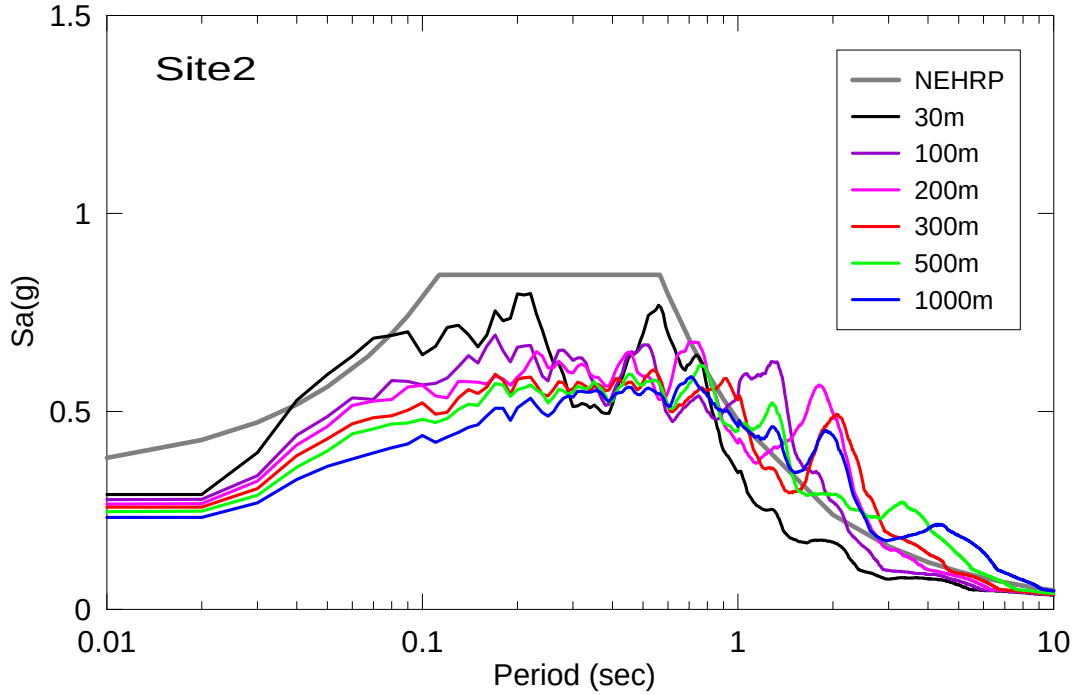

Figure B 11 Computed PSHA(FF)(2011) UHRS for 30m, 100m, 200m, 300m, 500m, 1000m soil-columns and NEHRP design spectra. Lowlands, site 2.

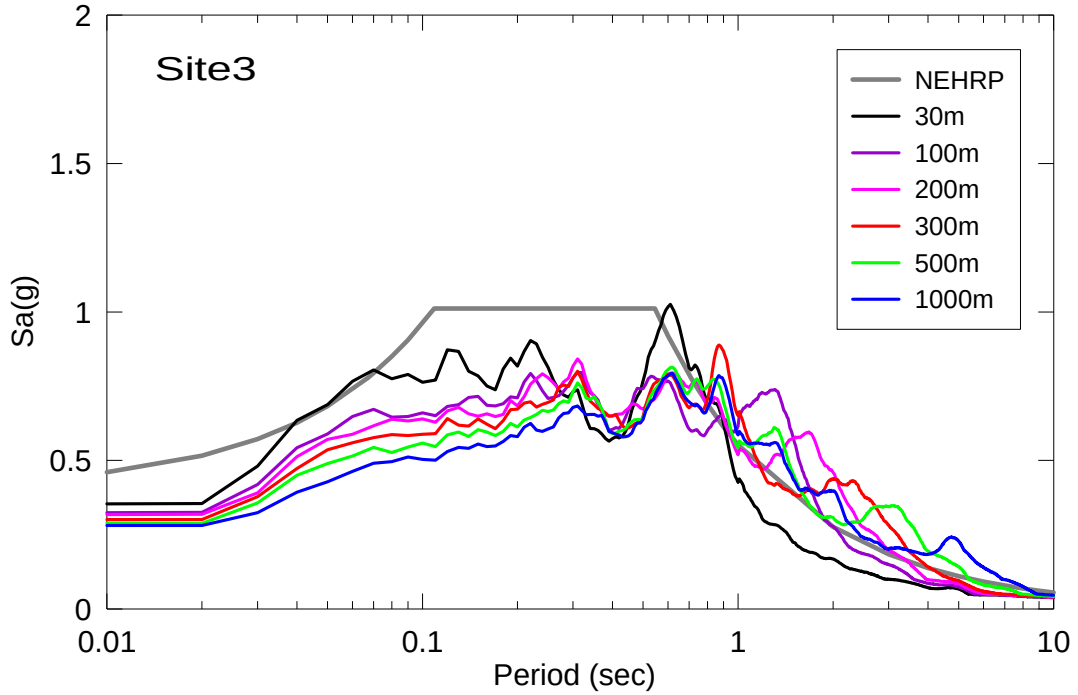

Figure B 12 Computed PSHA(FF)(2011) UHRS for 30m, 100m, 200m, 300m, 500m, 1000m soil-columns and NEHRP design spectra. Lowlands, site 3.

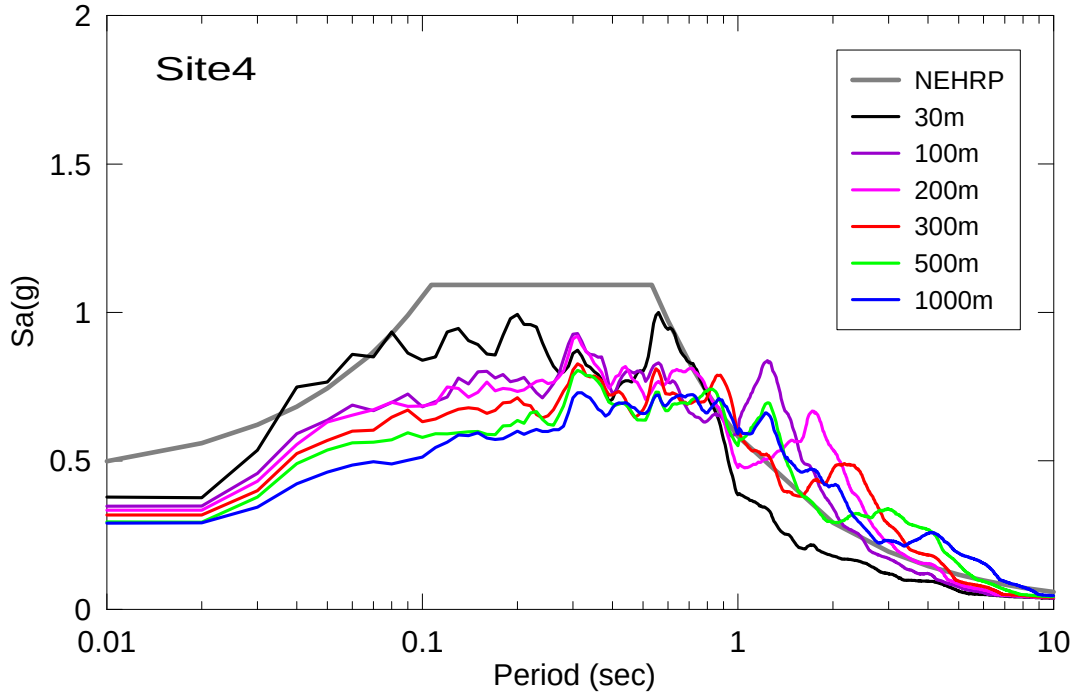

Figure B 13 Computed PSHA(FF)(2011) UHRS for 30m, 100m, 200m, 300m, 500m, 1000m soil-columns and NEHRP design spectra. Lowlands, site 4.

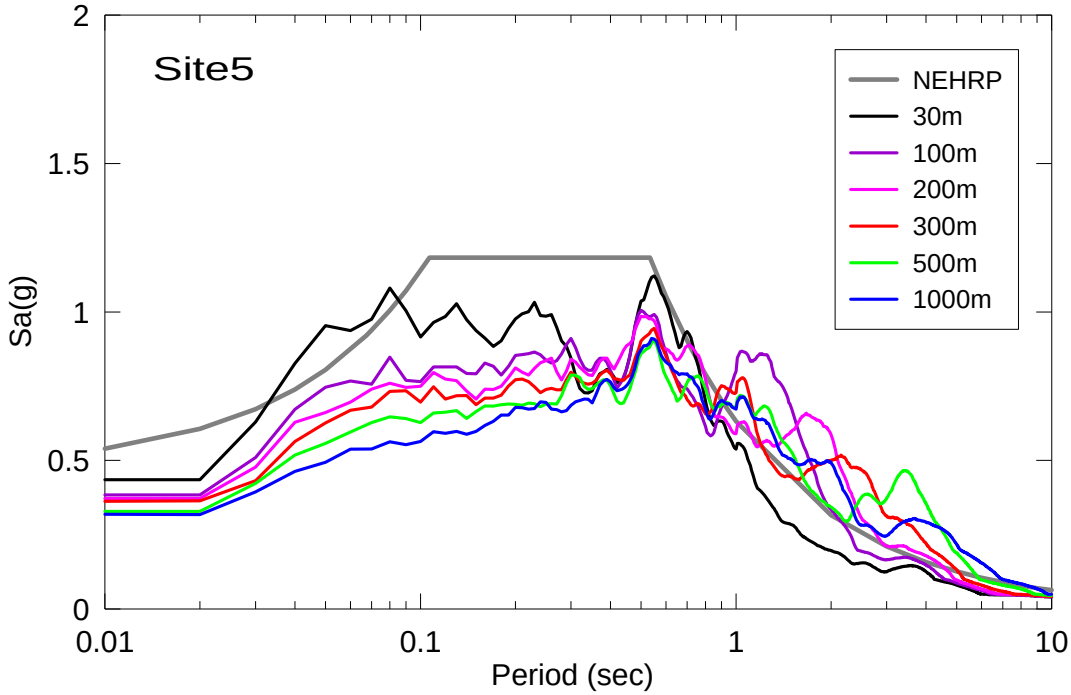

Figure B 14 Computed PSHA(FF)(2011) UHRS for 30m, 100m, 200m, 300m, 500m, 1000m soil-columns and NEHRP design spectra. Lowlands, site 5.

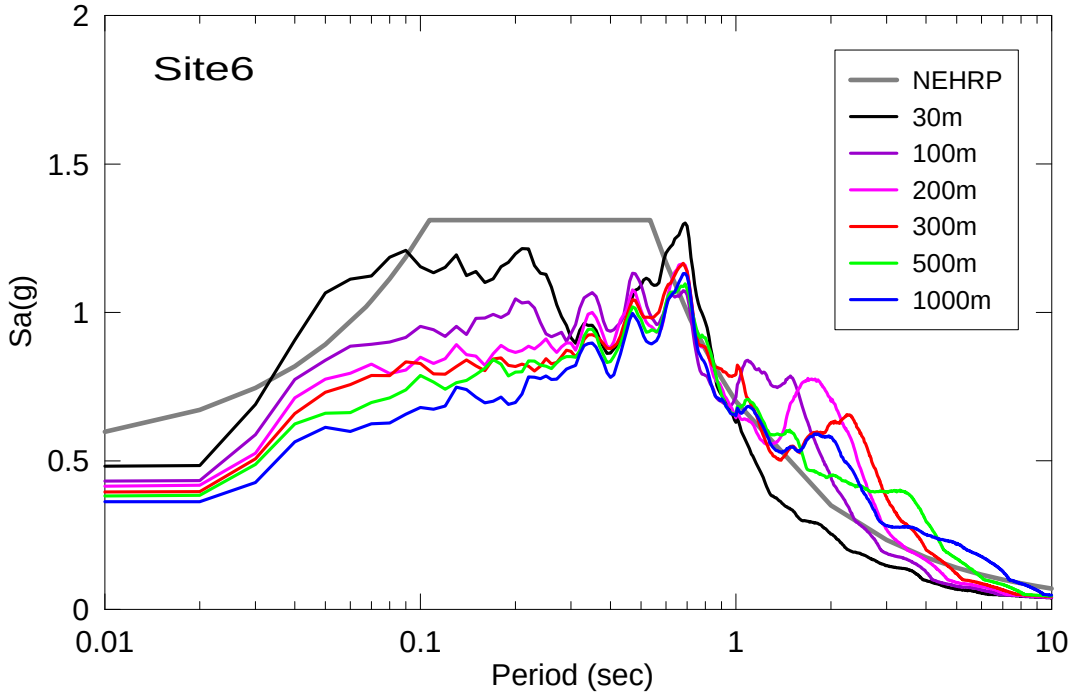

Figure B 15 Computed PSHA(FF)(2011) UHRS for 30m, 100m, 200m, 300m, 500m, 1000m soil-columns and NEHRP design spectra. Lowlands, site 6.

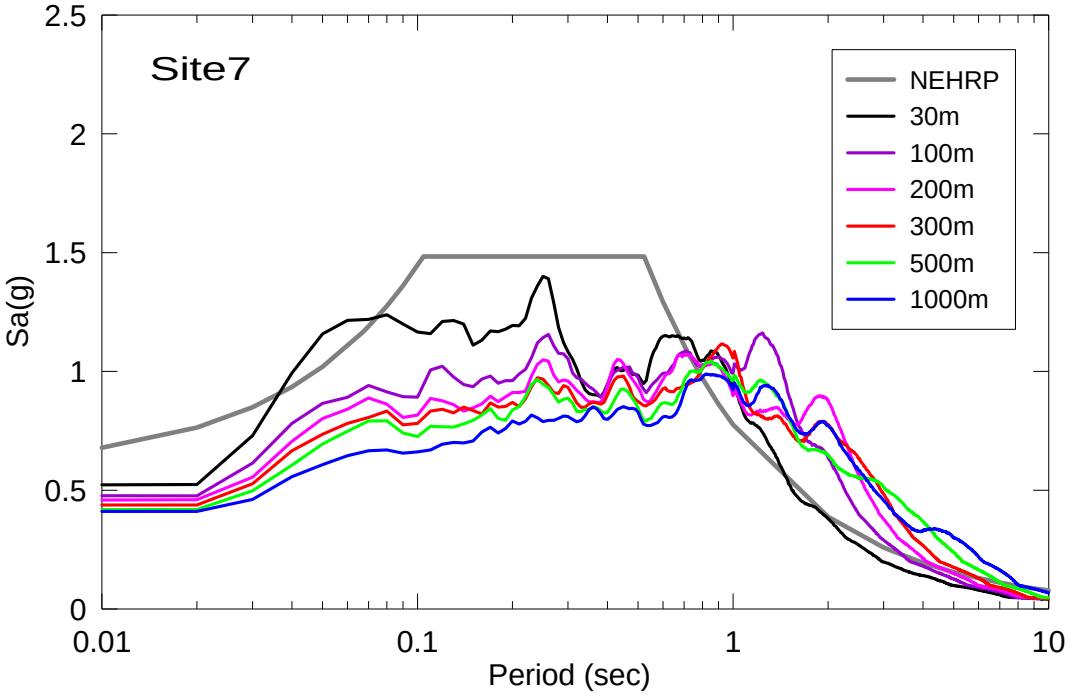

Figure B 16 Computed PSHA(FF)(2011) UHRS for 30m, 100m, 200m, 300m, 500m, 1000m soil-columns and NEHRP design spectra. Lowlands, site 7.

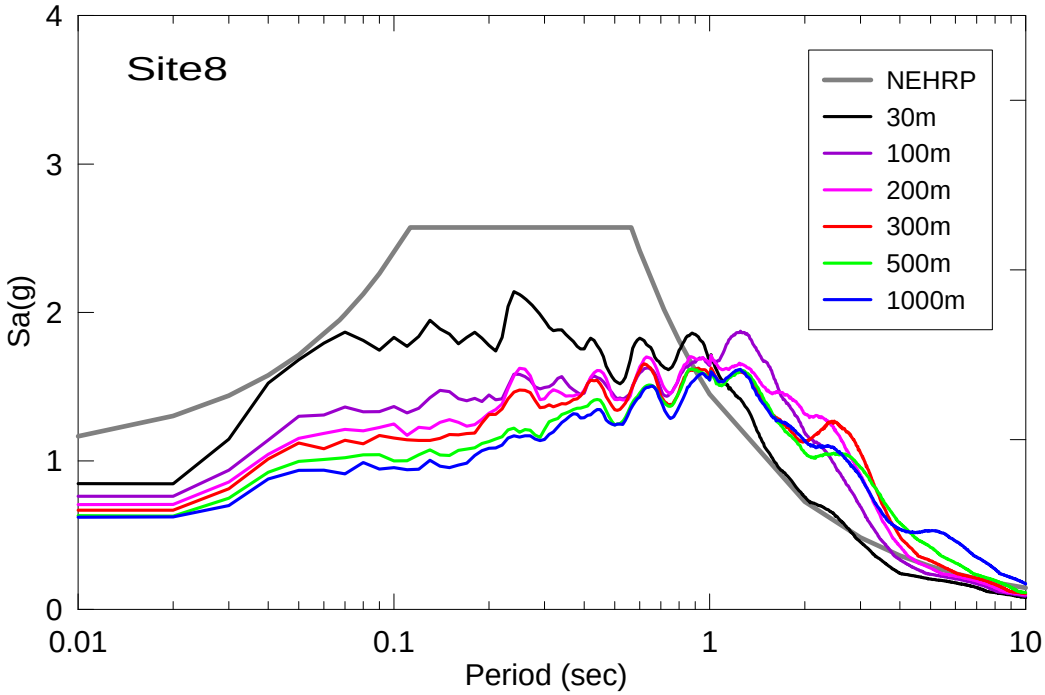

Figure B 17 Computed PSHA(FF)(2011) UHRS for 30m, 100m, 200m, 300m, 500m, 1000m soil-columns and NEHRP design spectra. Lowlands, site 8.

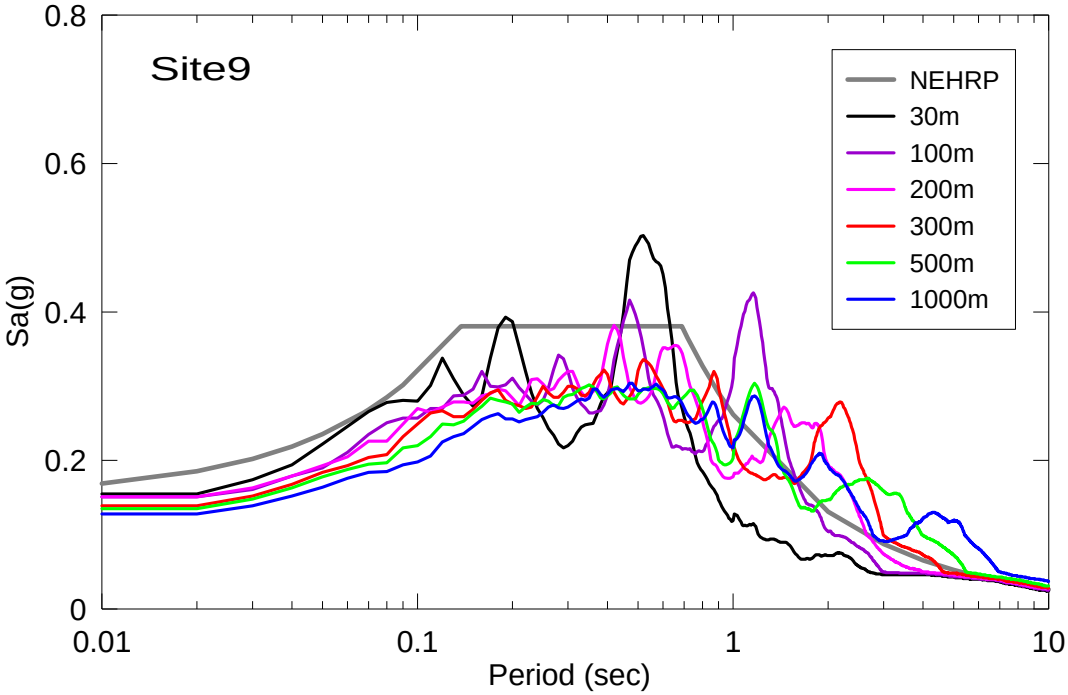

Figure B 18 Computed PSHA(FF)(2011) UHRS for 30m, 100m, 200m, 300m, 500m, 1000m soil-columns and NEHRP design spectra. Lowlands, site 9

APPENDIX C - Site Class E

Comparison of PSHA(FF)(2011) UHRS at different depth soil-columns (30m, 100m, 200m, 300m, 500m, 1000m) and NEHRP design spectra at uplands and lowlands

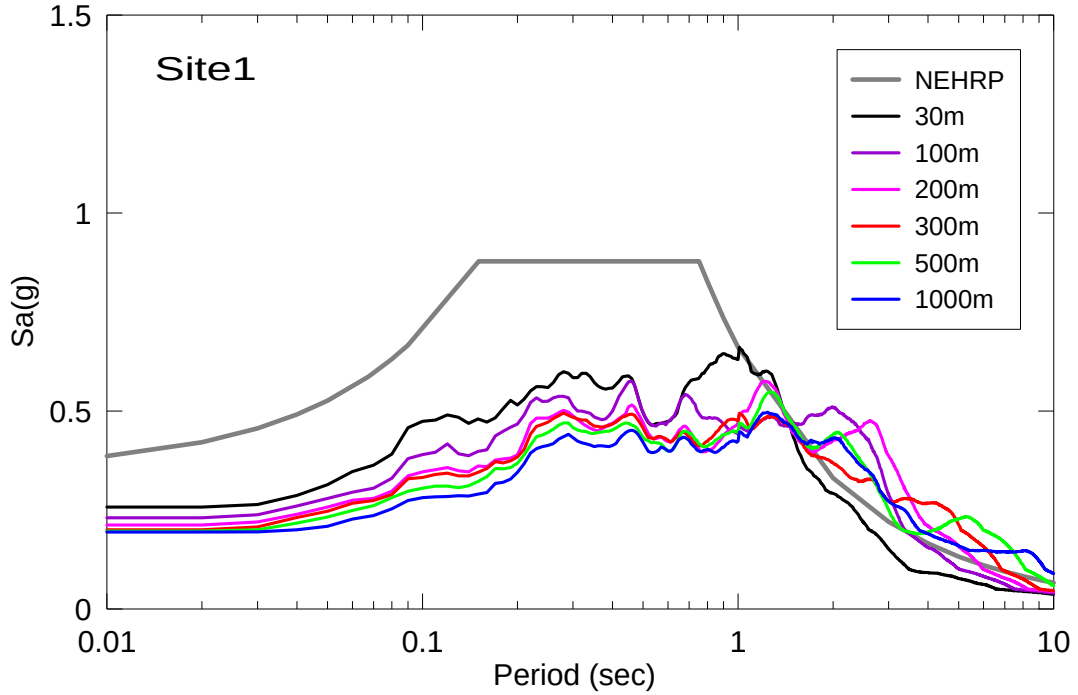

Figure C 1 Computed PSHA(FF)(2011) UHRS for 30m, 100m, 200m, 300m, 500m, 1000m soil-columns and NEHRP design spectra. Uplands, site 1.

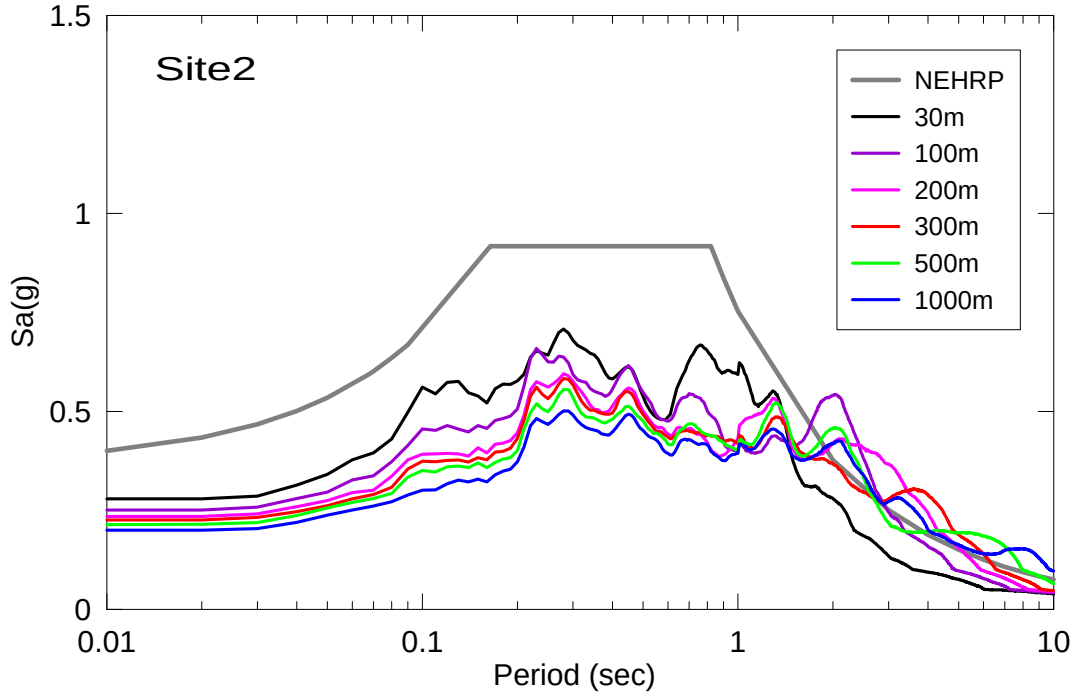

Figure C 2 Computed PSHA(FF)(2011) UHRS for 30m, 100m, 200m, 300m, 500m, 1000m soil-columns and NEHRP design spectra. Uplands, site 2.

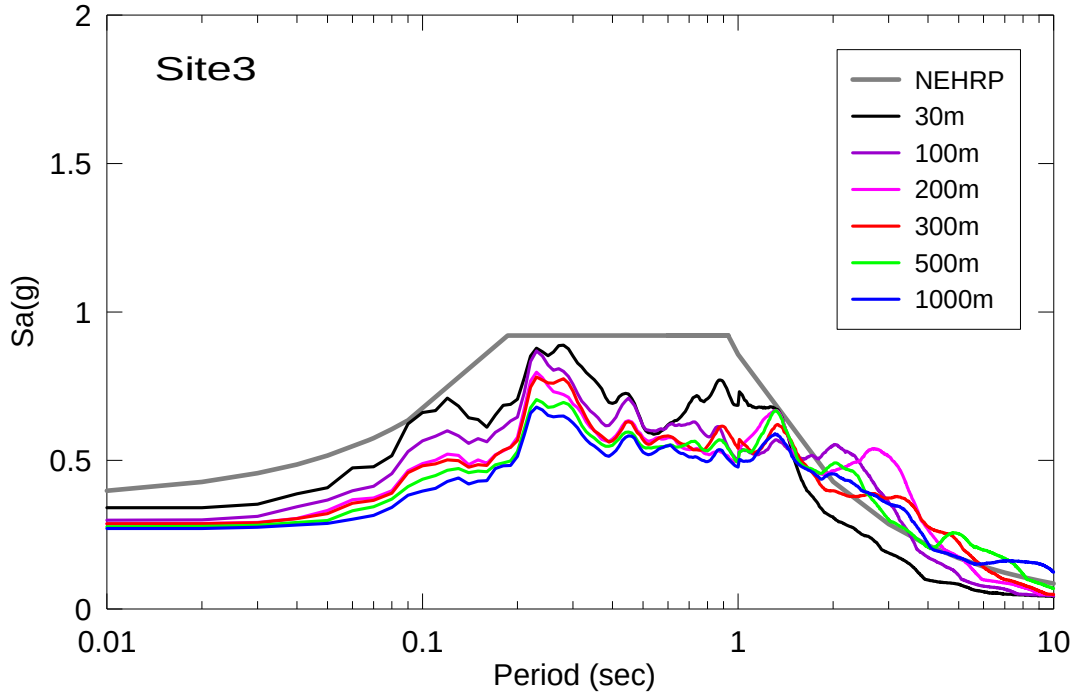

Figure C 3 Computed PSHA(FF)(2011) UHRS for 30m, 100m, 200m, 300m, 500m, 1000m soil-columns and NEHRP design spectra. Uplands, site 3.

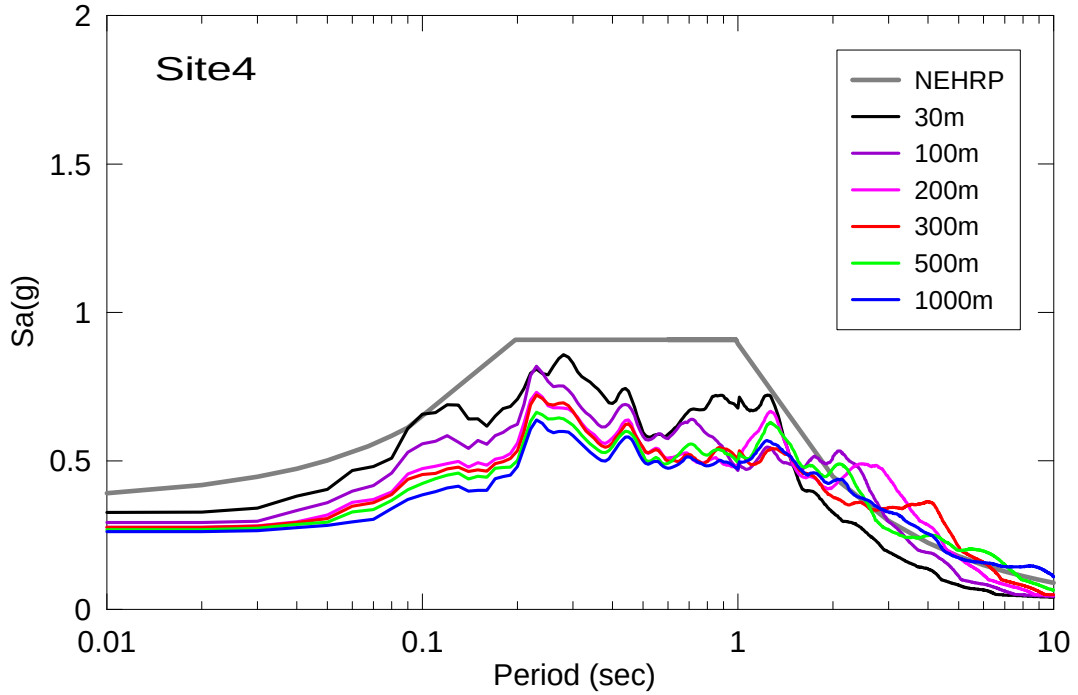

Figure C 4 Computed PSHA(FF)(2011) UHRS for 30m, 100m, 200m, 300m, 500m, 1000m soil-columns and NEHRP design spectra. Uplands, site 4.

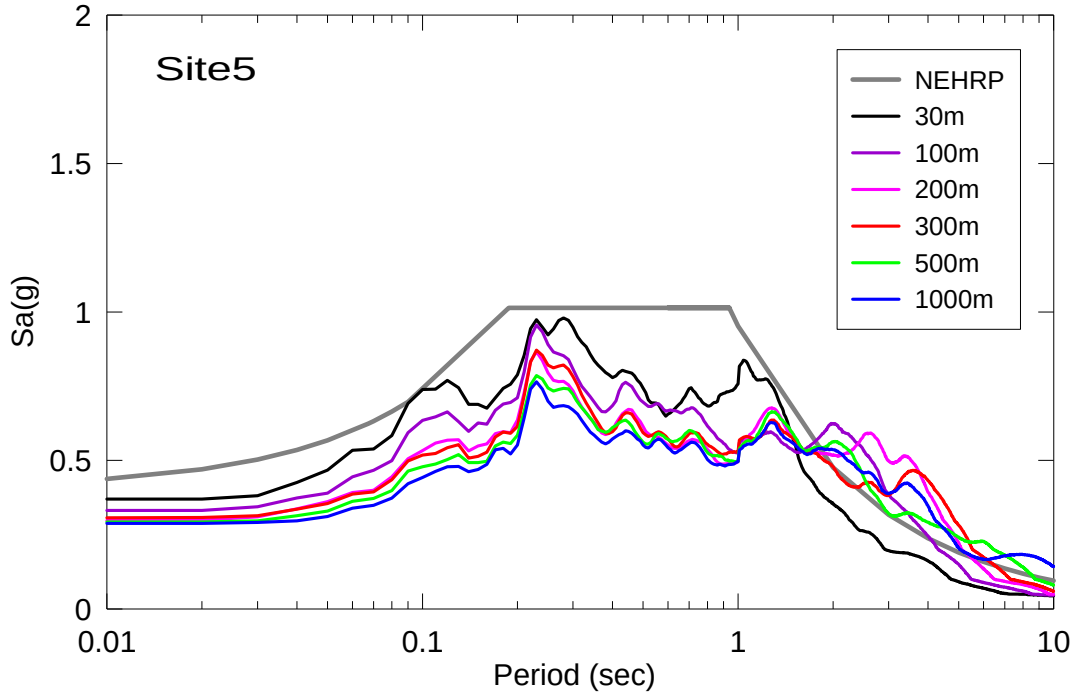

Figure C 5 Computed PSHA(FF)(2011) UHRS for 30m, 100m, 200m, 300m, 500m, 1000m soil-columns and NEHRP design spectra. Uplands, site 5.

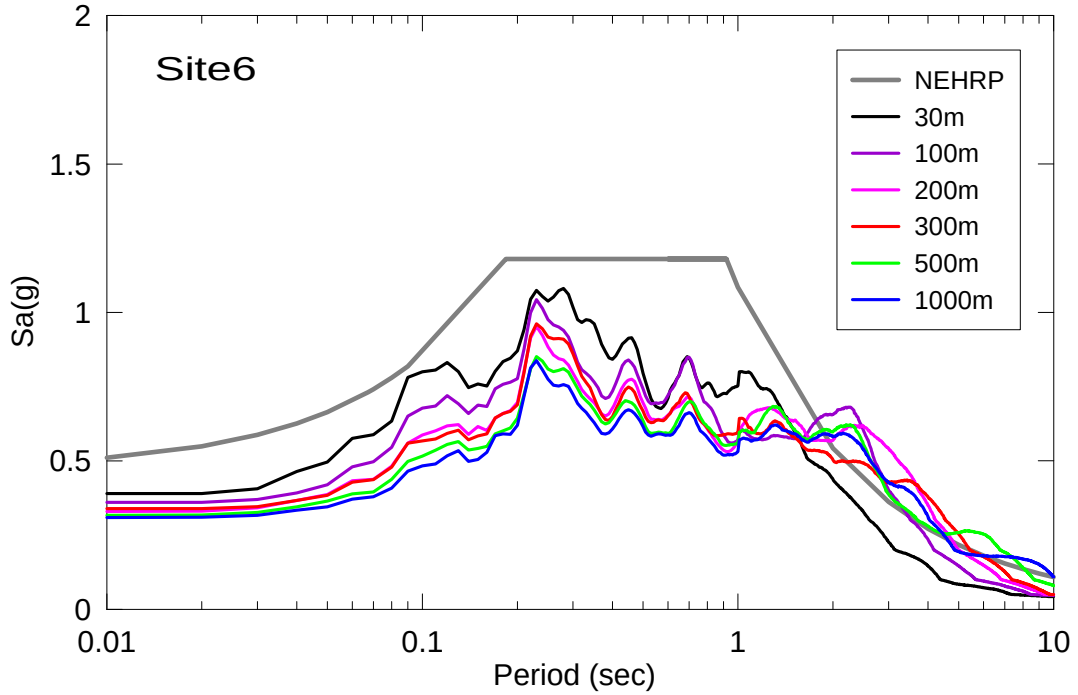

Figure C 6 Computed PSHA(FF)(2011) UHRS for 30m, 100m, 200m, 300m, 500m, 1000m soil-columns and NEHRP design spectra. Uplands, site 6.

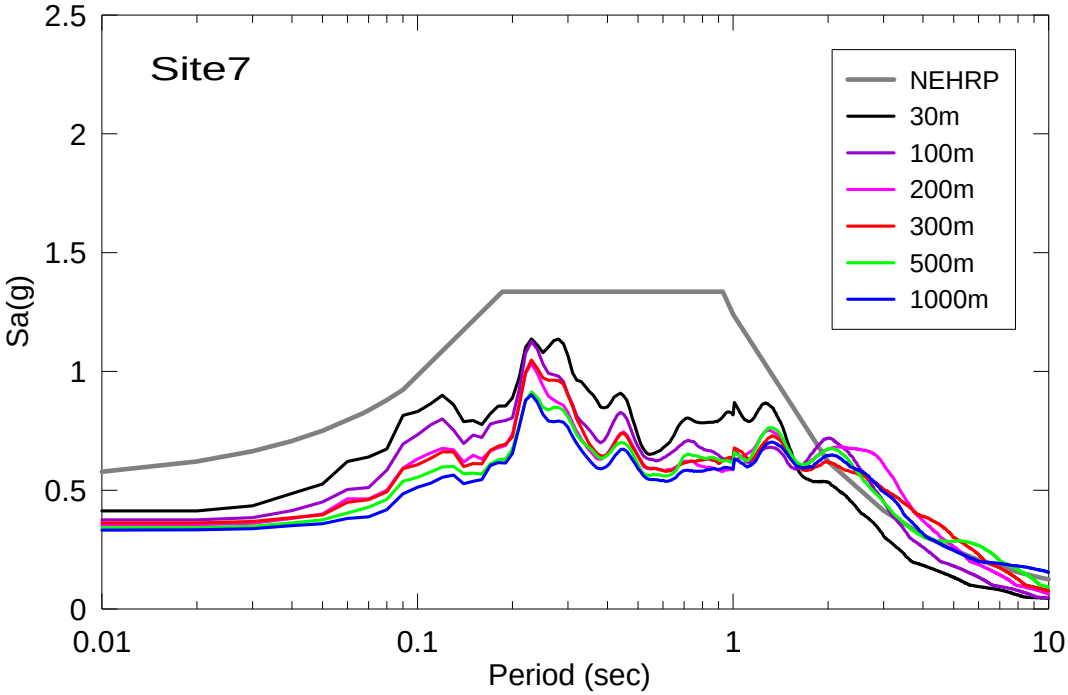

Figure C 7 Computed PSHA(FF)(2011) UHRS for 30m, 100m, 200m, 300m, 500m, 1000m soil-columns and NEHRP design spectra. Uplands, site 7.

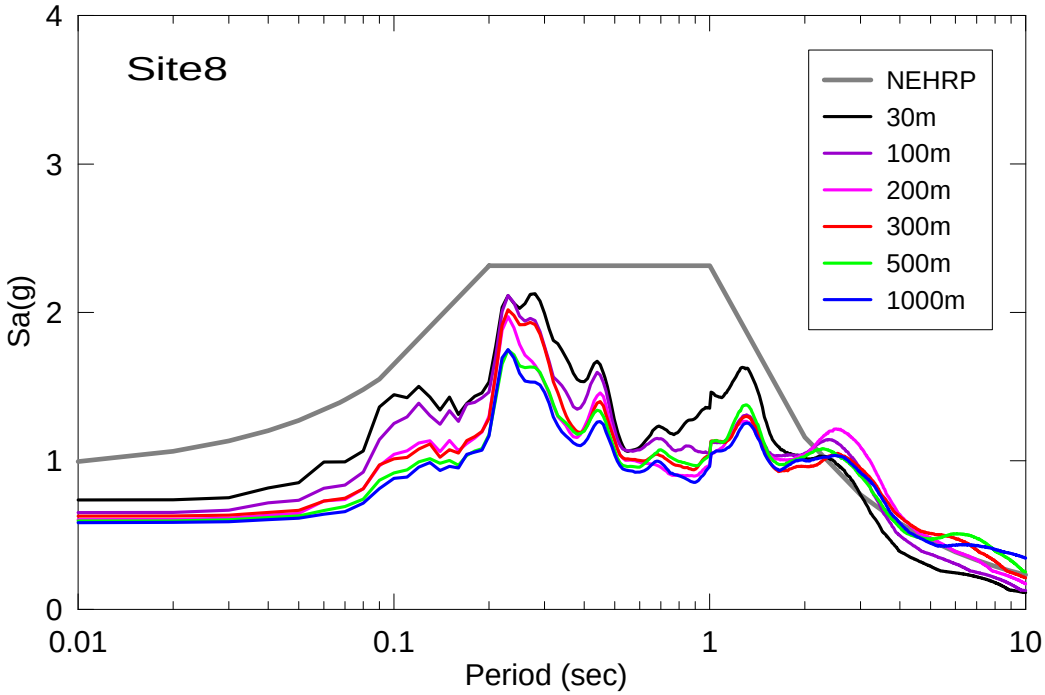

Figure C 8 Computed PSHA(FF)(2011) UHRS for 30m, 100m, 200m, 300m, 500m, 1000m soil-columns and NEHRP design spectra. Uplands, site 8.

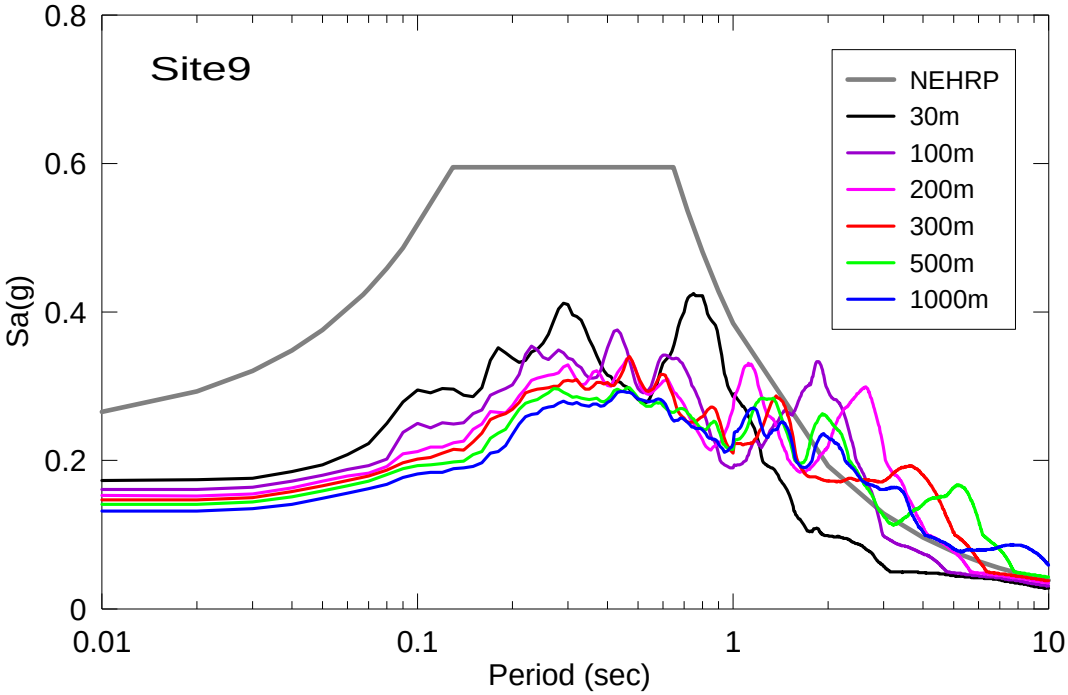

Figure C 9 Computed PSHA(FF)(2011) UHRS for 30m, 100m, 200m, 300m, 500m, 1000m soil-columns and NEHRP design spectra. Uplands, site 9.

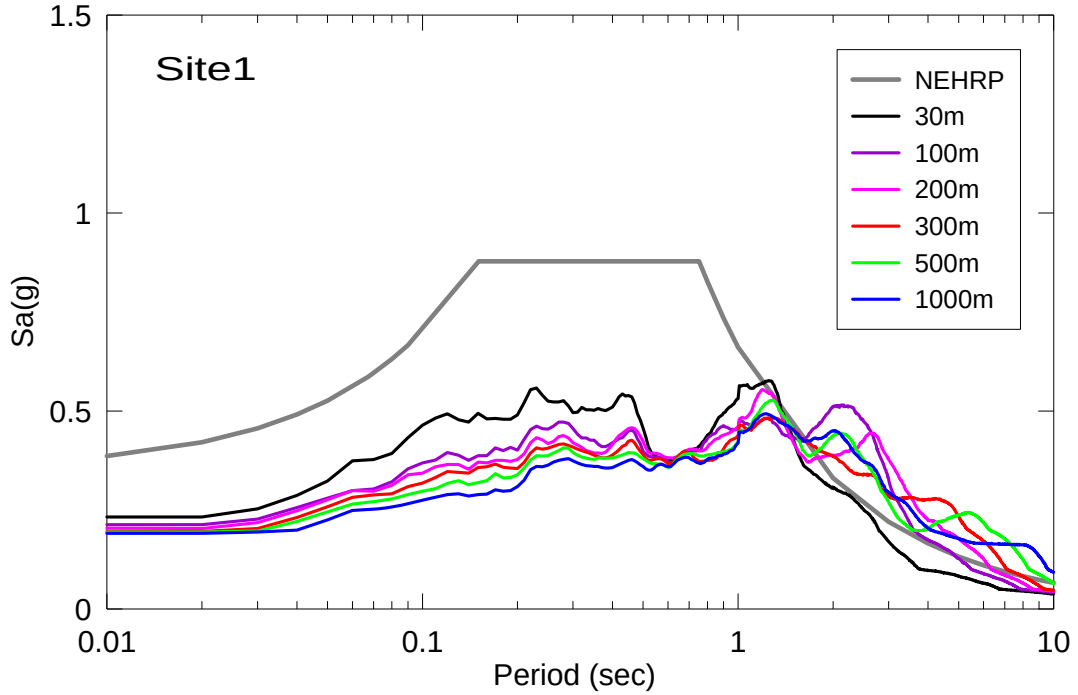

Figure C 10 Computed PSHA(FF)(2011) UHRS for 30m, 100m, 200m, 300m, 500m, 1000m soil-columns and NEHRP design spectra. Lowlands, site 1.

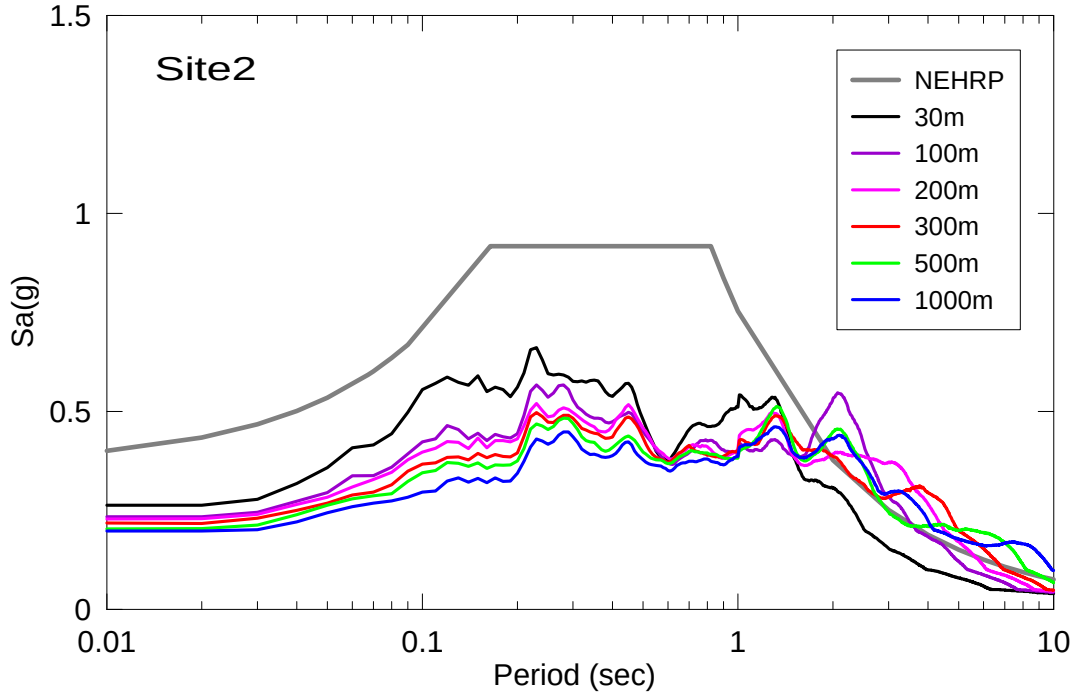

Figure C 11 Computed PSHA(FF)(2011) UHRS for 30m, 100m, 200m, 300m, 500m, 1000m soil-columns and NEHRP design spectra. Lowlands, site 2.

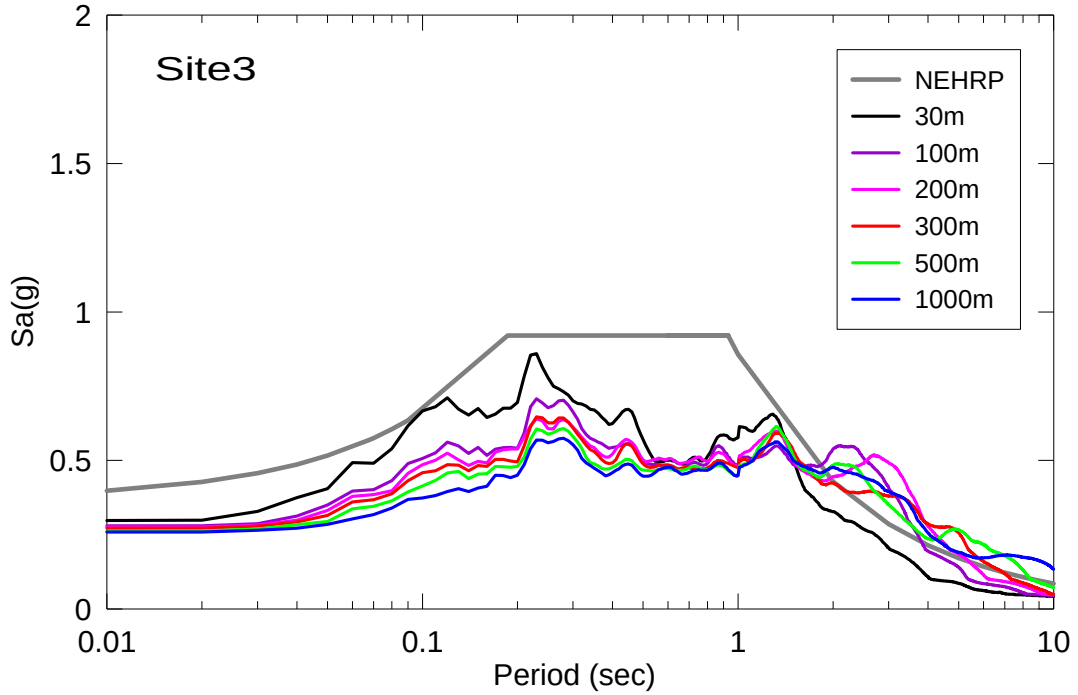

Figure C 12 Computed PSHA(FF)(2011) UHRS for 30m, 100m, 200m, 300m, 500m, 1000m soil-columns and NEHRP design spectra. Lowlands, site 3.

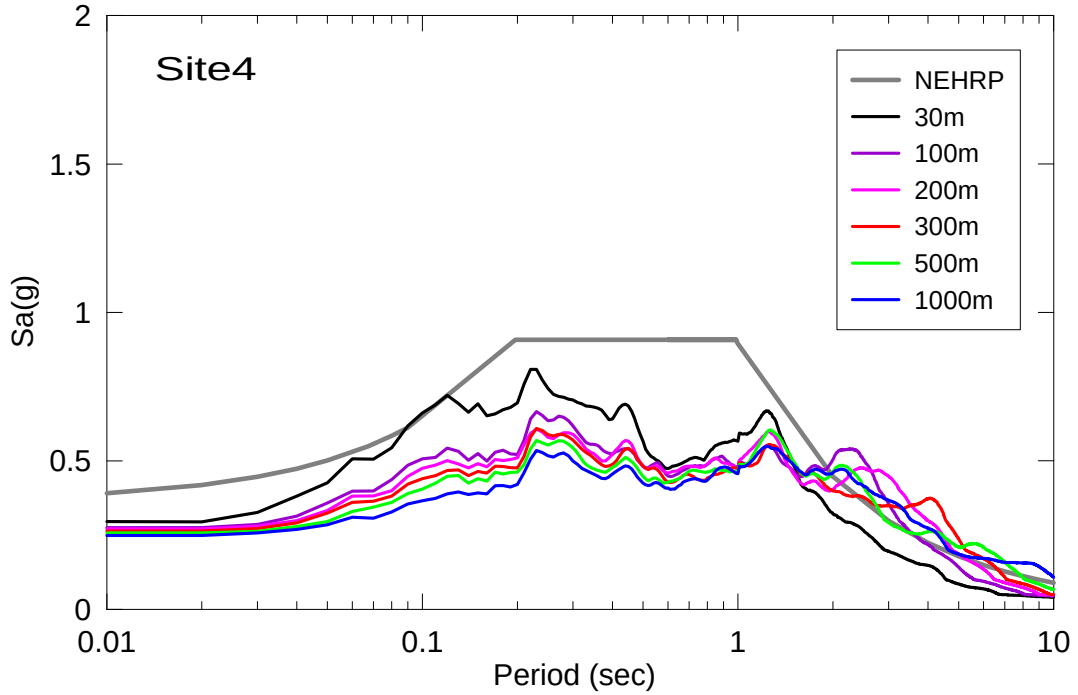

Figure C 13 Computed PSHA(FF)(2011) UHRS for 30m, 100m, 200m, 300m, 500m, 1000m soil-columns and NEHRP design spectra. Lowlands, site 4.

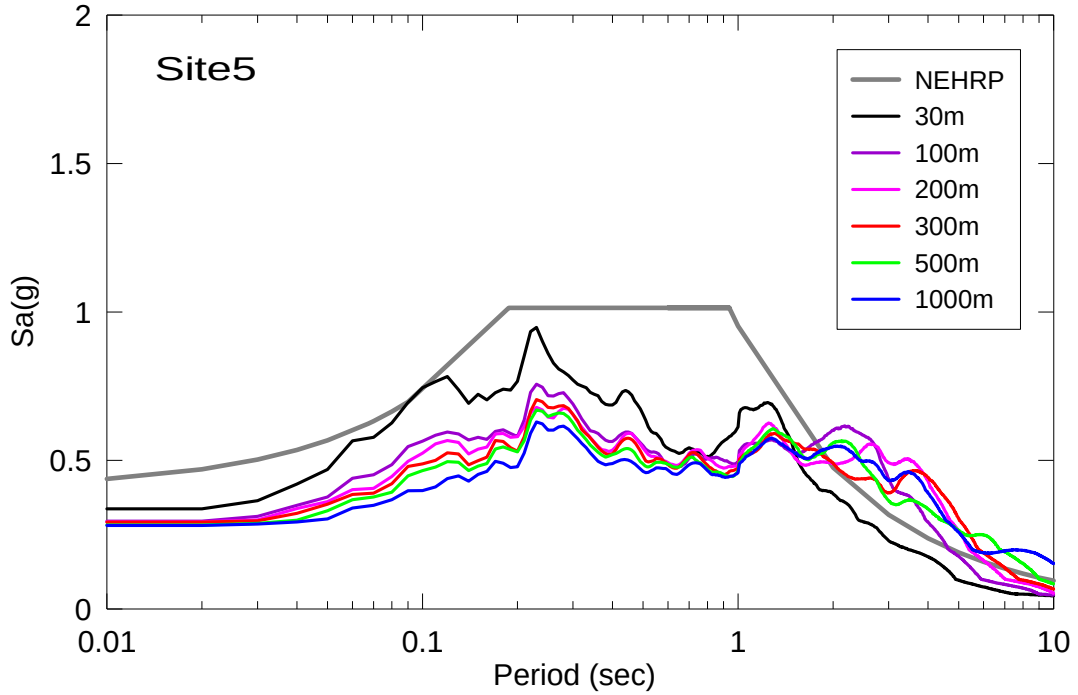

Figure C 14 Computed PSHA(FF)(2011) UHRS for 30m, 100m, 200m, 300m, 500m, 1000m soil-columns and NEHRP design spectra. Lowlands, site 5.

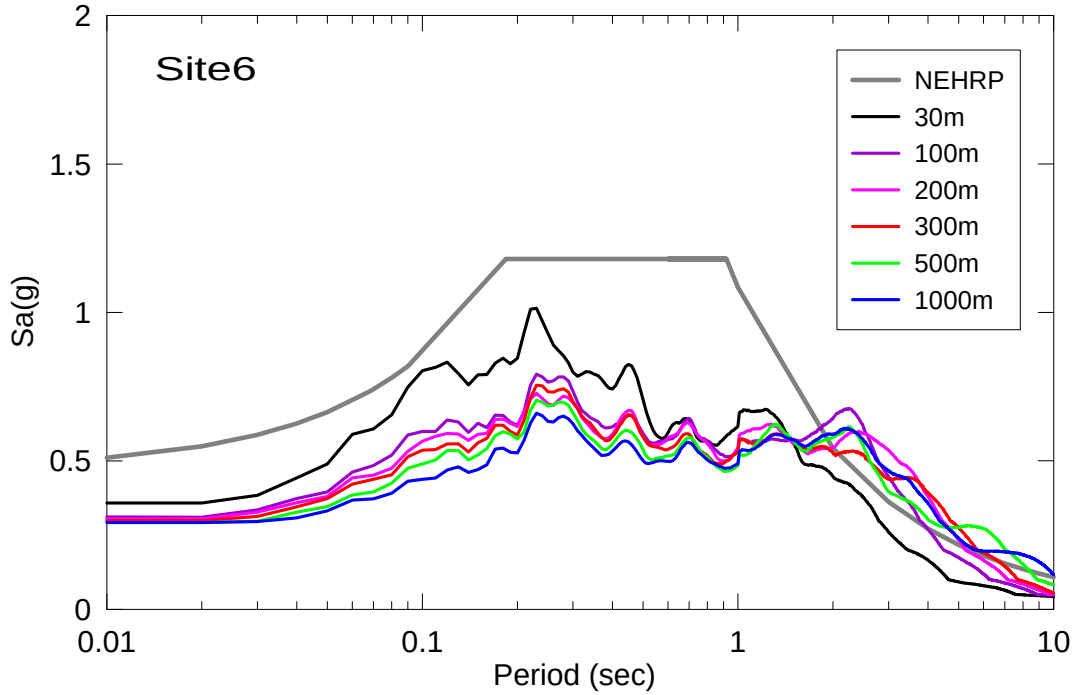

Figure C 15 Computed PSHA(FF)(2011) UHRS for 30m, 100m, 200m, 300m, 500m, 1000m soil-columns and NEHRP design spectra. Lowlands, site 6.

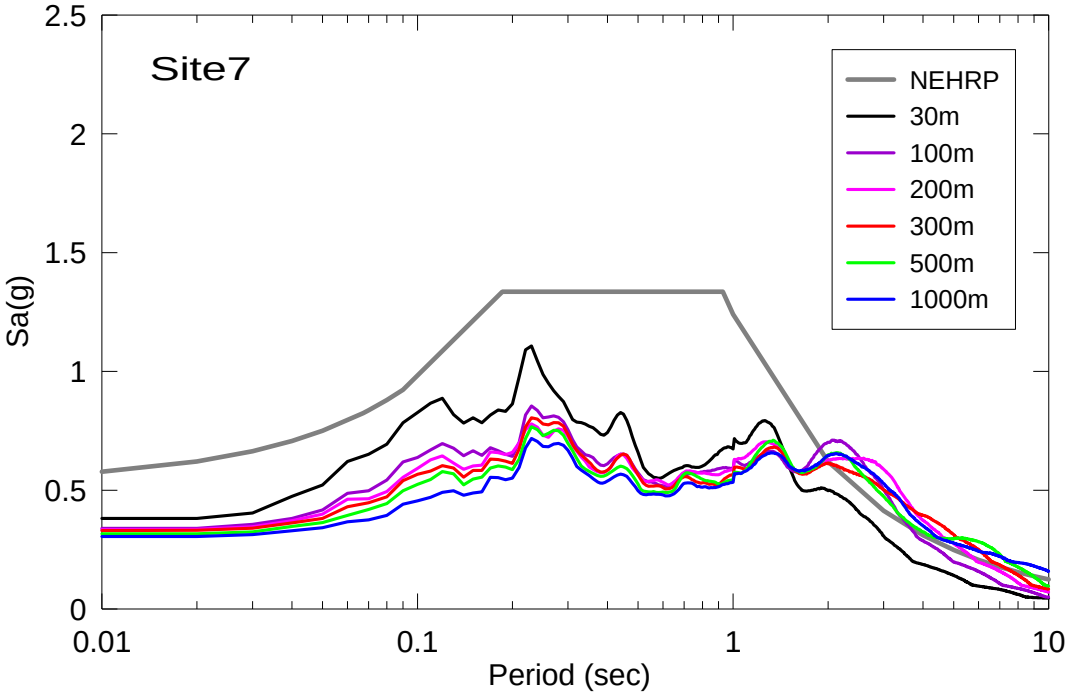

Figure C 16 Computed PSHA(FF)(2011) UHRS for 30m, 100m, 200m, 300m, 500m, 1000m soil-columns and NEHRP design spectra. Lowlands, site 7.

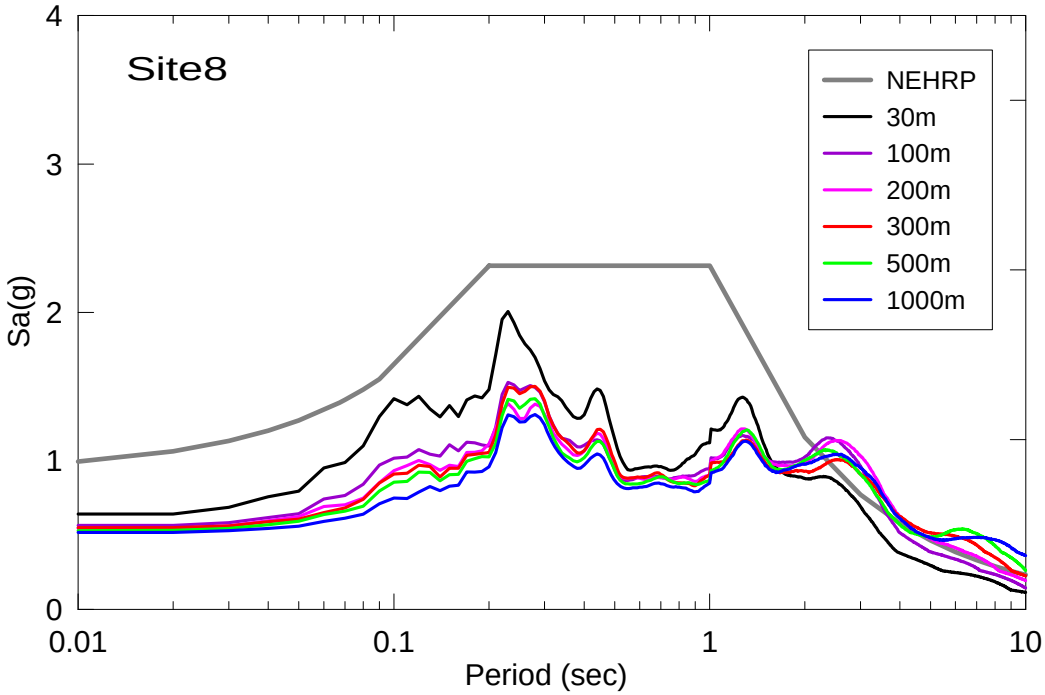

Figure C 17 Computed PSHA(FF)(2011) UHRS for 30m, 100m, 200m, 300m, 500m, 1000m soil-columns and NEHRP design spectra. Lowlands, site 8.

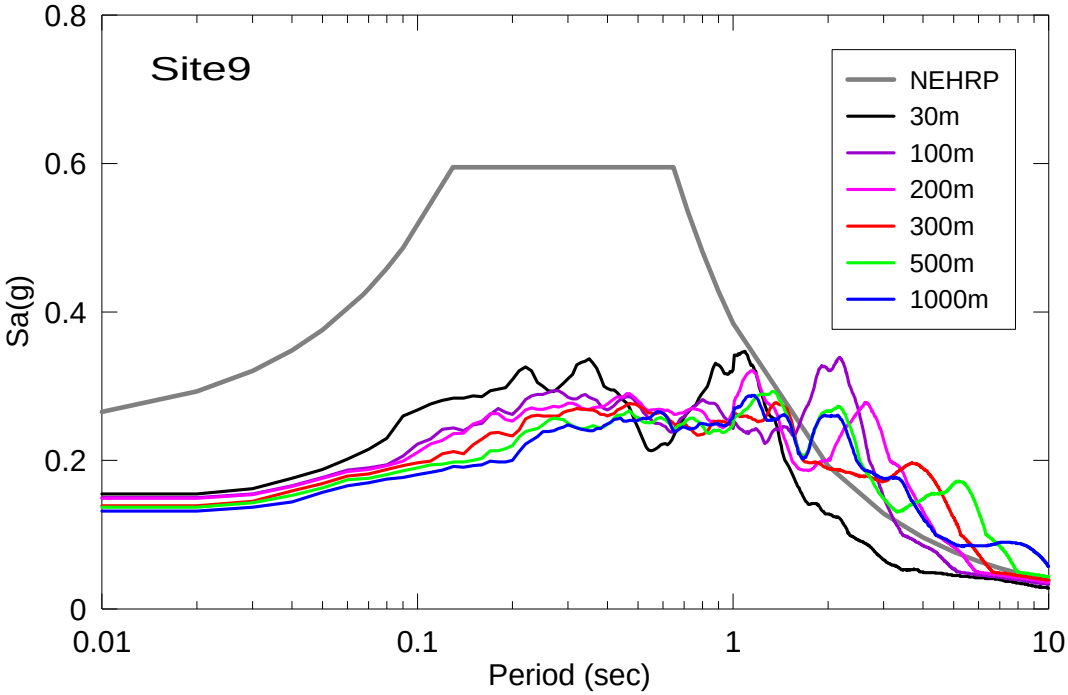

Figure C 18 Computed PSHA(FF)(2011) UHRS for 30m, 100m, 200m, 300m, 500m, 1000m soil-columns and NEHRP design spectra. Lowlands, site 9